Loughborough University

This item was submitted to Loughborough's Institutional Repository (https://dspace.lboro.ac.uk/) by the author and is made available under the following Creative Commons Licence conditions.

creative commons

COMMONS DEED

Attribution-NonCommercial-NoDerivs 2.5

You are free:

- to copy, distribute, display, and perform the work

Under the following conditions:

Attribution. You must attribute the work in the manner specified by the author or licensor.

Noncommercial. You may not use this work for commercial purposes.

No Derivative Works. You may not alter, transform, or build upon this work.

- For any reuse or distribution, you must make clear to others the license terms of this work.
- Any of these conditions can be waived if you get permission from the copyright holder.

Your fair use and other rights are in no way affected by the above.

This is a human-readable summary of the Legal Code (the full license).

Disclaimer

For the full text of this licence, please go to:
http://creativecommons.org/licenses/by-nc-nd/2.5/

Polynomial Matrix Decomposition Techniques for Frequency Selective MIMO Channels

By

Martin Raymond Davies

A Doctoral Thesis

Submitted in partial fulfillment of the requirements

for the award of

Doctor of Philosophy of Loughborough University

February, 2010

© by Martin Raymond Davies, 2010

Abstract

For a narrowband, instantaneous mixing multi-input, multi-output (MIMO) communications system, the channel is represented as a scalar matrix. In this scenario, singular value decomposition (SVD) provides a number of independent spatial subchannels which can be used to enhance data rates or to increase diversity. Alternatively, a QR decomposition can be used to reduce the MIMO channel equalization problem to a set of single channel equalization problems.

In the case of a frequency selective MIMO system, the multipath channel is represented as a polynomial matrix. Thus conventional matrix decomposition techniques can no longer be applied. The traditional solution to this broadband problem is to reduce it to narrowband form by using a discrete Fourier transform (DFT) to split the broadband channel into N narrow uniformly spaced frequency bands and applying scalar decomposition techniques within each band. This describes an orthogonal frequency division multiplexing (OFDM) based system.

However, a novel algorithm has been developed for calculating the eigenvalue decomposition of a para-Hermitian polynomial matrix, known as the sequential best rotation (SBR2) algorithm. SBR2 and its QR based derivatives allow a true polynomial singular value and QR decomposition to be formulated. The application of these algorithms within frequency selective MIMO systems results in a fundamentally new approach to exploiting spatial diversity.

Polynomial matrix decomposition and OFDM based solutions are compared for a wide variety of broadband MIMO communication systems. SVD is used to create a robust, high gain communications channel for ultra low signal-to-noise ratio (SNR) environments. Due to the frequency selective nature of the channels produced by polynomial matrix decomposition, additional processing is required at the receiver resulting in two distinct equalization techniques based around turbo and Viterbi equalization. The proposed approach is found to provide identical performance to that of an existing OFDM scheme while supporting a wider range of access schemes. This work is then extended to QR decomposition based communications systems, where the proposed polynomial approach is found to not only provide superior bit-error-rate (BER) performance but significantly reduce the complexity of transmitter design. Finally both techniques are combined to create a multi-user MIMO system that provides superior BER performance over an OFDM based scheme. Throughout the work the robustness of the proposed scheme to channel state information (CSI) error is considered, resulting in a rigorous demonstration of the capabilities of the polynomial approach.

Acknowledgements

I would like to thank Dr. Sangarapillai Lambotharan and Prof. Jonathon Chambers at Loughborough University, Prof. John McWhirter at Cardiff University and Prof. Ian Proudler at QinetiQ, Malvern for their continued support throughout my PhD study. I would also like to additionally thank my industrial sponsor, QinetiQ and the Engineering and Physical Sciences Research Council for funding my PhD studies.

Publications

- M. Davies, S. Lambotharan and J. McWhirter, "Polynomial Matrix SVD for MIMO Broadband Beamforming," 7^{th} *IMA International Conference on Mathematics in Signal Processing, Cirencester*, pp. 148-152, December, 2006

- M. Davies, S. Lambotharan and J. McWhirter, "Broadband MIMO Beamforming using Spatial-Temporal Filters and Polynomial Matrix Decomposition," 15^{th} *International Conference on Digital Signal Processing, Cardiff*, pp. 579-582, July, 2007

- M. Davies, S. Lambotharan, J. Chambers and J. McWhirter, "Broadband MIMO Beamforming for Frequency Selective Channels Using the Sequential Best Rotation Algorithm," 67^{th} *IEEE Vehicular Technology Conference - Spring, Singapore*, pp. 1147-1151, May, 2008

- M. Davies, S. Lambotharan, J. Foster, J. Chambers and J. McWhirter, "Polynomial Matrix QR Decomposition for Broadband MIMO Wireless Communications," 7^{th} *IMA International Conference on Mathematics in Signal Processing, Cirencester*, pp. 139-142, December, 2008

- M. Davies, S. Lambotharan, J. Foster, J. Chambers and J. McWhirter, "Polynomial Matrix QR Decomposition and Iterative Decoding of Frequency Selective MIMO Channels," *IEEE Wireless Communications and Networking Conference 2009, Budapest*, pp. 1-6, April, 2009

- M. Davies, S. Lambotharan, J. Foster, J. Chambers and J. McWhirter, "A Polynomial QR Decomposition Based Turbo Equalization Technique for Frequency Selective MIMO Channels," 69^{th} *IEEE Vehicular Technology Conference - Spring, Barcelona*, pp. 1-5, April, 2009

- J. Foster, J. McWhirter, M. Davies and J. Chambers, "An Algorithm for Calculating the QR and Singular Value Decomposition of Polynomial Matrices," *IEEE Transactions on Signal Processing*, vol. 58, no. 3, March, 2010

Contributions

- **Application of the sequential best rotation (SBR2) algorithm to obtain spatial diversity techniques in frequency selective MIMO channels.**

  For a frequency flat multi-input multi-output (MIMO) system the singular value decomposition has the ability to provide multiple spatial channels for data transmission. In a frequency selective MIMO scenario the problem is represented as a polynomial matrix and the SVD can no longer be applied. To obtain spatial diversity techniques for this scenario, repeated applications of the SBR2 algorithm have been used to perform a polynomial matrix singular value decomposition. Two types of receiver processing are proposed to overcome the delay spread in the subchannels, Viterbi equalization for exponentially decaying channels, and Turbo equalization for constant profile channels. The diversity performance of the dominant channel provided by the SBR2 based broadband decomposition is evaluated against transmit antenna selection and conventional MIMO-OFDM approaches. The SBR2 approach is shown to provide equal or superior bit-error-rate (BER) performance while also providing a range of benefits applicable to time domain multiple access schemes.

- **Application of polynomial matrix QR decomposition for iterative decoding of frequency selective MIMO channels.**

  Using the turbo equalization strategy developed previously, polynomial matrix QR decomposition is used to reduce the MIMO channel equalization problem to a set of single channel equalization problems for a wide range of Bell Laboratories Layered Space Time (BLAST) architecture wireless communication systems. The proposed approach is again evaluated against an identical MIMO-OFDM solution. The work is shown to have significant advantages, both in terms of superior BER performance and reduced amplifier complexity within the transmitter.

- **Polynomial matrix decomposition for downlink spatial multiplexing in frequency selective MIMO channels.**

  Combining beamforming at the transmitter using the SBR2 algorithm and channel equalization using polynomial matrix QR decomposition at the receiver, an entirely time domain multi-user MIMO system is created. By designing independent orthogonal spatial transmit vectors for each user at the transmitter, multiple users are able to operate within the same shared spectrum with

minimal cross-user interference. The proposed approach is evaluated against an identical MU-MIMO OFDM solution and found to provide superior BER performance due to the exploitation of the frequency selective fading properties of the MU-MIMO channel in the receiver.

Contents

List of Figures

List of Tables

List of Algorithms

List of Abbreviations

AOA	Angle of Arrival
AWGN	Additive White Gaussian Noise
BDFE	Block Division Feedback Equalization
BER	Bit Error Rate
BLAST	Bell Laboratories Layered Space-Time
BPSK	Binary Phase Shift Keying
BSS	Blind Source Separation
CCI	Co-Channel Interference
CDMA	Code Division Multiple Access
CIR	Channel Impulse Response
CP	Cyclic Prefix
CPGR	Complete Polynomial Givens Rotation
CSI	Channel State Information
D-BLAST	Diagonal Bell Laboratories Layered Space-Time
DFT	Discrete Fourier Transform
DMT	Discrete Multitone
DMMT	Discrete Matrix Multitone
DSP	Digital Signal Processing
DVB	Digital Video Broadcasting
ECC	Error Correction Coding
EDGE	Enhanced Data Rates for GSM Evolution
EM	Electromagnetic
EPGR	Elementary Polynomial Givens Rotation
ESPRIT	Estimation of Signal Parameters by Rotational Invariance Techniques
EVD	Eigenvalue Decomposition
FDM	Frequency Division Multiplexing
FDMA	Frequency Division Multiple Access
FFT	Fast Fourier Transform
FIR	Finite Impulse Response

GSM	Global System for Mobile Communications
H-BLAST	Horizontal Bell Laboratories Layered Space-Time
IBI	Interbin Interference
IEEE	Institute of Electrical and Electronics Engineers
IFB	Independent Frequency Band
IFFT	Inverse Fast Fourier Transform
IIR	Infinite Impulse Response
IPEEC	International Partnership for Energy Efficient Cooperation
ISI	Intersymbol Interference
LLR	Log Likelihood Ratio
LOS	Line of Sight
LSE	Least Squares Error
MAP	Maximum a Posteriori
MATLAB	Matrix Laboratory
MIMO	Multiple Input Multiple Output
MISO	Multiple Input Single Output
MMSE	Minimum Mean Square Error
MSE	Mean Square Error
MU-MIMO	Multi-User Multiple Input Multiple Output
MUSIC	Multiple Signal Classification
ODO	Optimal Detection Ordering
OFDM	Orthogonal Frequency Division Multiplexing
PAPR	Peak to Average Power Ratio
PM	Polynomial Matrix
PMEVD	Polynomial Matrix Eigenvalue Decomposition
PMQRD	Polynomial Matrix QR Decomposition
PMSVD	Polynomial Matrix Singular Value Decomposition
QRD	QR Decomposition
QPSK	Quadrature Phase Shift Keying
RF	Radio Frequency
SBR2	Sequential Best Rotation using 2^{nd} Order Statistics
SDMA	Space Division Multiple Access

SIMO	Single Input Multiple Output
SISO	Single Input Single Output
SNR	Signal to Noise Ratio
SOVA	Soft Output Viterbi Algorithm
SVD	Singular Value Decomposition
TAS	Transmitter Antenna Selection
TDMA	Time Division Multiple Access
V-BLAST	Vertical Bell Laboratories Layered Space-Time
WLAN	Wireless Local Area Network
WSS	Wide Sense Stationary

List of Notation

$E[\cdot]$	Expectation operator
$\mathbb{L}(\cdot)$	Log likelihood ratio
$\boldsymbol{I}_p$	$p \times p$ identity matrix
$\underline{\boldsymbol{A}}(z)$	Polynomial matrix
$\|\cdot\|_F$	Frobenius norm
$\widetilde{(\cdot)}$	Paraconjugation
$(\cdot)_*$	Complex conjugate
$(\cdot)^H$	Hermitian conjugate of a matrix or vector
$(\cdot)^T$	Transposition of a matrix or vector
$pinv$	Pseudoinverse of a matrix
$trace$	Trace of a matrix

List of Symbols

α	Probability of starting state for MAP decoder
$\boldsymbol{A}$	Generic scalar matrix
$\underline{\boldsymbol{A}}(z)$	Generic polynomial matrix
β	Number of iterations & Probability of ending state for MAP decoder
B	Bandwidth
$\underline{\boldsymbol{B}}(z)$	Delay matrix
c	Coded output
C	Channel capacity
$\boldsymbol{D}$	Discrete Fourier transform matrix
e	Error
ϵ	Stopping criteria
E_{rel}	Relative error
E_s	Total energy available at the transmitter over a symbol period
$\underline{\boldsymbol{F}}(z)$	Transmitter FIR filter bank
γ	Transmit energy & Probability of transition state for MAP decoder
$\underline{\boldsymbol{G}}(z)$	Transmitter FIR filter bank & Product of rotation matrix and delay matrix & EPGR
$\boldsymbol{H}$	Instantaneous mixing MIMO channel matrix
$\underline{\boldsymbol{H}}(z)$	Convolutive mixing MIMO channel matrix
j	Complex operator
k	Tone index
L	Polynomial length
$\boldsymbol{\Lambda}$	Diagonal matrix
$\underline{\boldsymbol{\Lambda}}(z)$	Polynomial diagonal matrix
M	MMSE Equalizer length
$\boldsymbol{M}$	Transmit filter bank for instantaneous mixing MIMO-MU
$\underline{\boldsymbol{M}}(z)$	Transmit filter bank for convolutive mixing MIMO-MU
M_r	Number of receive antennas
M_t	Number of transmit antennas
μ	Waterpouring constant & Truncation parameter

$\boldsymbol{n}$	Additive Gaussian noise process
N	FFT order & Number of time slots of channel
N_t	Length of training sequence
ψ	Exponential decaying factor
$\boldsymbol{P}$	Permutation matrix
$\underline{\boldsymbol{P}}$	Generic polynomial matrix & Paraunitary polynomial matrix
$\boldsymbol{Q}$	Unitary matrix from QR decomposition & Jacobi rotation matrix
$\underline{\boldsymbol{Q}}(z)$	Paraunitary matrix from PMQRD
r	Number of orthogonal channels
$\boldsymbol{R}$	Upper triangular matrix & Complex scalar matrix
$\underline{\boldsymbol{R}}(z)$	Polynomial upper triangular matrix & Para-Hermitian polynomial matrix
σ^2	Noise variance
s	State
$\boldsymbol{S}$	Set of source signals
τ	Polynomial index
T	Length of source signals
$\boldsymbol{U}$	Unitary matrix from SVD
$\underline{\boldsymbol{U}}(z)$	Paraunitary matrix from PMSVD
$\boldsymbol{V}$	Unitary matrix from SVD
$\underline{\boldsymbol{V}}(z)$	Paraunitary matrix from PMSVD
w	MMSE weight vector
x	Interleaved output
$\boldsymbol{Y}$	Set of receive signals
z^{-1}	Unit delay operator

Chapter 1

Introduction

Motivation

The date of the invention of the radio and to whom it should be credited is frequently debated. It is widely accepted that it should be attributed to Marconi, who in the spring of 1895 transmitted the first signal using a free propagating electromagnetic (EM) wave as a carrier [1]. Using Branly's coherer to detect EM waves, essentially loose iron fillings in a tube connected in a circuit with a battery and a galvanometer [2] and a spark gap transmitter invented by Hertz [3], Marconi was able to receive signals up to a distance of one mile from his laboratory in Bolgona, Italy. In 1896 Marconi moved to England and would go onto perform several ground breaking experiments. In particular in May 1897 messages were exchanged between Lavernock Point and Flat Holm island, in the Bristol Channel, at a distance of nine miles [1]. In December 1901 Marconi successfully completed the first transatlantic transmission and the radio age was born.

Radio would revolutionize the shipping industry, which even in 1900 was still reasonably dangerous [4]. Previous methods of communication largely relied on flares or lamps for signaling, and ships rarely sank in situations involving perfect visibility. Radio would also become a staple technology for the military, and the first world war would drive the development of smaller, lightweight units for use in aircraft, in turn leading to vacuum tubes with improved performance and reliability [5].

The first electronic computers appeared around the time of the second world war to quickly and accurately develop firing tables for guns used by the military [6]. The invention of the transistor in 1947 and subsequent fabrication of the first practical integrated circuit in 1959 [7] lead to digital signal processing (DSP) becoming a major area of interest in the mid 1960's [8]. Rapid advances in DSP and computing, in particular the advent of the fast Fourier transform (FFT) in 1965 [9] have led to the wide range of speech and image processing techniques available today.

The first real merging of radio and computing was in 1971. ALOHANET, the first computer network based on packet radio was developed at the University of Hawaii and enabled computer sites at seven campuses spread out over four islands to communicate with a central computer via radio

transmission [10]. However the high cost and low speed of wireless networking compared to wired Ethernet cabling prevented any commercial success. With the introduction of the wireless local area networking standard (WLAN) IEEE 802.11[11] in 1997, interest in wireless networking has renewed. Although data rates are still significantly lower than cable and coverage is limited to a few tens of meters, WLAN's are becoming the preferred Internet access method in many homes, offices, and campus environments due to their convenience and freedom from wires [10].

Conversely, cellular phones have experienced continued explosive growth since their introduction in the 1980's. Almost absurdly, in November 2007 worldwide cellular phone subscriptions reached 3.3 billion, equivalent to half the global population [12]. This statistic is slightly out of context, as several countries (including Britain) have a mobile penetration of over 100%, i.e. some owners have multiple phones, however the untapped commerical potential is vast.

Rapid progress in radio technology is continuously creating new and improved services at lower costs, resulting in the increase of air-time usage and subscribers. Around the turn of the century wireless service revenues were growing at approximately 40% per year. As a consequence wireless system designers are faced with an ever growing number of challenges. In particular the diminishing availability of radio spectrum versus the continuing increase in subscribers, demand for higher data rates and coverage by base stations and lower infrastructure and operating costs [13]. Wireless multiple-input, multiple-output (MIMO) systems have the potential to solve all these problems.

MIMO systems utilize multiple antennas at the transmitter and receiver to exploit the spatial properties of the propagating environment and offer several key benefits over conventional single-input, single-output (SISO) systems, in particular the ability to exploit the spatial properties of the wireless channel.

Diversity Gain

When the received signal power in a wireless SISO system drops significantly, the channel is said to be in a fade which is predominantly caused by two mechanisms, macroscopic and microscopic fading. Macroscopic or slow fading is attributed to the disappearance of noticeably strong contributing paths between transmitter and receiver due to intrusion of propagation environment features such as buildings [14]. Microscopic or fast fading refers to the rapid fluctuations of the received signal in space, time and frequency, and is caused by the signal scattering off objects between the transmitter and receiver [13]. For a wireless MIMO channel, the signal path between any single transmit antenna and any single receive antenna can be considered independent, providing the transmit antennas are spaced a suitable distance apart from each other and also the receive antennas are spaced likewise. As inde-

pendent signal paths have a low probability of experiencing deep fades simultaneously [10], by sending data over multiple independent paths the effects of fading can be mitigated, and is termed spatial diversity. Spatial diversity is highly desirable, as unlike frequency or temporal diversity techniques, it does not require additional signal bandwidth or transmission time.

Array Gain

The received signal power in a MIMO system can also be increased by coherent combining of signals. For example signals arriving at the receive antennas have different amplitudes and phases. The receiver can combine the signals coherently so that the resulting signal-to-noise ratio (SNR) is enhanced [3]. This is termed array gain.

Spatial Multiplexing

Spatial multiplexing (SM) refers to the linear increase in capacity of a MIMO system with the number of antenna transmit-receive pairs over a SISO system for the same bandwidth and with no additional power expenditure [3]. Encoding architectures such as Bell Laboratories Layered Space Time (BLAST) [15] transmit an independent symbol at each transmit antenna at each symbol period, and a MIMO system consisting of eight transmit and eight receive antennas has been shown to have a capacity of more than forty times that of a SISO system with identical total radiated transmit power and bandwidth [15]. Spatial multiplexing can only be exploited in MIMO channels.

Interference Reduction

CCI or co-channel interference arises due to frequency reuse in wireless channels. If the desired signal and interferers occupy the same temporal frequency band, then temporal filtering cannot be used to separate signal from interference [16]. However, as the desired and interference signals originate from different spatial locations, spatial separation can be used to separate signal from interference. Processing signals at an antenna array is termed beamforming, and allows pencil beams to be formed to radiate or receive energy from a specific spatial location.

Aside from increasing frequency reuse and improving network capacity, beamforming forms the centrepiece of cognitive radio [17, 18]. When portions of the electromagnetic spectrum are scanned it is found that there exist frequency bands that are largely unoccupied most of the time or only partially occupied. This is termed a spectrum hole [17] - i.e. a band of frequencies assigned to a primary user, but at a particular time and specific geographical location, the band is not being utilized by that user. Cognitive radio is an enabling technology that allows a secondary user to access a spectrum hole. The benefit of this is twofold, firstly it allows the primary user to lease spectrum holes and maximise

their investment and potentially lower the cost of their spectrum licence. Secondly, it allows efficient utilization of the precious electromagnetic spectrum.

Polynomial Matrix Decompositions

For a narrowband, instantaneous mixing scenario the MIMO channel matrix can be viewed as a matrix of complex scalar elements. Matrix decomposition techniques such as singular value decomposition (SVD) and QR decomposition (QRD) are fundamental components of techniques used to obtain spatial diversity. However in the broadband case where the signals are convolutively mixed, the problem is represented as a matrix consisting of complex polynomial elements. The matrix therefore is essentially three-dimensional and existing matrix decomposition techniques can no longer be applied.

Typically this polynomial matrix time domain problem is solved in the frequency domain [19, 20], known as a MIMO orthogonal frequency division multiplexing (OFDM) scheme. This separates the broadband problem into multiple narrowband problems, where conventional scalar matrix decomposition techniques can be applied.

However an entirely novel algorithm for calculating polynomial matrix eigenvalue decomposition (PMEVD) has been developed in [21]. Known as the sequential best rotation algorithm (SBR2) its application allows a polynomial matrix singular value decomposition (PMSVD) to be applied directly to the polynomial channel matrix. Continuing research into the operation of the SBR2 algorithm has also led to the development of an algorithm for calculating a polynomial matrix QR decomposition (PMQRD) [22].

The motivation therefore is to analyse polynomial matrix decomposition techniques and apply them to the broadband, convolutive mixing MIMO problem to create novel MIMO communications systems which operate entirely in the time domain. Although the work presented in this thesis is focused predominantly on wireless MIMO channels, the matrix decompositions are generic and can be applied to any MIMO channel.

Problem Statement and Aims of Thesis

The SBR2 algorithm allows the eigenvalue decomposition of a para-Hermitian polynomial matrix to be calculated [21]. It was developed initially for solving convolutive blind source separation (BSS) and can be used to enforce strong decorrelation upon a set of convolutively mixed signals. Additionally, SBR2 research has yielded an algorithm for calculating polynomial matrix QR decomposition [22]. These algorithms provide the foundations for the research presented in this thesis. The main aims of this thesis are now described below:

1. In a narrowband MIMO scenario where the received signals are instantaneously mixed, a scalar matrix is sufficient to describe the mixing. Paulraj, Nabar and Gore [3] have shown that for this scenario, performing the SVD would provide a number of independent spatial subchannels (commonly referred to as modes) which can be used to enhance the data rates or to obtain increased diversity. The motivation therefore is to apply the SBR2 algorithm to frequency selective MIMO channels to calculate PMSVD, extending the decomposition presented in [3] to a broadband MIMO scenario. As the proposed scheme operates using spatio-temporal filters in the time domain, further processing is required at the receiver to overcome delay spread in the modes. Therefore efficient channel equalization is also a key design issue.

2. Secondly, using a technique for PMQRD, based on applying the same elementary paraunitary operations used in the SBR2 algorithm, this thesis aims to continue to exploit spatial diversity in frequency selective MIMO channels. This decomposition reduces the MIMO channel equalization problem to a set of decision feedback based single channel equalization problems [23, 24]. However unlike PMSVD, PMQRD only requires channel knowledge at the receiver, hence it is highly suitable for broadcast applications.

3. Finally the work is extended to a multi-user MIMO scenario. Application of the SBR2 algorithm at the transmitter enables transmission of signals between the transmitting base station and a desired user within the null space between the transmitter and all other users [25]. To equalize the resulting frequency selective MIMO channel between transmitter and receiver, PMQRD is utilized at the receiver to reduce transmitter complexity.

Organization of Thesis

This thesis is organized as follows. Chapter two provides a review of space-time wireless communications techniques for both instantaneous mixing and convolutive mixing MIMO scenarios. The use of the SVD and QRD to obtain spatial diversity in frequency flat MIMO channels are explored, as well as existing techniques for calculating polynomial matrix decomposition. Finally, at the end of this chapter the estimation of the frequency selective MIMO channel using training sequences is discussed.

The third chapter details the operation of the SBR2 algorithm, which can be used to calculate the PMEVD of a para-Hermitian polynomial matrix. SBR2 makes use of "elementary paraunitary transformations" and constitutes a generalization of the classical Jacobi algorithm for conventional

Hermitian matrix diagonalization [21]. It is shown how the PMSVD of a polynomial matrix can be calculated by independently post and pre multiplying the polynomial matrix with its paraconjugate and applying the SBR2 algorithm to the resulting para-Hermitian matrix. This rotation matrix approach to polynomial matrix decomposition is then extended to an algorithm for calculating PMQRD [26], which no longer requires the input matrix to possess the para-Hermitian property. Finally it is shown how PMSVD can be performed using the PMQRD algorithm, resulting in a higher quality decomposition.

Throughout this thesis, frequency selective MIMO channels with both exponentially power delay and constant power profile are investigated. Channels with exponential power delay are used to model the channel properties applicable to outdoor cellular environments and channels with constant power profile are used to model the channel properties applicable to indoor wireless local area networks. The distribution of energy within the frequency selective MIMO channel directly affects the distribution of energy within the spatial-temporal channels produced by polynomial matrix decomposition, resulting in two fundamentally different equalization approaches. The fourth chapter focuses on exploiting the high gain properties of the dominant mode produced by PMSVD for both these scenarios. The performance of the SBR2 based scheme is evaluated against a transmitter antenna selection (TAS) based scheme, providing a time domain multiple access (TDMA) comparison. The SBR2 based scheme is also evaluated against a frequency domain MIMO orthogonal frequency division multiplexing (OFDM) SVD scheme.

The fifth chapter demonstrates how spatial diversity can be obtained in frequency selective MIMO channels using PMQRD. In particular this chapter focuses on the time domain solution to the MIMO channel equalization problem provided by PMQRD versus the frequency domain solution provided by MIMO-OFDM QRD. The fundamental difference between these two approaches is that PMQRD spreads the information within each transmitted symbol across the entire channel bandwidth, whereas OFDM constrains the information in each transmitted symbol to a single narrowband tone is explored. Individual tones may have low gain, due to the frequency selective nature of the channel, and consequently the PMQRD approach provides significant performance benefits. Throughout this chapter a wide range of transmitter architectures based on Bell Laboratories Layered Space Time (BLAST) [15] are explored.

The sixth chapter extends the work to a multi-user MIMO scenario. A downlink MIMO-MU scenario is considered consisting of a transmitting base station equipped with multiple antennas, and multiple receiving users also equipped with multiple antennas. Filter banks designed using the SBR2 algorithm are used to transmit spatially propagating data streams and reduce CCI. Building on

the work in chapter five, PMQRD is used to recover the individual streams. Again this time domain polynomial matrix approach is evaluated against a conventional frequency domain MIMO-MU OFDM approach.

The final chapter concludes this thesis and discusses further continuation of this work in the future. Appendices are included to provide additional simulation results that are not included in the main body of the text.

Notation

Throughout this thesis, matrices are denoted by upper case bold characters and vectors by lower case bold characters. Regular upper or lower case characters denote scalar quantities. $[\cdot]_{kl}$ denotes the (k,l)-th element of the matrix in the square brackets. The superscripts T and H denote the matrix transpose and Hermitian conjugate, respectively. $\boldsymbol{I}_p$ is used to denote the $p \times p$ identity matrix. Polynomial matrices and vectors are denoted respectively by underscored bold upper and lower case characters. The use of an underscore with scalar quantities denotes a polynomial with scalar coefficients. Any polynomial (matrix, vector, or scalar) with the qualifier (z) denotes a polynomial in the indeterminate variable z^{-1}. The $*$, used as a subscript, denotes complex conjugation of the coefficients in a polynomial matrix or vector. The use of $\widetilde{\ }$ above a polynomial matrix or vector denotes the paraconjugate, i.e. for a given polynomial matrix $\underline{\boldsymbol{A}}(z)$, $\underline{\widetilde{\boldsymbol{A}}}(z) = \underline{\boldsymbol{A}}_*^T(z^{-1})$. $\|\cdot\|_F$ will be used to denote the Frobenius norm (F-norm) of a polynomial matrix, which is simply the square root of sum of the squared F-norms for all coefficient matrices.

Chapter 2

Background to Space-Time Wireless Communications

2.1 Introduction

In this chapter the instantaneous mixing model is discussed and its subsequent exploitation in frequency flat MIMO systems. Firstly the application of scalar matrix decompositions to narrowband MIMO channels is considered. The singular value decomposition is used to create multiple parallel spatial sub-channels and the average bit-error-rate (BER) performance of the dominant sub-channel is shown to be far superior to that of a SISO channel with equal total radiated transmit power and bandwidth. As the multiple spatial sub-channels provided by SVD are orthogonal, they may be used simultaneously to increase system capacity. A waterpouring scheme [27] is used to find the optimum allocation of transmit energy over the sub-channels and theoretical capacity results are presented.

SVD requires knowledge of the wireless channel at both the transmitter and receiver. For a MIMO system where no feedback path exists between the receiver and transmitter, channel knowledge is only obtainable at the receiver. The transmitter will repeatedly transmit a training sequence, allowing for estimation of the channel by the receiver followed by a data sequence. For this scenario, QR decomposition is shown to reduce the MIMO channel equalization problem to a set of decision feedback based single channel equalization problems. BER results are presented to show the substantial increase in capacity obtained by QRD over a SISO channel with equal total radiated transmit power and bandwidth.

The main topic of this thesis, the convolutive mixing model for MIMO channels is then presented, alongside a review of existing techniques for solving the broadband MIMO problem, in particular the well known frequency domain based MIMO-OFDM approach as well as novel transceiver techniques based on convex optimization. Following on from this the operation of a wide range of techniques for polynomial matrix decomposition are presented, and their suitability for implementation within a MIMO communications system is discussed. This includes well known approaches to polynomial matrix decomposition such as Smith-McMillan decomposition and an FIR lossless decomposition based approach pioneered by Vaidyanathan [28].

The chapter concludes with channel estimation techniques applicable to frequency selective MIMO channels. Estimation of the channel state information (CSI) will become a significant component of simulations in subsequent chapters, allowing accurate representation of a real-world MIMO communications system.

2.2 Instantaneous Mixing

In an instantaneous mixing model, the wireless channel between a single transmit-receive antenna pair is represented as a single complex coefficient. This represents a scaling in amplitude due to attenuation by the propagating environment, and a phase shift that accounts for the propagation delay [21].

For a MIMO system consisting of M_t transmit and M_r receive antennas operating in an instantaneous mixing environment, the noise free channel can be represented as an $M_r \times M_t$ mixing matrix, $\boldsymbol{H}$. The element h_{ji} represents the channel between the i^{th} transmit antenna and j^{th} receive antenna, for $i = 1, 2, \ldots, M_t$ and $j = 1, 2, \ldots, M_r$. Hence a complex scalar matrix is sufficient to describe the mixing. This is termed a frequency flat system, as the bandwidth of the signal transmitted is less than the coherence bandwidth of the channel. Coherence bandwidth represents the maximum bandwidth over which two frequencies of a signal are likely to experience correlated amplitude fading [3]. For this reason it is also frequently refered to as a narrowband MIMO system.

Considering a set of source signals of length T, $\boldsymbol{s}(t) \in \mathbb{C}^{M_t \times 1}$, for $t \in \{0, 1, \ldots, T-1\}$ that are propagated through the MIMO channel, $\boldsymbol{H}$. The set of received signals, $\boldsymbol{y}(t) \in \mathbb{C}^{M_r \times 1}$ can be expressed as:

$$\boldsymbol{y} = \boldsymbol{H}\ \boldsymbol{s} + \boldsymbol{n} \tag{2.1}$$

where $\boldsymbol{n}(t)$ denotes an $M_r \times 1$ vector representing an additive Gaussian noise process with variance σ^2. Figure 2.1 shows the basic MIMO communications system structure.

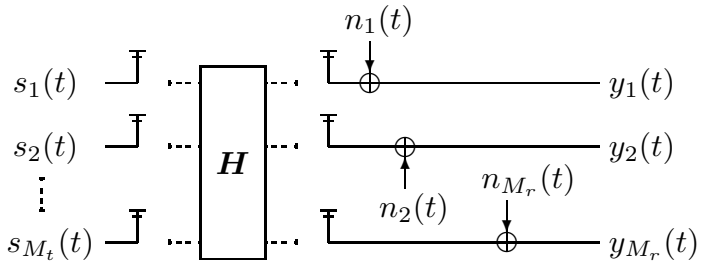

Figure 2.1: Basic MIMO communications structure.

2.2.1 Singular Value Decomposition

The Singular Value Decomposition (SVD) of the MIMO channel $\boldsymbol{H}$ is given in (2.2) where $\boldsymbol{U}$ and $\boldsymbol{V}$ are unitary matrices, such that $\boldsymbol{U}\boldsymbol{U}^H = \boldsymbol{U}^H\boldsymbol{U} = \boldsymbol{I}_{M_r}$ and $\boldsymbol{V}\boldsymbol{V}^H = \boldsymbol{V}^H\boldsymbol{V} = \boldsymbol{I}_{M_t}$ and Λ is a diagonal scalar matrix [29].

$$\boldsymbol{H} = \boldsymbol{U}\boldsymbol{\Lambda}\boldsymbol{V}^H \tag{2.2}$$

The process of using the i^{th} column of $\boldsymbol{V}$, $\boldsymbol{v}_i = [v_{1i}, v_{2i}, \ldots, v_{M_t i}]^T$ as a transmit beamformer and the i^{th} row of $\boldsymbol{U}^H$, i.e. $\boldsymbol{u}_i^H = \left[u_{i1}^H, u_{i2}^H, \ldots, u_{iM_r}^H\right]$ as a receive beamformer, is identical to passing the i^{th} signal through the i_{th} diagonal element of $\boldsymbol{\Lambda}$, i.e.

$$\begin{aligned} y_i(t) &= \boldsymbol{u}_i^H\ \boldsymbol{H}\ \boldsymbol{v}_i\ s_i(t) + \boldsymbol{u}_i^H\ n(t) \\ y_i(t) &= \boldsymbol{\lambda}_{ii}\ s_i(t) +\ n'(t) \end{aligned} \tag{2.3}$$

where $n'(t) = \boldsymbol{u}_i^H\ n(t)$. Figure 2.2 shows the MIMO communications system structure for the i^{th} transmitted signal. Due to the unitary property of $\boldsymbol{U}$ the statistical properties of the noise will be unchanged by filtering it with $\boldsymbol{u}_i^H$. For an $M_r \times M_t$ MIMO system, $\boldsymbol{\Lambda}$ will be a diagonal matrix containing $r = min\{M_r, M_t\}$ orthogonal channels, ordered in terms of power. Hence $\boldsymbol{\lambda}_{11} > \boldsymbol{\lambda}_{22} > \ldots > \boldsymbol{\lambda}_{rr}$. SVD can therefore be used to provide a number of independent spatial subchannels which can be used to enhance the data rates or to increase diversity [3].

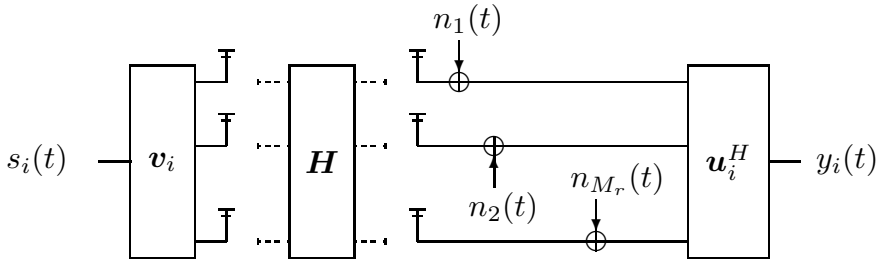

Figure 2.2: SVD MIMO communications structure for the i^{th} transmitted signal.

Figure 2.3 shows the bit error rate (BER) performance when using the dominant mode, $\boldsymbol{\lambda}_{11}$ exclusively for transmission for a range of MIMO orders. The total transmission power budget is identical in each MIMO scheme. The modulation scheme used is BPSK. BER results have been computed for 1000 Monte Carlo simulations. Diversity gain manifests itself in increasing the magnitude of the slope of the BER curve [3], clearly visible in the dramatic improvement in BER performance in a 2×2 MIMO system over a SISO system, for example a 12dB gain in SNR is observed at BER

10^{-2}.

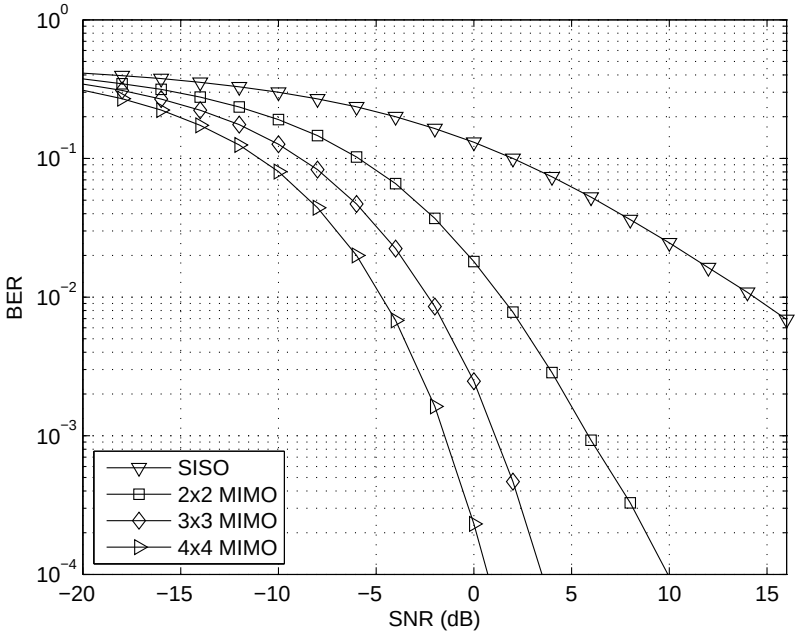

Figure 2.3: Average BER curves for dominant mode SVD instantaneous mixing channels.

MIMO Channel Capacity

Shannon introduced the concept of channel capacity, C, as the maximum rate at which information can be transmitted over a noisy channel [30, 31]. The channel capacity of any SISO channel is given by

$$C = \log_2 \left(1 + \frac{E_s}{\sigma^2} |h|^2\right) \text{ bits/sec} \tag{2.4}$$

where E_s denotes the total average energy available at the transmitter over a symbol period. As the channels provided by the SVD are orthogonal they may be used simultaneously for spatial multiplexing. The capacity of the MIMO channel is the sum of the individual parallel SISO channel capacities [3] and is given by

$$C = \sum_{i=1}^{r} \log_2 \left(1 + \frac{E_s \gamma_i}{M_t \sigma^2} |\boldsymbol{\lambda}_{ii}|^2\right) \tag{2.5}$$

where γ_i denotes the transmit energy in the i^{th} sub-channel and $\sum_{i=1}^{r} \gamma_i = M_t$. The optimal energy allocation of transmit energy over the sub-channels is found iteratively using the waterpouring algorithm [32].

Waterpouring Algorithm

The waterpouring algorithm for MIMO SVD is analogous to the waterpouring solutions for parallel Gaussian channels [27]. It takes p iterations up to a maximum of $p = r$ iterations. For the p^{th} iteration the constant μ is calculated as

$$\mu = \frac{M_t}{(r-p+1)} \left[1 + \frac{\sigma^2}{E_s} \sum_{i=1}^{r-p+1} \frac{1}{|\boldsymbol{\lambda}_{ii}|^2} \right] \tag{2.6}$$

Using this value of μ, the power allocated to the i^{th} sub-channel is calculated using

$$\gamma_i = \left(\mu - \frac{M_t \sigma^2}{E_s \, |\boldsymbol{\lambda}_{ii}|^2} \right), i = 1, 2, \ldots, r-p+1 \tag{2.7}$$

If the energy allocated to $\gamma_{r-p+1} < 0$ this channel is discarded and $\gamma_{r-p+1} = 0$. The algorithm is then re-run with p incremented by 1. The optimal waterpouring power allocation strategy is found when the power allocated to each spatial subchannel is non-negative [3].

Figure 2.4 shows the total capacity when using waterpouring in an SVD based system for a range of MIMO orders. The total transmission power budget is identical in each MIMO scheme. Results have been computed for 1000 Monte Carlo simulations. A wide sense stationary (WSS) situation has been considered where the channel coefficients have been assumed to be unchanged within each data block, but allowed to change between data blocks according to a zero mean complex circular Gaussian distribution. The tremendous increase in capacity afforded by MIMO is clearly visible, for example the capacity of a 4×4 MIMO system is almost four times greater than that of the equivalent SISO system at an SNR of 10dB.

2.2.2 QR Decomposition

SVD requires both the transmitter and receiver to have prior knowledge of the MIMO channel, $\boldsymbol{H}$. However in applications such as digital video broadcasting (DVB) the transmitter has no prior channel knowledge. For this scenario, QR decomposition can be applied at the receiver to exploit the diversity gain afforded by the MIMO channel. The QR decomposition of the $M_r \times M_t$ complex scalar channel matrix, $\boldsymbol{H}$ is given as:

$$\boldsymbol{H} = \boldsymbol{Q} \; \boldsymbol{R} \tag{2.8}$$

where $\boldsymbol{Q}$ is a $M_r \times M_r$ unitary matrix, so that $\boldsymbol{Q}\boldsymbol{Q}^H = \boldsymbol{Q}^H\boldsymbol{Q} = \boldsymbol{I}_{M_r}$ and $\boldsymbol{R}$ is a $M_r \times M_t$ upper triangular matrix. A set of source signals of length N, $\boldsymbol{s}(t) \in \mathbb{C}^{M_t \times 1}$ are propagated through the

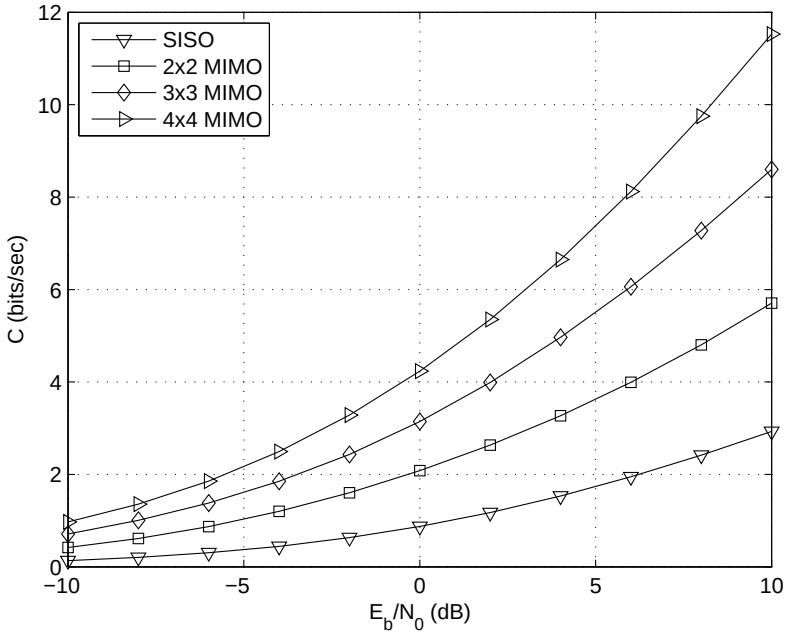

Figure 2.4: Average capacity curves for MIMO SVD instantaneous mixing channels.

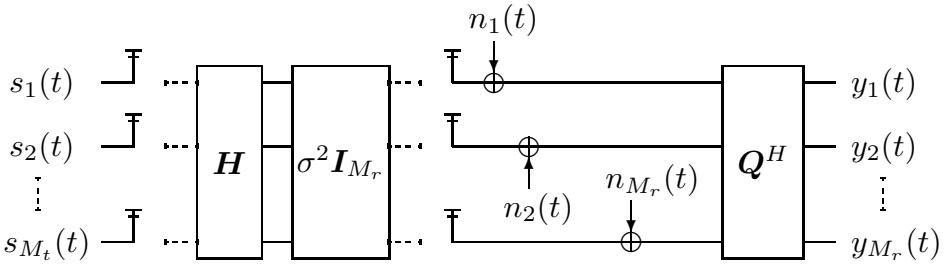

Figure 2.5: QR MIMO communications structure.

MIMO channel, received and filtered with $\boldsymbol{Q}^H$ as shown in Figure 2.5

The set of received signals, $\boldsymbol{y}$ is then expressed as:

$$\begin{aligned} \boldsymbol{y} &= \boldsymbol{Q}^H \, \boldsymbol{H} \, \boldsymbol{s} + \boldsymbol{Q}^H \, \boldsymbol{n} \\ \boldsymbol{y} &= \boldsymbol{R} \, \boldsymbol{s} + \boldsymbol{n}' \end{aligned} \tag{2.9}$$

where $\boldsymbol{n}' = \boldsymbol{Q}^H \, \boldsymbol{n}$. Again, due to the unitary property of $\boldsymbol{Q}$ the statistical properties of the noise will be unchanged by filtering it with $\boldsymbol{Q}^H$. The upper triangular property of the matrix $\boldsymbol{R}$ can now be exploited to transform the MIMO channel equalization problem into a set of M_r equalization problems

using back substitution. The M_t^{th} source signal is expressed as (2.10)

$$\boldsymbol{y}_{M_r} = \boldsymbol{r}_{M_r M_r}\ \boldsymbol{s}_{M_t} + \boldsymbol{n}'_{M_r} \tag{2.10}$$

Once $\boldsymbol{s}_{M_t}$ is retrieved, it can be used to cancel its contribution to $\boldsymbol{y}_{M_r-1}$ as follows

$$\boldsymbol{y}_{M_r-1} - \boldsymbol{r}_{M_r-1M_r}\ \boldsymbol{s}_{M_t} = \boldsymbol{r}_{M_r-1M_r-1}\ \boldsymbol{s}_{M_t-1} + \boldsymbol{n}'_{M_r-1} \tag{2.11}$$

which again is a single channel equalization problem. Therefore the i^{th} single channel equalization problem can be formulated as

$$\boldsymbol{y}_i - \sum_{j=i+1}^{M_r} r_{ij}\ s_j = r_{ii}\ s_i + n'_i \tag{2.12}$$

providing the streams $\boldsymbol{s}_{i+1} \ldots \boldsymbol{s}_{M_t}$ have been previously recovered.

As the transmitter has no knowledge of $\boldsymbol{H}$, an adaptive power transmission scheme cannot be implemented. Hence the total transmission power budget is allocated equally between the streams. For an $M_r = M_t$ MIMO QR system, assuming perfect interference cancellation between substreams the total system capacity can be expressed as

$$C = \sum_{i=1}^{M_t} \log_2 \left(1 + \frac{E_s}{M_t \sigma^2} |r_{ii}|^2\right) \tag{2.13}$$

Figure 2.6 shows the theoretical maximum throughput of a QR based system for a range of MIMO orders calculated using (2.13). The total transmission power budget is identical in each MIMO scheme. Results have been computed for 1000 Monte Carlo simulations. Once again the increase in throughput afforded by MIMO is clearly visible, for example the data rate of a 4×4 MIMO system is over three times greater than that of the equivalent SISO system at an SNR of 10dB.

2.3 Convolutive Mixing

In a convolutive mixing model, the bandwidth of the signal transmitted is greater than the coherence bandwidth of the channel. Hence the transmitted signal will experience frequency selective fading. The wireless channel between a single transmit-receive pair is therefore finite impulse response (FIR) in nature. This is due to the transmitted signal arriving at the receiver over multiple paths and with different time delays. Therefore, in the case of a frequency selective MIMO system, the noise

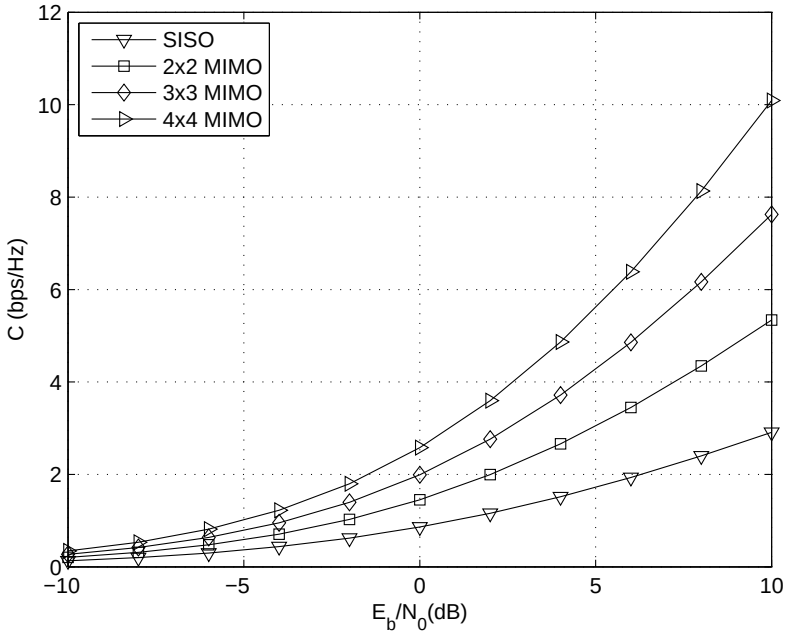

Figure 2.6: Average capacity curves for MIMO QR instantaneous mixing channels.

free multipath channel matrix can be expressed as a polynomial matrix, $\underline{\boldsymbol{H}}(z)$.

$$\underline{\boldsymbol{H}}(z) = \sum_{i=0}^{L-1} \boldsymbol{H}_i z^{-i} \tag{2.14}$$

where $\boldsymbol{H}_i \in \mathbb{C}^{M_r \times M_t}$ is the i^{th} matrix tap of the MIMO channel of length L, and z^{-1} is the unit delay operator. Thus its singular value and QR decomposition cannot be directly formulated and spatial diversity can no longer be exploited. A number of solutions for this frequency selective problem are now presented.

2.3.1 Space Time Vector Coding

Considering a set of source signals of length T, $\boldsymbol{s}(t) \in \mathbb{C}^{M_t \times 1}$ for $t \in \{0, 1, \ldots, T-1\}$ that are propagated through the MIMO channel, $\underline{\boldsymbol{H}}(z)$, the received signals $\boldsymbol{y}(t)$ may be expressed as

$$\underline{\boldsymbol{y}}(z) = \underline{\boldsymbol{H}}(z)\ \underline{\boldsymbol{s}}(z) \tag{2.15}$$

where $\underline{\boldsymbol{s}}(z)$ and $\underline{\boldsymbol{y}}(z)$ denote the algebraic power series

$$\begin{aligned} \underline{\boldsymbol{s}}(z) &= \sum_{t=-\infty}^{\infty} \boldsymbol{s}(t) z^{-t} \\ \underline{\boldsymbol{y}}(z) &= \sum_{t=-\infty}^{\infty} \boldsymbol{y}(t) z^{-t} \end{aligned} \tag{2.16}$$

Raleigh and Cioffi [33] have shown that rewriting $\boldsymbol{s}$ as an $M_t \times N$ column vector, $\boldsymbol{s}_{rc}$ the input-output equation for a limited data block may be expressed as

$$\boldsymbol{y}_{rc} = \boldsymbol{H}_{rc}\ \boldsymbol{s}_{rc} \tag{2.17}$$

where $\boldsymbol{H}_{rc}$ is an $M_r\,(N+L-1) \times M_t\,(N)$ matrix composed of $M_r \times M_t$ single-input single-output (SISO) subblocks.

$$\boldsymbol{H}_{rc} = \begin{bmatrix} \boldsymbol{H}_{rc\ 1,1} & \dots & \boldsymbol{H}_{rc\ 1,M_t} \\ \vdots & \ddots & \vdots \\ \boldsymbol{H}_{rc\ M_r,1} & \dots & \boldsymbol{H}_{rc\ M_r,M_t} \end{bmatrix} \tag{2.18}$$

with each subblock representing the channel convolution matrix for a single transmit-receive pair and possessing the well-known Toeplitz form. The structure of the subblock for the i^{th} transmit and j^{th} receive antenna is shown in (2.19). The SVD can then be applied to $\boldsymbol{H}_{rc}$. Raleigh and Cioffi term this approach Space-Time Vector Coding (STVC). The caveat of STVC is the associated computational complexity. The SVD of an $M_r\,(N+L-1) \times M_t\,(N)$ matrix must be computed which is unfeasible for even modest block lengths.

$$\boldsymbol{H}_{rc\ j,i} = \begin{bmatrix} h_{ji}(0) & 0 & \dots & \dots & \dots & \dots & \dots & 0 \\ h_{ji}(1) & h_{ji}(0) & 0 & \dots & \dots & \dots & \dots & 0 \\ \vdots & \ddots & \ddots & \ddots & \ddots & \ddots & \ddots & \vdots \\ 0 & h_{ji}(L-1) & \dots & h_{ji}(1) & h_{ji}(0) & 0 & \dots & 0 \\ \vdots & \ddots & \ddots & \ddots & \ddots & \ddots & \ddots & \vdots \\ 0 & \dots & 0 & h_{ji}(L-1) & \dots & h_{ji}(1) & h_{ji}(0) & 0 \end{bmatrix} \tag{2.19}$$

Although STVC structure is suggested as a theoretical means for achieving capacity [33], a reduced-complexity discrete matrix multitone (DMMT) technique is implemented by the authors to exploit the frequency selective MIMO channel. It is based on discrete multitone (DMT) [34] which is a technique that uses the discrete Fourier transform (DFT) to implement frequency-division multiplexing (FDM)

in SISO communications channels, this digital approach pioneered in the 70's is significantly less expensive and complex than its analogue counterpart. DMMT is essentially analogous to the OFDM approach presented below so it is not discussed in further detail.

2.3.2 Orthogonal Frequency Division Multiplexing

A typical solution to the frequency selective channel problem is to reduce it to a narrowband form by using a DFT to decompose the otherwise frequency selective channel of bandwidth B into N orthogonal frequency flat MIMO channels, each with bandwidth B/N [3]. Consider first a SISO frequency selective channel, $\underline{\boldsymbol{h}}(z)$, with polynomial length L. The transmitter first performs an inverse fast Fourier transform (IFFT) operation on the source signal of length T, $\boldsymbol{s}(t) \in \mathbb{C}^{1\times 1}$, for $t \in \{0, 1, \ldots, T-1\}$ to be transmitted. A cyclic prefix (CP) of length $(L-1)$ is then added prior to transmission. At the receiver the cyclic prefix is stripped off and an FFT is applied to the received signal, as shown in Figure 2.7.

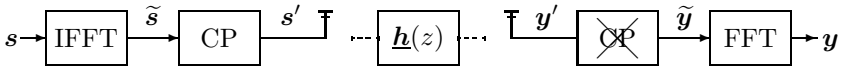

Figure 2.7: SISO OFDM communications structure.

The purpose of the cyclic prefix is that it renders the matrix for the block input-output description, $\boldsymbol{H}_c$ as circulant. Therefore the sequence $\widetilde{\boldsymbol{y}}$ may be expressed as

$$\widetilde{\boldsymbol{y}} = \boldsymbol{H}_c \, \widetilde{\boldsymbol{s}} \tag{2.20}$$

where

$$\boldsymbol{H}_c = \begin{bmatrix} h(0) & 0 & \ldots & 0 & 0 & h(L-1) & \ldots & h(1) \\ h(1) & h(0) & 0 & \ldots & 0 & 0 & \ddots & \vdots \\ \vdots & h(1) & h(0) & 0 & 0 & \ddots & 0 & h(L-1) \\ h(L-1) & \vdots & h(1) & \ddots & 0 & \ddots & 0 & 0 \\ 0 & h(L-1) & \vdots & \ddots & h(0) & \ddots & \ddots & 0 \\ \ddots & 0 & h(L-1) & \ddots & h(1) & h(0) & 0 & 0 \\ \ddots & \ddots & 0 & \ddots & \vdots & \ddots & \ddots & 0 \\ 0 & 0 & \ldots & 0 & h(L-1) & \ldots & h(1) & h(0) \end{bmatrix} \tag{2.21}$$

The eigenvalues of a circulant matrix comprise the DFT of the first row of the circulant matrix,

and conversely the first row of a circulant matrix is the inverse DFT of the eigenvalues [35]. Hence the eigendecomposition of $\boldsymbol{H}_c$ may be expressed as

$$\boldsymbol{H}_c = \boldsymbol{D}^H \, \boldsymbol{\Sigma} \, \boldsymbol{D} \tag{2.22}$$

Where $\boldsymbol{D}$ denotes the discrete Fourier transform matrix of order n defined by [29]

$$\boldsymbol{D}_n = \frac{1}{\sqrt{N}}(d_{jk}), \quad d_{jk} = \omega_n^{jk} \tag{2.23}$$

where

$$\omega_n = \exp(-2\pi\sqrt{-1}/n) = \cos(2\pi/n) - \sqrt{-1} \cdot \sin(2\pi/n) \tag{2.24}$$

and $\boldsymbol{\Sigma} = diag\,\{\sigma(0), \sigma(1), \ldots, \sigma(N-1)\}$, with

$$\sigma(k) = \sum_{i=0}^{L-1} h(l) \exp^{-\frac{j2\pi ki}{N}}, \; k = 0, 1, 2, \ldots, N-1 \tag{2.25}$$

$\sigma(k)$ for $k = 0, 1, \ldots, N-1$ is the sampled frequency response of the channel, where k represents the tone index. Using $1/\sqrt{N}$ as the normalization factor in (2.23) conveniently ensures that the resulting DFT matrix, $\boldsymbol{D}$ is unitary. As the IFFT of the transmitted signal, $\widetilde{\boldsymbol{s}} = \boldsymbol{D}^H \boldsymbol{s}$ and the FFT of the received signal, $\boldsymbol{y} = \boldsymbol{D}\widetilde{\boldsymbol{y}}$, and exploiting the unitary property of the normalized DFT matrix ($\boldsymbol{D}\boldsymbol{D}^H = \boldsymbol{I}$), the received signal becomes

$$\begin{aligned} \boldsymbol{y} &= \boldsymbol{D} \, \boldsymbol{D}^H \, \boldsymbol{\Sigma} \, \boldsymbol{D}\boldsymbol{D}^H \boldsymbol{s} \\ \boldsymbol{y} &= \boldsymbol{\Sigma} \, \boldsymbol{s} \end{aligned} \tag{2.26}$$

The frequency selective SISO channel has therefore been decoupled into N parallel flat fading channels. OFDM is readily extended to MIMO frequency selective channels. For the MIMO scenario the IFFT and CP operation is carried out individually on the data stream to be transmitted on each antenna, prior to propagation. At the receiver the removal of the CP and FFT is carried out on each individual received stream as shown in Figure 2.8. Where $\boldsymbol{s}_i$ denotes the i^{th} transmitted stream of length N symbols for $i = 1, 2, \ldots, M_t$ and $\boldsymbol{y}_j$ denotes the j^{th} received stream of length N symbols for $j = 1, 2, \ldots, M_r$.

The matrix $\boldsymbol{H}\,[k]$ is the frequency response of the narrowband MIMO channel corresponding to

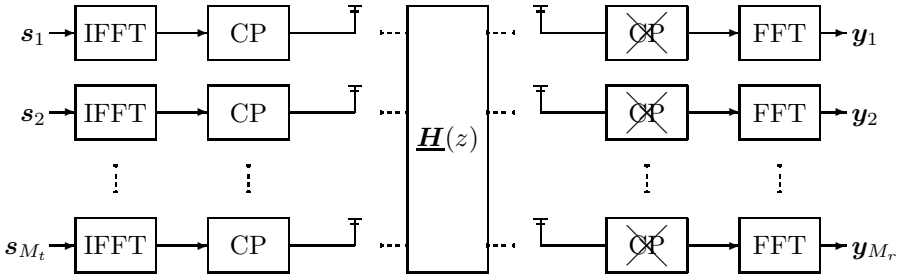

Figure 2.8: MIMO OFDM communications structure.

the k^{th} tone and is related to the MIMO channel matrix $\underline{\boldsymbol{H}}(z)$ by

$$\boldsymbol{H}[k] = \sum_{i=0}^{L-1} \boldsymbol{H}_i \exp^{-\frac{j2\pi ki}{N}} \tag{2.27}$$

The standard scalar SVD and QRD may then be applied within each narrowband tone to provide multiple spatial subchannels. Typically for efficient implementation of the FFT, N is chosen to be a power of 2 [36]. It is important to note that MIMO-OFDM is a block based communications system, with each transmitter or receiver operating on data N blocks in length. It therefore requires significant storage for DFT's and is unsuitable for decoding continuous streams of data.

2.3.3 Transceiver Optimization

Vucic and Boche have proposed a novel technique for transceiver optimization for frequency selective MIMO channels [37]. The transmitter and receiver are equipped with linear, causal FIR filters $\underline{\boldsymbol{G}}(z)$ and $\underline{\boldsymbol{F}}(z)$, respectively as shown in Figure 2.9. The system operates under the assumption that the receiver has perfect channel state information (CSI) and that the transmitter has imperfect CSI.

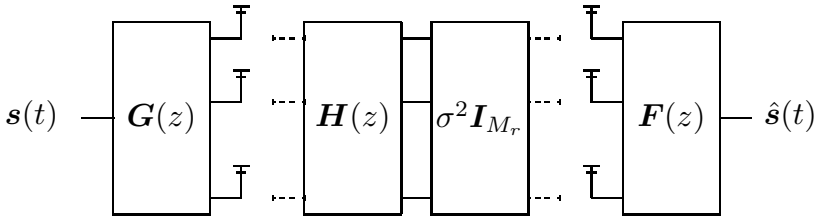

Figure 2.9: Transceiver optimization communications structure.

The mean square error (MSE) between the transmitted signal, $\boldsymbol{s}(n)$ and estimate of the received signal, $\hat{\boldsymbol{s}}(n)$, (2.28) is used as a performance measure. Using a minimax approach to transceiver optimization, the authors have developed an iterative framework capable of providing a robust solution

for a broad range of MIMO scenarios. Critically however, due to the intricacy of the problems, convergence to the global optimum is not guaranteed [37].

$$E\left\{\|\boldsymbol{s}(n)-\hat{\boldsymbol{s}}(n)\|_2^2\right\} \tag{2.28}$$

Due to the uniqueness of this approach and the associated computational complexity, this work has not been considered as it is an optimization problem and therefore distinctly different to the matrix decomposition approach presented in this thesis. For this same reason, similar methods such as the redundant FIR precoder approach proposed by Mertins [38] have also not been considered. As with Vucic and Boche, Mertins does not discuss the associated computational complexity of his approach or the performance of his system in terms of BER and therefore does not provide sufficient motivation for a direct comparison between transceiver optimization and matrix decomposition approaches.

2.3.4 Polynomial Matrix Decomposition Techniques

A handful of numerical procedures currently exist for calculating polynomial matrix decomposition or factorization. Perhaps the most well known is Smith-McMillan decomposition [28], however there is little work on polynomial matrix techniques equivalent to the EVD, SVD and QRD for scalar matrices. Vaidyanathan [28] has shown that any finite degree polynomial matrix can be factorized into a series of paraunitary matrices consisting of rotation and delay matrices. Regalia and Huang [39] have further extended this work to compute the EVD of a 2×2 paraunitary polynomial matrix. Finally Lambert [40, 41] has developed a distinct technique for calculating the EVD of polynomial matrices using the DFT.

Smith Form of a Polynomial Matrix

For a generic $p \times q$ polynomial matrix, $\underline{\boldsymbol{P}}(z)$, simpler forms such as triangular and diagonal can be obtained by performing elementary operations on the matrix [42]. There exist three types of elementary row operations that may be carried out on $\underline{\boldsymbol{P}}(z)$:

- Interchange two rows.
- Multiply a row by a non-zero constant.
- Add a polynomial multiple of a row to another row.

They are performed by pre-multiplying $\underline{\boldsymbol{P}}(z)$ with an appropriate square matrix, termed an elementary matrix. Additionally there exist three types of elementary column operations, defined identically. Elementary matrices are unimodular, in that the i^{th} matrix tap, $\boldsymbol{P}_i z^{-i}$ is a square polynomial matrix

with determinant ± 1. The product of any two unimodular matrices is also unimodular and the inverse of a unimodular matrix is unimodular. Repeated applications of various row operations amount to pre-multiplication of $\underline{\boldsymbol{P}}(z)$ with a $p \times p$ unimodular matrix. Similarly, repeated applications of various column operations amount to post-multiplication of $\underline{\boldsymbol{P}}(z)$ by a $q \times q$ unimodular matrix [28].

Smith-McMillan Form

The Smith-McMillan form of the frequency selective MIMO channel matrix, $\underline{\boldsymbol{H}}(z)$ is defined as

$$\underline{\boldsymbol{H}}(z) = \underline{\boldsymbol{W}}(z)\ \underline{\boldsymbol{\Lambda}}(z)\ \underline{\boldsymbol{V}}(z) \tag{2.29}$$

where $\underline{\boldsymbol{W}}(z)$ and $\underline{\boldsymbol{V}}(z)$ are $M_r \times M_r$ and $M_t \times M_t$ unimodular matrix polynomials in z respectively and $\underline{\boldsymbol{\Lambda}}(z)$ is an $M_r \times M_t$ diagonal matrix.

So far it appears that the problem of polynomial matrix diagonalization is already solved. Smith-McMillan decomposition can be used to design polynomial filter banks at the transmitter and receiver to create multiple spatial sub-channels and waterpouring can then be applied to maximize channel capacity. Critically however the transmit and receive filter banks do not posses the para-unitary property obtained through polynomial matrix singular value decomposition. i.e. $\underline{\boldsymbol{V}}(z)\ \widetilde{\underline{\boldsymbol{V}}}(z) \neq \boldsymbol{I}_{M_t}$ and $\underline{\boldsymbol{W}}(z)\ \widetilde{\underline{\boldsymbol{W}}}(z) \neq \boldsymbol{I}_{M_r}$. Therefore when using $\underline{\boldsymbol{W}}(z)$ as a receive filter bank the noise power is no longer preserved and consequently the gain of the spatial sub-channels no longer accurately reflect a gain in SNR. Additionally the statistical properties of the noise will no longer be preserved which may present further problems for equalization and decoding schemes. For example the Viterbi algorithm assumes that the received sequence is corrupted by an additive white Gaussian noise process [31].

Therefore Smith decomposition has not been considered in this thesis, as it does not constitute an extension of the scalar matrix decomposition techniques to polynomial matrices and is an independent problem in its own right.

FIR Lossless Decomposition

If $\underline{\boldsymbol{H}}(z)$ denotes the MIMO channel matrix of a causal system, then it is said to be lossless if the FIR filter representing the multipath between each transmit-receive pair is stable. Additionally the channel matrix must possess the paraunitary property, i.e. $\widetilde{\underline{\boldsymbol{H}}}(z)\ \underline{\boldsymbol{H}}(z) = \underline{\boldsymbol{H}}(z)\ \widetilde{\underline{\boldsymbol{H}}}(z) = \boldsymbol{I}$. Vaidyanathan [28] has shown that any lossless polynomial matrix can be factorised into a series of paraunitary matrices comprised of rotation and delay matrices. At each step in the process, a rotation and delay matrix are factored out of the lossless polynomial matrix, $\underline{\boldsymbol{H}}_N(z)$, resulting in a lossless polynomial matrix where the degree of the system, N has been reduced by unity [43].

The following example details the factorization for a 2×2 lossless system and Vaidyanathan has subsequently generalized this work to paraunitary polynomial matrices of any dimension, provided it is of fixed degree. For a 2×2 lossless system, the polynomial channel matrix may be written as

$$\underline{\boldsymbol{H}}_N(z) = \sum_{n=0}^{L} \boldsymbol{H}(n) z^{-n}, \ \boldsymbol{H}(L) \neq 0 \tag{2.30}$$

Where N denotes the degree of the determinant of $\underline{\boldsymbol{H}}(z)$. The determinant of $\underline{\boldsymbol{H}}_N(z)$ is equal to a single delay, i.e. of the form $|\underline{\boldsymbol{H}}_N(z)| = \chi z^{-N}$ where $\chi \neq 0$. For the trivial scalar matrix case, $L = 0$ then $\boldsymbol{h}(0)$ is a real unitary matrix and can always be represented as

$$\boldsymbol{h}(0) = \alpha \begin{bmatrix} \cos(\theta_0) & -\sin(\theta_0) \\ \sin(\theta_0) & \cos(\theta_0) \end{bmatrix} \begin{bmatrix} 1 & 0 \\ 0 & \pm 1 \end{bmatrix} \tag{2.31}$$

where $\alpha = \sqrt{|\chi|}$. Assuming $L > 0$, then the first step of factorization is to formulate a Givens rotation [29] matrix, $\boldsymbol{Q}_N$ and a delay matrix, $\underline{\boldsymbol{\Lambda}}(z)$ such that when they are applied to another polynomial matrix, $\underline{\boldsymbol{H}}_{N-1}(z)$ results in

$$\underline{\boldsymbol{H}}_N(z) = \underbrace{\begin{bmatrix} \cos(\theta_N) & -\sin(\theta_N) \\ \sin(\theta_N) & \cos(\theta_N) \end{bmatrix}}_{\boldsymbol{Q}_N} \underbrace{\begin{bmatrix} 1 & 0 \\ 0 & z^{-1} \end{bmatrix}}_{\underline{\boldsymbol{\Lambda}}(z)} \underline{\boldsymbol{H}}_{N-1}(z) \tag{2.32}$$

where $\underline{\boldsymbol{H}}_{N-1}(z)$ is also a lossless polynomial matrix. Therefore $\underline{\boldsymbol{H}}_N(z)$ is expressed in terms of another 2×2 lossless polynomial matrix, $\underline{\boldsymbol{H}}_{N-1}(z)$, whose degree of the determinant has been reduced by unity, and therefore the degree of the overall system has been reduced. Essentially a lossless degree-one building block has been extracted to obtain a reduced remainder, $\underline{\boldsymbol{H}}_{N-1}(z)$. This process can then be repeated, with $\underline{\boldsymbol{H}}_{N-1}(z)$ expressed in terms of $\underline{\boldsymbol{H}}_{N-2}(z)$ and so forth until the matrix $\underline{\boldsymbol{H}}_0(z)$ is obtained, with determinant $|\underline{\boldsymbol{H}}_0(z)| = \chi$. Therefore $\underline{\boldsymbol{H}}_N(z)$ can be expressed as

$$\underline{\boldsymbol{H}}_N(z) = \boldsymbol{Q}_N \ \underline{\boldsymbol{\Lambda}}(z) \ \boldsymbol{Q}_{N-1} \ \underline{\boldsymbol{\Lambda}}(z) \ \ldots \boldsymbol{Q}_1 \ \underline{\boldsymbol{\Lambda}}(z) \ \alpha \ \boldsymbol{Q}_0 \begin{bmatrix} 1 & 0 \\ 0 & \pm 1 \end{bmatrix} \tag{2.33}$$

The ability to factorize any paraunitary polynomial matrix in this manner provided the original motivation for McWhirter to develop his EVD algorithm for para-Hermitian polynomial matrices [21]. The caveat of Vaidyanathan's approach (and a problem not present with the SBR2 algorithm and its derivatives) is that FIR lossless decomposition only ever implements a unit delay in one step. Consider

a paraunitary polynomial matrix of degree 100, but containing only two non-zero coefficient matrices ($\underline{\boldsymbol{H}}_0$ and $\underline{\boldsymbol{H}}_{100}$). This decomposition would require 100 stages and is computationally inefficient.

Two-channel FIR Lossless Decomposition

Regalia and Huang [39] have considered the problem of adaptively optimizing a two-channel lossless FIR filter bank using eigenstructure algorithms. Using the fixed degree parametrization proposed by Vaidyanathan [28] they re-formulate the problem as a state-space approach and propose an iterative solution that avoids the problems of local minima associated with gradient descent techniques while also reducing the computational complexity by an order of magnitude when compared to gradient descent techniques. However their solution is only applicable to the 2×2 case and also suffers from the unit delay step component of FIR lossless decomposition.

Lambert's Approach to Multichannel Blind Deconvolution

The problem of broadband blind signal separation in the context of convolutive mixing has been addressed by Lambert [41, 40]. By adapting standard eigenvalue routines, factorizations, decompositions and matrix algorithms and using abstract algebra/group theoretic concepts and information theoretic principles, he has developed an EVD for polynomial matrices. Using a DFT to represent the mixing in the frequency domain, Householder reflections are used to obtain the eigenvalues. Lambert's routine focuses on 2×2 polynomial matrices. However it can be readily extended to large matrices, by applying the routine to a series of 2×2 sub-matrices of the matrix to obtain a diagonal matrix [43]. As Lambert's approach involves the approximate inversion of FIR filters in the frequency domain, it is fundamentally different from SBR2 and its derivatives presented in this thesis.

2.4 Channel Estimation

Accurate estimation of the frequency selective MIMO channel is critical to the performance of wireless communications systems. Inaccuracies in the CSI will result in sub-optimum performance and often system failure. To estimate $\underline{\boldsymbol{H}}(z)$ a training sequence known to both transmitter and/or receiver is used [44]. A training sequence of length N_t, $\boldsymbol{s}_t(n) \in \mathbb{C}^{M_t \times 1}$ for $n \in \{0, 1, \ldots, N_t - 1\}$ is propagated through the MIMO wireless channel, $\underline{\boldsymbol{H}}(z)$. The received training sequence, $\boldsymbol{Y}_t$ is expressed as an $(N_t + L - 1) \times M_r$ matrix, i.e.

$$\boldsymbol{Y}_t = \boldsymbol{S}_t \; \boldsymbol{H}_t + \boldsymbol{n} \tag{2.34}$$

where $\boldsymbol{S}_t$ is an $(N_t + L - 1) \times (M_t \; L)$ matrix comprised of $(N_t + L - 1) \times L$ subblocks, with each sub-

block representing the convolution matrix of the training sequence transmitted from a given transmit antenna and possessing the well-known Toeplitz form and $\boldsymbol{H}_t$ is an $(M_t\ L) \times M_r$ matrix containing the channel coefficients in column vector form, i.e.

$$\boldsymbol{H}_t = \begin{bmatrix} h_{11}(0) & \dots & h_{M_t 1}(0) \\ h_{11}(1) & \dots & h_{M_t 1}(1) \\ \vdots & & \vdots \\ h_{11}(L-1) & & h_{M_t 1}(L-1) \\ \vdots & & \vdots \\ h_{1M_r}(0) & \dots & h_{M_t M_r(0)} \\ h_{1M_r}(1) & \dots & h_{M_t M_r(1)} \\ \vdots & & \vdots \\ h_{1M_r}(L-1) & \dots & h_{M_t M_r(L-1)} \end{bmatrix} \tag{2.35}$$

2.4.1 Zero-Forcing Channel Estimation

A simple zero-forcing solution can be implemented by calculating the pseudo-inverse of $\boldsymbol{S}_t$. Pseudo-inversion is so called as it allows for the calculation of the inverse of non-square matrices. Defining the scalar matrix $\boldsymbol{A} \in \mathbb{R}^{m \times n}$, the pseudo-inverse of $\boldsymbol{A}$, denoted $\boldsymbol{X}$ of dimensions $n \times m$ is defined to be the unique matrix that satisfies the four *Moore-Penrose* conditions [29]:

$$\begin{aligned} \boldsymbol{A}\ \boldsymbol{X}\ \boldsymbol{A} &= \boldsymbol{A} \\ \boldsymbol{X}\ \boldsymbol{A}\ \boldsymbol{X} &= \boldsymbol{X} \\ (\boldsymbol{A}\ \boldsymbol{X})^T &= \boldsymbol{A}\ \boldsymbol{X} \\ (\boldsymbol{X}\ \boldsymbol{A})^T &= \boldsymbol{X}\ \boldsymbol{A} \end{aligned} \tag{2.36}$$

The estimate of the channel, $\hat{\boldsymbol{H}}_t$ can now simply be calculated by

$$\hat{\boldsymbol{H}}_t = pinv(\boldsymbol{S}_t)\ \boldsymbol{Y}_t \tag{2.37}$$

where $pinv(\boldsymbol{S}_t)$ denotes the pseudoinverse of the matrix $\boldsymbol{S}_t$. In practice this zero forcing approach is rarely implemented, and instead the least squared error (LSE) discussed below is used, due to its

increased performance at low signal to noise ratios. As the LSE solution minimizes the summation of the squared error in the presence of channel noise it becomes the zero-forcing solution when no noise is present.

2.4.2 Least Squares Error Channel Estimation

Defining the error between the received signal, $\boldsymbol{Y}_t$ and the transmitted signal, $\boldsymbol{S}_t$ as

$$\boldsymbol{E} = (\boldsymbol{Y}_t - \boldsymbol{S}_t\hat{\boldsymbol{H}}_t) \tag{2.38}$$

where $\hat{\boldsymbol{H}}_t$ denotes the estimate of the channel matrix, $\boldsymbol{H}_t$. The LSE approach seeks to minimize the summation of the square error, i.e.

$$\begin{aligned} J &= trace(\boldsymbol{E}^H\boldsymbol{E}) \\ &= (\boldsymbol{Y}_t - \boldsymbol{S}_t\hat{\boldsymbol{H}}_t)^H(\boldsymbol{Y}_t - \boldsymbol{S}_t\hat{\boldsymbol{H}}_t) \\ &= \boldsymbol{Y}_t^H\boldsymbol{Y}_t - \boldsymbol{Y}_t^H\boldsymbol{S}_t\hat{\boldsymbol{H}}_t - \hat{\boldsymbol{H}}_t^H\boldsymbol{S}_t^H\boldsymbol{Y}_t + \hat{\boldsymbol{H}}_t^H\boldsymbol{S}_t^H\boldsymbol{S}_t\hat{\boldsymbol{H}}_t \end{aligned} \tag{2.39}$$

where $trace(\boldsymbol{E}^H\boldsymbol{E})$ denotes the sum of the elements on the main diagaonal of $\boldsymbol{E}^H\boldsymbol{E}$. Differentiating with respect to $\hat{\boldsymbol{H}}_t^H$ results in

$$\frac{\delta J}{\delta \hat{\boldsymbol{H}}_t} = \boldsymbol{S}_t^H\boldsymbol{Y}_t + \boldsymbol{S}_t^H\boldsymbol{S}_t\hat{\boldsymbol{H}}_t = 0 \tag{2.40}$$

Re-arranging in terms of $\hat{\boldsymbol{H}}_t$ simply results in

$$\hat{\boldsymbol{H}}_t = (\boldsymbol{S}_t^H\boldsymbol{S}_t)^{-1}\ \boldsymbol{S}_t^H\boldsymbol{Y}_t \tag{2.41}$$

It should be noted, that typically if the rank of the matrix $\boldsymbol{S}_t$ is $M_t(L)$, then typically $pinv(\boldsymbol{S}_t) = (\boldsymbol{S}_t^H\boldsymbol{S}_t)^{-1}\boldsymbol{S}_t^H$. For this scenario the zero forcing solution (2.37) is identical to the LSE equation, (2.41).

2.4.3 Implementation

In practice it is desirable that the training sequence, $\boldsymbol{S}_t$ is uncorrelated, so that $E\left\{\boldsymbol{S}_t^H\ \boldsymbol{S}_t\right\} \approx M_t(L)\times\boldsymbol{I}_{M_t(L)}$. This ensures that the channel for each transmit-receive pair is estimated independently and prevents $(\boldsymbol{S}_t^H\boldsymbol{S}_t)^{-1}$ becoming singular. Increasing the length of N_t increases the accuracy of the decomposition, at the cost of spectral efficiency. The relative error for the estimate of the channel,

$\underline{\boldsymbol{H}}(z)$ is defined as

$$E_{rel} = \frac{\left\| \underline{\boldsymbol{H}}(z) - \underline{\hat{\boldsymbol{H}}}(z) \right\|_F}{\| \underline{\boldsymbol{H}}(z) \|_F} \tag{2.42}$$

where $\underline{\hat{\boldsymbol{H}}}(z)$ denotes the polynomial estimate of the MIMO frequency selective channel. Figure 2.10 shows the average relative error in LSE channel estimation for a range of training sequences.

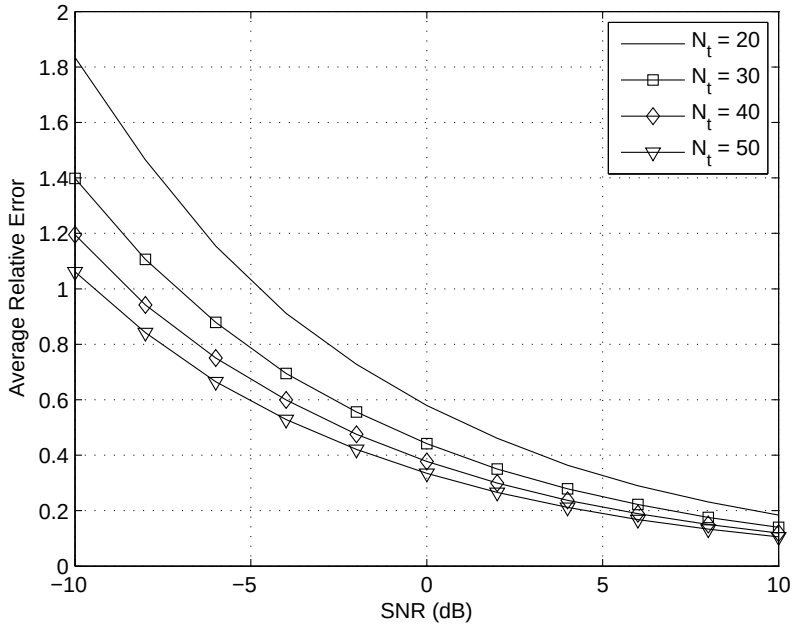

Figure 2.10: Average relative error in channel estimation for a 3×3 MIMO channel with polynomial length $L = 5$ and training sequences of lengths N_t averaged over 1000 Monte Carlo simulations.

Even with a relatively low SNR it is possible to obtain a reasonably accurate estimation of the channel, for example a relative error of 0.27 at an SNR of 2dB for a training sequence of length $N_t = 50$. This can be considered as accurate as performing a polynomial matrix decomposition on a known channel matrix and recalculating the channel matrix from the polynomial matrices produced by the decomposition results in a relative error between the reconstituted matrix and the known channel matrix of a similar magnitude. Hence at SNR's of greater than 2dB relative errors introduced by polynomial matrix decomposition dominate the effects of those produced by inaccurate channel state information. This is discussed in greater depth in the next chapter.

Recently there has been a great deal of research for MMSE channel estimation in MIMO-OFDM systems, namely due to MIMO-OFDM based 4G broadband wireless technology [45]. In particular the exploitation of spatial and frequency correlations within the MIMO channel[46, 47]. Blind-channel estimation, whereby channel state information (CSI) is obtained by using the statistical properties

of transmitted signals [48], and thus avoids sending any pilot symbols or training sequences is also a topic of current research interest, as it maximizes spectral efficiency. However only the simple LSE channel estimator demonstrated here has been implemented throughout this thesis, as it is only needed to quantify the effects of channel estimation error on the performance of MIMO systems based on PMSVD and PMQRD.

2.5 Conclusion

In this chapter the benefits of singular value and QR decomposition for MIMO flat fading channels have been clearly demonstrated. In particular how spatial diversity can be exploited to increase overall system capacity. The frequency selective MIMO problem has been introduced, in the form of convolutive mixing and an overview of existing solutions to the broadband problem has been presented. The treatment of MIMO-OFDM is of special importance, as this will become the performance yardstick for which the techniques proposed in this thesis are measured against in subsequent chapters.

Existing techniques and numerical procedures for operating on polynomial matrices have been reviewed. It is important to note that there are no existing techniques for achieving the polynomial matrix singular value and QR decompositions presented in this thesis. Finally the estimation of channel state information has been covered, which will become integral to accurate simulation of the performance of a real-world frequency selective MIMO system.

The scene therefore is now set, and the focus of this thesis will now be on the application and analysis of polynomial matrix decomposition to frequency selective channels to obtain performance benefits identical to those observed in frequency flat MIMO channels, while providing an entirely time domain based solution.

Chapter 3

Polynomial Matrix Decomposition Techniques

3.1 Introduction

In the previous chapter the significant performance benefits of performing singular value and QR decomposition for instantaneous mixing MIMO channels were shown. In this chapter the operation of the algorithms that allow for the singular value and QR decomposition of polynomial matrices are introduced, allowing for the generalization of the previous work to frequency selective MIMO channels.

The chapter begins by showing how the Eigenvalue decomposition (EVD) of a real symmetric scalar matrix can be formulated using Jacobi rotation matrices [29]. This work is then extended to the polynomial matrix eigenvalue decomposition (PMEVD) of a para-Hermitian polynomial matrix, which is performed using the sequential best rotation (SBR2) method [21]. SBR2 was initially developed for the blind separation of signals that have been mixed in a convolutive manner [49]. For this scenario SBR2 forms the first stage in a multi-stage blind source separation (BSS) algorithm and is used to decorrelate the convolutively mixed signals. A second stage uses 4^{th} order statistics and allows the calculation of a hidden rotation matrix [49], allowing for further separation of the source signals. SBR2's operation and efficient implementation is discussed prior to the work being extended to show how multiple applications of the SBR2 algorithm can be used to calculate the polynomial matrix singular value decomposition (PMSVD) of a generic complex polynomial matrix.

The underlying Jacobi rotation approach of the SBR2 algorithm is then applied within a polynomial matrix QR decomposition (PMQRD) algorithm to calculate the PMQRD of a generic complex polynomial matrix. Finally it is shown how PMSVD can be performed entirely with the PMQRD algorithm, and how the SBR2 approach is no longer necessary for future implementations.

3.2 SBR2 Operation for PMEVD

The EVD of a complex symmetric scalar matrix $\boldsymbol{R}$ is given in (3.1) where $\boldsymbol{V}$ is a unitary matrix,

such that $\boldsymbol{V}\boldsymbol{V}^H = \boldsymbol{V}^H\boldsymbol{V} = \boldsymbol{I}_p$ and $\boldsymbol{D}$ is a diagonal matrix consisting of eigenvalues.

$$\boldsymbol{V}\ \boldsymbol{R}\ \boldsymbol{V}^H = \boldsymbol{D} \tag{3.1}$$

This diagonalization of $\boldsymbol{R}$ is achieved using Jacobi rotation matrices [29]. Initially, the largest in magnitude off-diagonal element of $\boldsymbol{R}$ is located, assumed to be the p, q^{th} element, i.e. $r_{pq} = [\boldsymbol{R}]_{pq}$. This search can either be restricted to the upper triangular or lower triangular part of $\boldsymbol{R}$ due to its Hermitian property. The rotation angle θ which is used to annihilate the off-diagonal element r_{pq} of matrix $\boldsymbol{R}$ is chosen such that:

$$\cot 2\theta = \frac{r_{qq} - r_{pp}}{2r_{pq}} \tag{3.2}$$

The corresponding Jacobi rotation matrix, $\boldsymbol{Q}_{pq}$ is then given by

$$\boldsymbol{Q}_{pq} \equiv \begin{bmatrix} 1 & \dots & 0 & \dots & 0 & \dots & 0 \\ \vdots & \ddots & \vdots & & \vdots & & \vdots \\ 0 & \dots & c_{pp} & \dots & s_{pq} & \dots & 0 \\ \vdots & & \vdots & \ddots & \vdots & & \vdots \\ 0 & \dots & -s_{qp} & \dots & c_{qq} & \dots & 0 \\ \vdots & & \vdots & & \vdots & \ddots & \vdots \\ 0 & \dots & 0 & \dots & 0 & \dots & 1 \end{bmatrix} \tag{3.3}$$

where $c = \cos(\theta)$ and $s = \sin(\theta)$, and their subscripts denote the element location in the matrix. This matrix is orthogonal by construction. To diagonalize matrix $\boldsymbol{R}$ using Jacobi rotation matrices a sequence of such orthogonal (similarity) transformations are applied of the form:

$$\boldsymbol{R}' = \boldsymbol{Q}_{pq}^T\ \boldsymbol{R}\ \boldsymbol{Q}_{pq} \tag{3.4}$$

Each application of rotation matrices $\boldsymbol{Q}_{pq}$ and $\boldsymbol{Q}_{pq}^T$ will zero two elements of $\boldsymbol{R}$ and the sequence of such matrices is chosen so as to eliminate the dominant off-diagonal elements at each step. Successive transformations will partially undo previously zeroed elements, but off diagonal terms will eventually tend to zero, resulting in a diagonal matrix $\boldsymbol{D}$, to within some target precision whose elements correspond to the eigenvalues of $\boldsymbol{R}$:

$$\boldsymbol{D} = \boldsymbol{Q}_{\beta}^T \dots \boldsymbol{Q}_1^T\ \boldsymbol{R}\ \boldsymbol{Q}_1 \dots \boldsymbol{Q}_{\beta} \tag{3.5}$$

where β is an unspecified number of iterations. Therefore by performing a sequence of orthogonal similarity updates, $\boldsymbol{R}$ is diagonalized.

3.2.1 SBR2 Algorithm

Similar to the scalar EVD, the input to the SBR2 algorithm [21] is a para-Hermitian polynomial matrix, which may be expressed as

$$\underline{\boldsymbol{R}}(z) = \sum_{\tau=-\tau_{max}}^{\tau_{max}} z^{-\tau} \boldsymbol{R}(\tau) \tag{3.6}$$

where $\boldsymbol{R}(\tau) \in \mathbb{C}^{p\times p}$ and τ represents the polynomial index.

$$\begin{aligned} [\boldsymbol{R}(\tau)]_{kl} &= r_{kl}(\tau) = r^*_{lk}(-\tau) \\ &= [\boldsymbol{R}(-\tau)]^*_{lk}\,,\ k,l \in \{1,2,\ldots,p\} \end{aligned} \tag{3.7}$$

The SBR2 algorithm will calculate the PMEVD of $\underline{\boldsymbol{R}}(z)$ as in (3.8) where $\underline{\boldsymbol{D}}(z)$ is a diagonal polynomial matrix and $\underline{\boldsymbol{P}}(z)$ is a paraunitary polynomial matrix and $\widetilde{\underline{\boldsymbol{P}}}(z)$ is its paraconjugate.

$$\underline{\boldsymbol{P}}(z)\ \underline{\boldsymbol{R}}(z)\ \widetilde{\underline{\boldsymbol{P}}}(z) = \underline{\boldsymbol{D}}(z) \tag{3.8}$$

3.2.2 Extension to Polynomial Matrices

SBR2 expands the Jacobi rotation matrix approach to para-Hermitian polynomial matrices. Initially the dominant off-diagonal coefficient of the input polynomial matrix $\underline{\boldsymbol{R}}(z)$ is located, i.e. the off-diagonal coefficient whose magnitude is greatest. Once again this search can be restricted to either the upper triangular or lower triangular part of $\underline{\boldsymbol{R}}(z)$ due to its para-Hermitian property. $\underline{\boldsymbol{B}}(z)$, a delay matrix is constructed to shift the dominant off-diagonal coefficient to the zero delay lag, z^{-0}. A Jacobi rotation matrix $\boldsymbol{Q}$ is then designed to drive the dominant coefficient to zero resulting in a new polynomial matrix, $\underline{\boldsymbol{R}}'(z)$.

If we denote $\underline{\boldsymbol{G}}(z)$ the product of the rotation matrix $\boldsymbol{Q}$ and the delay matrix $\underline{\boldsymbol{B}}(z)$ then $\underline{\boldsymbol{R}}'(z)$ is given explicitly by:

$$\underline{\boldsymbol{R}}'(z) = \underline{\boldsymbol{G}}(z)\ \underline{\boldsymbol{R}}(z)\ \widetilde{\underline{\boldsymbol{G}}}(z) \tag{3.9}$$

The delay matrix $\underline{\boldsymbol{B}}(z)$ is defined as a $p \times p$ polynomial identity matrix with the exception of the

k^{th} diagonal element, which is z^{-t}, i.e.

$$\underline{\boldsymbol{B}}^{(k,t)}(z) = \begin{bmatrix} \boldsymbol{I}_{k-1} & 0 & 0 \\ 0 & z^{-t} & 0 \\ 0 & 0 & \boldsymbol{I}_{p-k} \end{bmatrix} \tag{3.10}$$

This process can be repeated iteratively until the magnitude of the maximum off-diagonal coefficient is approximately zero, to within some target precision. This is determined by the ratio, denoted ϵ of the maximum off-diagonal element to the sum of the Frobenius norms of the coefficients of the diagonalized matrix, i.e. $\|diag\left(\underline{\boldsymbol{D}}(z)\right)\|_F$, see [21], in which a proof of convergence of the algorithm is given.

The paraunitary matrix, $\widetilde{\underline{\boldsymbol{P}}}_\beta(z)$ is defined as:

$$\widetilde{\underline{\boldsymbol{P}}}_\beta(z) = \widetilde{\underline{\boldsymbol{G}}}_1(z)\ \widetilde{\underline{\boldsymbol{G}}}_2(z) \ldots \widetilde{\underline{\boldsymbol{G}}}_\beta(z) \tag{3.11}$$

where β represents an unspecified number of iterations. After β iterations (3.9) results in:

$$\underline{\boldsymbol{D}}_\beta(z) = \underline{\boldsymbol{P}}_\beta(z)\ \underline{\boldsymbol{R}}(z)\ \widetilde{\underline{\boldsymbol{P}}}_\beta(z) \tag{3.12}$$

which is clearly the PMEVD of $\underline{\boldsymbol{R}}(z)$.

3.2.3 Preliminary Results

Figures 3.1 and 3.2 show a 5×5 para-Hermitian polynomial matrix of polynomial length 9 and its subsequent diagonalization using the SBR2 algorithm. Each figure depicts the impulse response of the corresponding channel transfer function. From Figure 3.2 it is observed that SBR2 successfully diagonalizes the input para-Hermitian matrix. By recalculating the initial input para-Hermitian matrix $\underline{\boldsymbol{R}}(z)$ from $\underline{\boldsymbol{D}}(z)$ and $\underline{\boldsymbol{P}}(z)$ calculated by SBR2, and comparing it with the original $\underline{\boldsymbol{R}}(z)$, the relative error for the decomposition can be calculated, i.e.

$$E_{rel} = \frac{\left\| \underline{\boldsymbol{R}}(z) - \left(\widetilde{\underline{\boldsymbol{P}}}(z)\ \underline{\boldsymbol{D}}(z)\ \underline{\boldsymbol{P}}(z) \right) \right\|_F}{\|\underline{\boldsymbol{R}}(z)\|_F} \tag{3.13}$$

For the example shown $E_{rel} = 7.987 \times 10^{-3}$, which is reasonably small, confirming the validity of the approach taken of generalizing the Jacobi method for calculating the EVD of scalar matrices to polynomial form. However with each delay step, at each iteration of the algorithm, the order of the

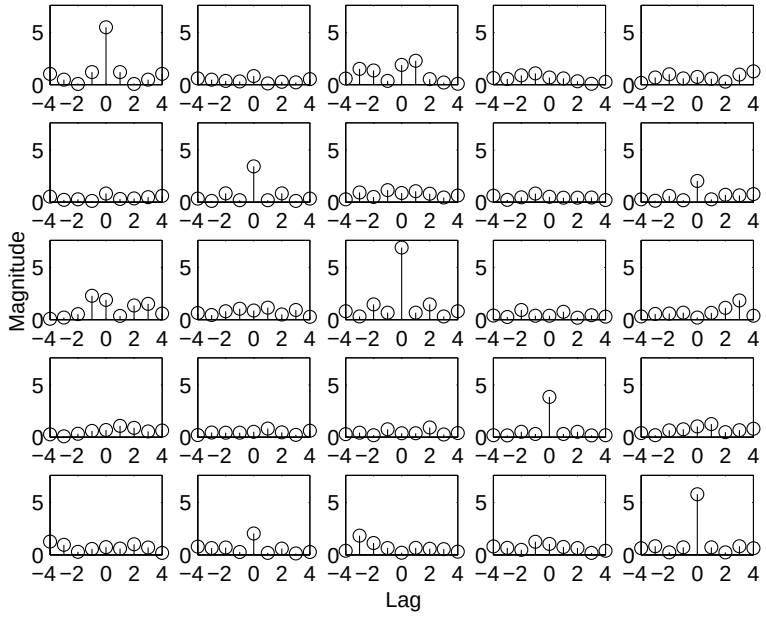

Figure 3.1: Input para-Hermitian matrix, $\underline{\boldsymbol{R}}(z)$ of polynomial length 9.

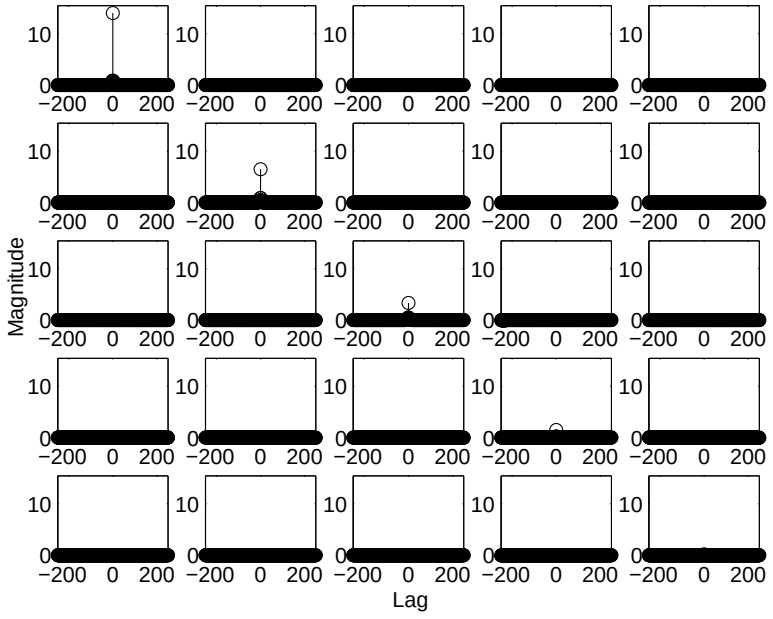

Figure 3.2: Diagonalized output matrix $\underline{\boldsymbol{D}}(z)$ calculated using SBR2. Stopping criteria of maximum polynomial order of 501 for both $\underline{\boldsymbol{D}}(z)$ and $\underline{\boldsymbol{P}}(z)$.

polynomial matrix being diagonalized increases, often after a series of iterations becoming unnecessarily large [50]. This is a natural consequence of using an FIR filter to compute the PMEVD. At every

iteration new coefficient matrices are created at both ends of the matrix to accommodate the shifted coefficients. Hence the order of the polynomial $\boldsymbol{D}_{i+1}(z)$ is greater than $\boldsymbol{D}_i(z)$ for $i = 1, 2, \ldots, \beta - 1$. In the example shown in Figure 3.2, the maximum polynomial order of the diagonalized matrix calculated by SBR2 has been limited to 501. In the original SBR2 algorithm [21], additional stopping criteria are implemented such as a limit on the maximum number of iterations and a convergence criteria, ϵ. If the smallest off-diagonal element is less than the product of ϵ and the reference value given in (3.14), then the input para-Hermitian matrix $\underline{\boldsymbol{R}}(z)$ is deemed sufficiently diagonalized.

$$\frac{\left\| \underline{\boldsymbol{R}}(z)\widetilde{\underline{\boldsymbol{R}}}(z) \right\|_F}{p} \tag{3.14}$$

As the polynomial order of the diagonalized matrix increases at every iteration, the computational cost of the algorithm quickly becomes a limiting factor. Hence in the example shown, maximal polynomial order has been used a stopping criteria as opposed to a limit on the maximum number of iterations or convergence criteria. Critically, this maximum polynomial limit is reached prior to the magnitude of the maximum off-diagonal coefficient becoming approximately zero and therefore limits the quality of the decomposition.

3.2.4 Limiting Polynomial Matrices Order Within SBR2

Polynomial matrix growth within the SBR2 algorithm has a significant impact on performance with storage requirements becoming excessively large and the subsequent increase in the process of searching for the largest in magnitude off-diagonal coefficient through an ever increasing matrix. New coefficient matrices constructed at every iteration typically consist entirely of zeros except for coefficients in the l^{th} row or column of the matrix. Further delays applied to the matrix in subsequent iterations often result in outer coefficient matrices containing a small fraction of the total Frobenius norm of the input matrix, $\underline{\boldsymbol{R}}(z)$ and occasionally outer coefficient matrices consisting entirely of zeros. Therefore to reduce computational complexity, Foster, *et al* [50] have proposed that a small proportion of the Frobenius norm of $\underline{\boldsymbol{R}}(z)$ is allowed to be lost at each iteration of the algorithm. By truncating $\underline{\boldsymbol{R}}(z)$ in this way the order of the resulting diagonalized matrix $\underline{\boldsymbol{D}}(z)$ is significantly reduced. Ta, *et al* [51] have also proposed a similar method for shortening the order of polynomial matrices produced by the SBR2 algorithm. Their approach reduces the order of the paraunitary matrix, $\underline{\boldsymbol{P}}(z)$ while containing the loss in paraunitary property under a given upper bound.

The approach of Foster [50] introduces an additional stopping criteria, the total maximal amount of the Frobenius norm of $\underline{\boldsymbol{R}}(z)$ which can be lost over all iterations may also be introduced to prevent

the small faction in energy lost become excessive over a large number of iterations. Figure 3.3 repeats the diagonalization of the matrix shown in Figure 3.1 but allows a maximal fraction of 1×10^{-6} of the F-Norm of $\underline{\boldsymbol{R}}(z)$ to be lost per iteration. For comparative purposes, Figure 3.4 shows the corresponding element, $\underline{\boldsymbol{R}}_{11}(z)$ of the input para-Hermitian polynomial matrix to the SBR2 algorithm. Note the significant increase in magnitude of the zero lag element in Figure 3.3 post diagonalization.

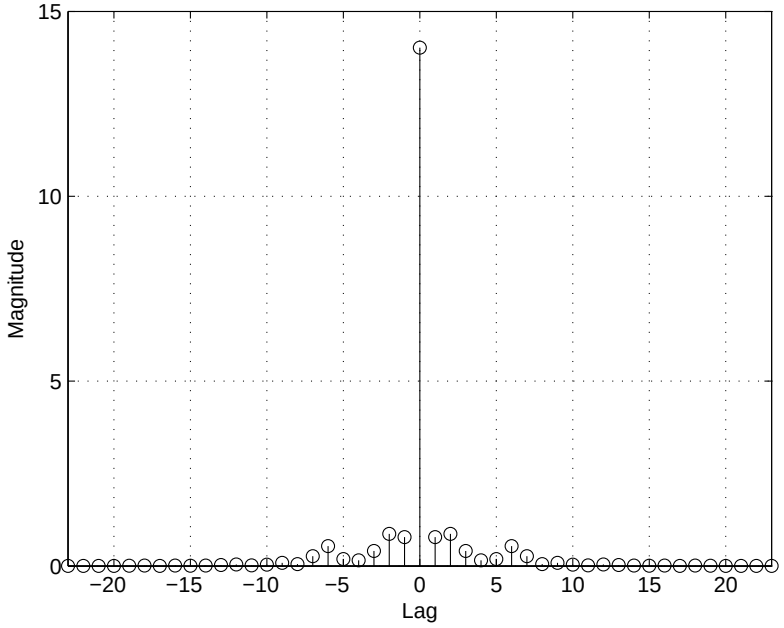

Figure 3.3: Dominant mode of the diagonalized output matrix $\underline{\boldsymbol{D}}(z)$ calculated using SBR2 with truncation parameters $\mu = 1 \times 10^{-6}$ and $\epsilon = 1 \times 10^{-4}$.

As can be clearly seen, the polynomial order of the resulting diagonal matrix has been reduced to 41, at a marginal cost of increasing the relative error of the decomposition to $E_{rel} = 17.0469 \times 10^{-3}$. Critically the stopping criteria of $\epsilon = 1 \times 10^{-4}$ has been reached, and polynomial matrix size is no longer a limiting factor. The number of iterations required was 932 [1].

Table 3.1 compares the computational complexity of SBR2 diagonalizing the matrix in Figure 3.1 with and without the trimming function. Numerical values have been taken directly from the MATLAB profiler. Only the results for the key SBR2 functions are presented [2]. Self time is the time spent in a function excluding the time spent in it's child functions. The key functions are as follows:

[1] The computational cost of an iteration of the SBR2 algorithm depends on the order of the matrix being diagonalized, and hence the time required for locating the maximum off-diagonal element and addressing the amount of memory required for the bulk delay matrix. Therefore the number of iterations has little significance on actual computational cost and should not be considered as such.

[2] The SBR2 algorithm has been implemented entirely within the MATLAB environment. Code has been written efficiently as possible but there has been no attempt to increase speed by implementing code in C++ and compiling them as *.mex* functions.

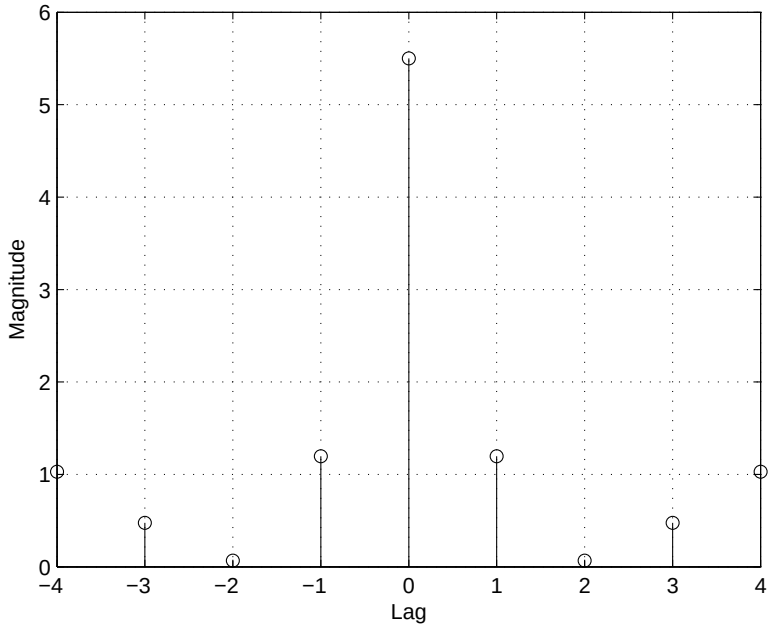

Figure 3.4: $\underline{\boldsymbol{R}}_{11}(z)$ of the input para-Hermitian polynomial matrix to the SBR2 algorithm.

- **SBR2 Main** - The main SBR2 function.
- **Max Element** - Locates the maximum off-diagonal element. In this implementation the search is restricted to the upper triangular component.
- **Left Rotate** - Applies the rotation matrix from the left hand side. This function will be called twice, for calculating the updated $\underline{\boldsymbol{R}}'(z)$ and the updated paraunitary matrix $\underline{\boldsymbol{P}}(z)$.
- **Left Shift** - Applies the bulk delay matrix from the left hand side. Again this function will be called twice, for calculating the updated $\underline{\boldsymbol{R}}'(z)$ and the updated paraunitary matrix $\underline{\boldsymbol{P}}(z)$
- **Right Rotate** - Applies the rotation matrix from the right hand side.
- **Right Shift** - Applies the bulk delay matrix from the right hand side.

$\underline{\widetilde{\boldsymbol{P}}}(z)$ is calculated directly from $\underline{\boldsymbol{P}}(z)$ once matrix diagonalization is complete to reduce the number of calls to *Right Rotate* and *Right Shift*.

As can be clearly seen from Table 3.1 the overall computational time of the algorithm has been reduced by over 95%. As the focus of this thesis is the application of polynomial matrix decomposition to frequency selective MIMO channels and not the development of computationally efficient algorithms, there will be little further discussion on computational complexity. However as we shall see in Chapter 4, other key components of the MIMO communications system, in particular the turbo

	SBR2 - no trimming			SBR2 - with trimming		
Function	*Calls*	*Total Time (s)*	*Self Time (s)*	*Calls*	*Total Time (s)*	*Self Time (s)*
SBR2 Main	1	173.3	152.9	1	4	2.2
Max Element	2307	9.6	9.6	933	0.8	2
Left Rotate	4612	4.2	4.2	1864	0.3	0.3
Left Shift	4612	1.9	1.9	1864	0.1	0.1
Right Rotate	2306	1.8	1.8	932	0.1	0.1
Right Shift	2306	0.7	0.7	932	0.1	0.1

Table 3.1: Computational complexity analysis for SBR2 with and without trimming functions, for a 5×5 MIMO channel with polynomial length 5.

decoder are far higher in computational complexitity. As turbo decoding is already part of the third generation partnership project (3GPP) standards for mobile networking [52] it is reasonable to assume SBR2 and its derivatives could easily be implemented in hardware for real-time communications.

3.3 Polynomial Matrix Singular Value Decomposition

The PMSVD of the polynomial channel, $\underline{\boldsymbol{H}}(z)$, is shown in (3.15) where $\underline{\boldsymbol{U}}(z)$ and $\widetilde{\underline{\boldsymbol{V}}}(z)$ are paraunitary polynomial matrices, so that $\widetilde{\underline{\boldsymbol{U}}}(z)\ \underline{\boldsymbol{U}}(z) = \boldsymbol{I}$ and $\widetilde{\underline{\boldsymbol{V}}}(z)\ \underline{\boldsymbol{V}}(z) = \boldsymbol{I}$ and $\underline{\boldsymbol{\Lambda}}(z)$ is a diagonal polynomial matrix.

$$\underline{\boldsymbol{H}}(z) = \underline{\boldsymbol{U}}(z)\ \underline{\boldsymbol{\Lambda}}(z)\ \widetilde{\underline{\boldsymbol{V}}}(z) \tag{3.15}$$

$\underline{\boldsymbol{U}}(z)$ and $\widetilde{\underline{\boldsymbol{V}}}(z)$ are obtained from the polynomial decomposition of $\underline{\boldsymbol{H}}(z)\ \widetilde{\underline{\boldsymbol{H}}}(z)$ and $\widetilde{\underline{\boldsymbol{H}}}(z)\ \underline{\boldsymbol{H}}(z)$. By separately post and pre multiplying the channel matrix with its paraconjugate and re-arranging in terms of $\underline{\boldsymbol{\Lambda}}(z)$ we obtain the pair of equations in (3.16).

$$\begin{aligned} \underline{\boldsymbol{\Lambda}}(z)\ \widetilde{\underline{\boldsymbol{\Lambda}}}(z) &= \widetilde{\underline{\boldsymbol{U}}}(z)\ \underline{\boldsymbol{H}}(z)\ \widetilde{\underline{\boldsymbol{H}}}(z)\ \underline{\boldsymbol{U}}(z) \\ \widetilde{\underline{\boldsymbol{\Lambda}}}(z)\ \underline{\boldsymbol{\Lambda}}(z) &= \widetilde{\underline{\boldsymbol{V}}}(z)\ \widetilde{\underline{\boldsymbol{H}}}(z)\ \underline{\boldsymbol{H}}(z)\ \underline{\boldsymbol{V}}(z) \end{aligned} \tag{3.16}$$

Forming the para-Hermitian input to SBR2 by post multiplying the polynomial channel matrix with its paraconjugate, i.e. $\underline{\boldsymbol{R}}(z) = \underline{\boldsymbol{H}}(z)\ \widetilde{\underline{\boldsymbol{H}}}(z)$ and comparing the first equation in (3.16) and (3.8) shows that the paraunitary diagonalizing matrix calculated by the SBR2 algorithm, $\widetilde{\underline{\boldsymbol{P}}}(z) \equiv \underline{\boldsymbol{U}}(z)$

Repeating this operation with the para-Hermitian input to SBR2 formed from the pre multiplication of the paraconjugate of the polynomial channel matrix and the polynomial channel matrix itself, i.e. $\underline{\boldsymbol{R}}(z) = \widetilde{\underline{\boldsymbol{H}}}(z)\ \underline{\boldsymbol{H}}(z)$ yields the paraunitary matrix, $\underline{\boldsymbol{V}}(z)$ as $\widetilde{\underline{\boldsymbol{P}}}(z) \equiv \underline{\boldsymbol{V}}(z)$.

Finally, $\underline{\boldsymbol{\Lambda}}(z)$ is calculated from (3.15) as $\widetilde{\underline{\boldsymbol{U}}}(z)\ \underline{\boldsymbol{H}}(z)\ \underline{\boldsymbol{V}}(z)$. $\underline{\boldsymbol{\Lambda}}(z)$ has been calculated in this manner as computing $\underline{\boldsymbol{\Lambda}}(z)$ directly from the diagonal output of SBR2 (3.8), $\underline{\boldsymbol{D}}(z)$ is a complex mathematical problem in its own right and outside the scope of this thesis. Therefore a true PMSVD has been

performed on $\underline{\boldsymbol{H}}(z)$ by applying the SBR2 algorithm twice.

3.3.1 Simulation Results

Figure 3.5 shows a MIMO system with five antennas at the transmitter and receiver. The temporal length of the channel between each transmitter and receiver is five and the channel has a constant power delay profile with equal average gain for each tap. Figure 3.6 shows its subsequent diagonalization using multiple applications of the SBR2 algorithm. The relative error of this decomposition, i.e.

$$E_{rel} = \frac{\left\| \underline{\boldsymbol{H}}(z) - \left(\underline{\boldsymbol{U}}(z)\ \underline{\boldsymbol{\Lambda}}(z)\ \widetilde{\underline{\boldsymbol{V}}}(z) \right) \right\|_F}{\left\| \underline{\boldsymbol{H}}(z) \right\|_F} \tag{3.17}$$

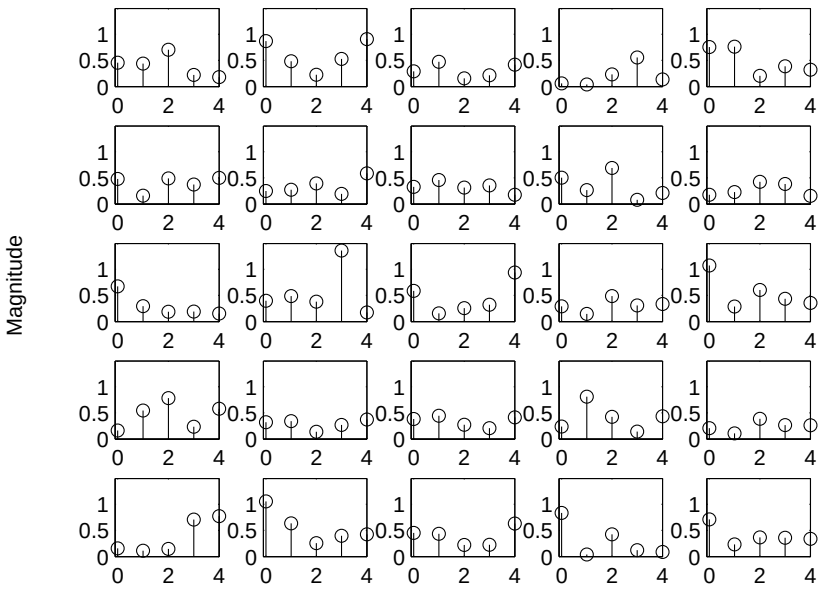

Figure 3.5: Input polynomial matrix, $\underline{\boldsymbol{H}}(z)$ of polynomial length 5.

was 63.6×10^{-3}. As a comparison, Figure 3.7 shows the relative error in channel estimation of $\underline{\boldsymbol{H}}(z)$ for a training sequence of length $N_t = 50$, averaged over 1000 Monte Carlo simulations using an MMSE channel estimator. PMSVD is then performed on the MMSE estimate, $\underline{\hat{\boldsymbol{H}}}(z)$ and then $\underline{\boldsymbol{H}}(z)$ is reconstructed from (3.15) and its relative error calculated. As can be seen the additional relative error introduced from PMSVD does not significantly increase the relative error already present in the channel estimator.

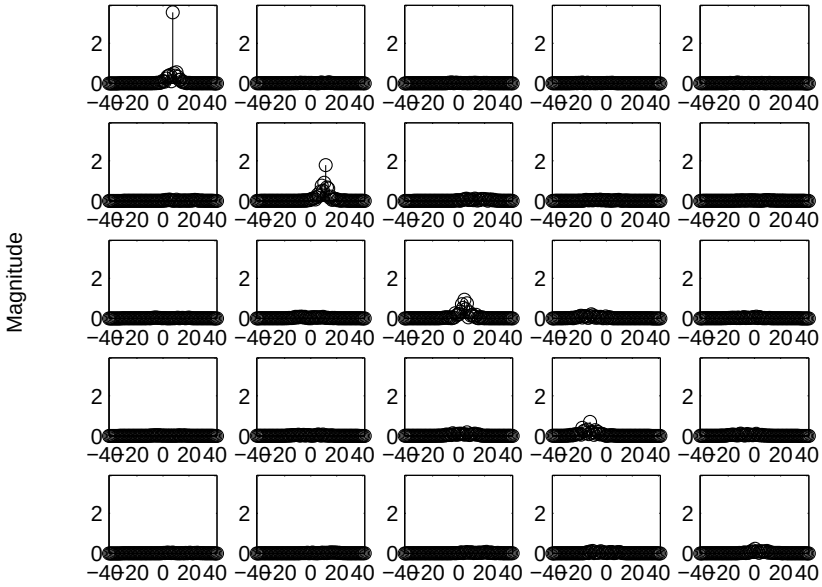

Figure 3.6: Output diagonalized polynomial matrix produced by PMSVD, $\mu = 1 \times 10^{-6}$, $\epsilon = 1 \times 10^{-4}$.

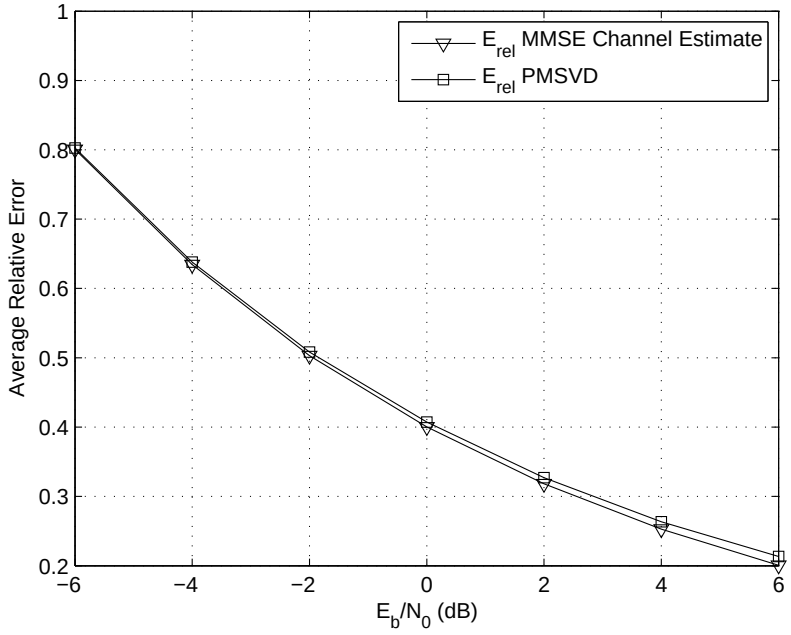

Figure 3.7: Average relative error in channel estimation for $\underline{\boldsymbol{H}}(z)$, with training sequence of length $N_t = 50$ averaged over 1000 Monte Carlo simulations.

3.3.2 Alternate PMSVD Approaches

This approach to PMSVD is often criticized, as perfect channel knowledge is unobtainable in the

real world. Hence the presence of channel estimation errors in $\underline{\boldsymbol{H}}(z)$ is exasipated when forming the para-Hermitian input to SBR2. Although unfavourable, for the majority of this PhD this was the only algorithm available to calculate the PMSVD of a polynomial matrix.

McWhirter has proposed a method for directly calculating the PMSVD of $\underline{\boldsymbol{H}}(z)$ operating directly on $\underline{\boldsymbol{H}}(z)$. Golub [29] has shown that the SVD of a scalar matrix can be calculated directly using Givens rotations and McWhirter's solution is a generalization of this to polynomial matrices using the bulk delay and rotation approach developed in the SBR2 algorithm. Due to the para-Hermitian property of the input polynomial matrix to the SBR2 algorithm, at each iteration the effect of the bulk delay component of $\underline{\boldsymbol{G}}(z)$ will be counter-acted by that of $\widetilde{\underline{\boldsymbol{G}}}(z)$. However this will not be the case when operating directly on $\underline{\boldsymbol{H}}(z)$ and hence independent rotations applied from the left and right may cause energy to leave the zero lag diagonal elements, resulting in the development of a significantly different approach to that of SBR2. This algorithm is currently still in development and no work has been currently published on its operation.

It is also possible to calculate the PMSVD directly on $\underline{\boldsymbol{H}}(z)$ using the PMQRD algorithm. This PMQRD approach to PMSVD results in a highly efficient implementation and is discussed on page 42. Due to its recent conception it has been implemented in this thesis but not in the detail afforded to the SBR2 based evaluation. As will be seen it significantly further improves the computational time of calculating a PMSVD.

3.4 Polynomial Matrix QR Decomposition

The QR decomposition of a $p \times q$ scalar matrix $\boldsymbol{A}$ is defined as:

$$\boldsymbol{A} = \boldsymbol{Q}\ \boldsymbol{R} \tag{3.18}$$

where $\boldsymbol{Q}$ is a $p \times p$ unitary matrix, so that $\boldsymbol{Q}\boldsymbol{Q}^H = \boldsymbol{Q}^H\boldsymbol{Q} = \boldsymbol{I}_p$ and $\boldsymbol{R}$ is a $p \times q$ upper triangular matrix. One method for computing the unitary matrix Q is by calculating a series of Givens[3] rotations, where each rotation will drive one of the elements beneath the diagonal of the matrix $\boldsymbol{A}$ to zero [29]. The elements of $\boldsymbol{A}$ below the diagonal are zeroed in a particular order to ensure that successive rotations do not undo previously zeroed elements. There are several different orderings that can be implemented, however for the purposes of this thesis the elements are eliminated starting with the uppermost left element and then moving across elements beneath the diagonal in each row from left to right, before

[3]It is important to note that Givens rotations are no different from Jacobi rotations. In the context of Jacobi methods for the symmetric eigenvalue problem, Jacobi rotations form the core operation. Therefore it is commonplace to refer to Jacobi rotations in the context of eigenvalue decomposition and Givens rotations in the context of QR decomposition.

moving to the next row down.

3.4.1 Polynomial Matrix QR Decomposition

The $p \times q$ polynomial matrix $\underline{\boldsymbol{A}}(z)$ is defined as

$$\underline{\boldsymbol{A}}(z) = \sum_{i=t_1}^{t_2} \boldsymbol{A}_i z^{-i} \tag{3.19}$$

Where $\boldsymbol{A}_i \in \mathbb{C}^{p \times q}$ is the i^{th} matrix tap of the polynomial matrix, $i \in \mathbb{Z}, t_1 < t_2$ and z^{-1} is the unit delay operator. The polynomial QR decomposition of $\underline{\boldsymbol{A}}(z)$ is shown in (3.20) where $\underline{\boldsymbol{Q}}(z)$ is a paraunitary polynomial matrix, so that $\underline{\boldsymbol{Q}}(z)\widetilde{\underline{\boldsymbol{Q}}}(z) = \boldsymbol{I}_p$ and $\underline{\boldsymbol{R}}(z)$ is an upper triangular polynomial matrix.

$$\underline{\boldsymbol{A}}(z) = \underline{\boldsymbol{Q}}(z)\ \underline{\boldsymbol{R}}(z) \tag{3.20}$$

Elementary Polynomial Givens Rotation

An elementary polynomial Givens rotation (EPGR) [22] is a Givens rotation preceded by an elementary time shift matrix as follows:

$$\begin{aligned} \underline{\boldsymbol{G}}^{(\alpha,\theta,\phi,t)}(z) &= \begin{bmatrix} e^{j\alpha}\cos\theta & e^{j\phi}\sin\theta \\ -e^{-j\phi}\sin\theta & e^{-j\alpha}\cos\theta \end{bmatrix} \begin{bmatrix} 1 & 0 \\ 0 & z^t \end{bmatrix} \\ &= \begin{bmatrix} e^{j\alpha}\cos\theta & z^t e^{j\phi}\sin\theta \\ -e^{-j\phi}\sin\theta & z^t e^{-j\alpha}\cos\theta \end{bmatrix} \end{aligned} \tag{3.21}$$

where j denotes the imaginary constant and θ the rotation angle. In the simplest case, defining a 2×1 polynomial vector as $\underline{\boldsymbol{a}}(z) \in \mathbb{C}^{2\times 1}$, the object of the EPGR is to drive a specific coefficient from the polynomial element $\underline{a}_2(z)$ to zero.

$$\begin{bmatrix} e^{j\alpha}\cos\theta & z^t e^{j\phi}\sin\theta \\ -e^{-j\phi}\sin\theta & z^t e^{-j\alpha}\cos\theta \end{bmatrix} \begin{bmatrix} \underline{a}_1(z) \\ \underline{a}_2(z) \end{bmatrix} = \begin{bmatrix} \underline{a}'_1(z) \\ \underline{a}'_2(z) \end{bmatrix} \tag{3.22}$$

For example, to zero the coefficient $a_2(i)$ then the lag parameter in the EPGR matrix is set as $t = i$ and the rotation angles are chosen [26] such that

$$\tan\theta = \frac{|a_2(t)|}{|a_1(0)|}, \phi = -\arg(a_2(t)), \alpha = -\arg(a_1(0)) \tag{3.23}$$

resulting in $a'_2(0) = 0$. The application of the EPGR renders $a'_1(0)$ real. Note that if $|a_1(0)| = 0$

in (3.23), then set $\theta = \pi/2$ [43]. An EPGR is paraunitary by construction as each component of the matrix, i.e. the Givens rotation and the elementary time shift matrix are both paraunitary.

Complete Polynomial Givens Rotation

Successive EPGR's can be applied iteratively to the 2×1 polynomial vector $\underline{\boldsymbol{a}}(z)$ to drive all coefficients of the polynomial element $\underline{a}_2(z)$ arbitrarily close to zero. The coefficients of $\underline{a}_2(z)$ are zeroed in order of maximum magnitude. At each iteration, the coefficient of maximum amplitude is zeroed and the complete series of EPGR's required constitutes a complete polynomial Givens rotation (CPGR) [22, 26], denoted by the matrix $\underline{\boldsymbol{G}}^{(2,1)}(z)$, where the superscripts denote the position of the polynomial element that the matrix is attempting to annihilate. A matrix of this form can be applied to $\underline{\boldsymbol{a}}(z)$ resulting in

$$\underline{\boldsymbol{G}}^{(2,1)}(z) \begin{bmatrix} \underline{a}_1(z) \\ \underline{a}_2(z) \end{bmatrix} \cong \begin{bmatrix} \underline{a}'_1(z) \\ 0 \end{bmatrix} \tag{3.24}$$

3.4.2 PMQRD Algorithm

A CPGR can be applied to the polynomial matrix $\underline{\boldsymbol{A}}(z)$ to drive one of the polynomial elements to zero, e.g.

$$\underline{\boldsymbol{A}}'(z) = \underline{\boldsymbol{G}}^{(j,k)}(z)\ \underline{\boldsymbol{A}}(z) \tag{3.25}$$

where $\underline{\boldsymbol{G}}^{(j,k)}(z)$ is the CPGR matrix designed to drive all coefficients of $\underline{a}_{j,k}(z)$ sufficiently small, resulting in a new polynomial matrix, $\underline{\boldsymbol{A}}'(z)$ [22, 26]. The CPGR applies an iterative sequence of EPGR matrices. Each EPGR is formulated as a $p \times p$ identity matrix with the exception of the four elements positioned at the intersection of rows j and k with columns j and k. These elements are given by the 2×2 sub-matrix, $\underline{\boldsymbol{G}}^{(\alpha,\theta,\phi,t)}(z)$ as in (3.22), where for example if the dominant coefficient is $a_{j,k}(i)$, then the lag parameter is set as $t = i$ and the coefficients required for calculating the rotation angles are $a_2(t) = a_{jk}(i)$ and $a_1(0) = a_{k,k}(0)$.

Zeroing the polynomial elements of $\underline{\boldsymbol{A}}(z)$ beneath the diagonal in the order previously described is now a simple case of applying successive CPGR matrices. Defining the paraunitary matrix $\underline{\boldsymbol{Q}}_\beta(z)$ as:

$$\underline{\widetilde{\boldsymbol{Q}}}_\beta(z) = \underline{\boldsymbol{G}}_\beta(z) \ldots \underline{\boldsymbol{G}}_2(z)\ \underline{\boldsymbol{G}}_1(z) \tag{3.26}$$

where β represents an unspecified number of iterations. After β iterations (3.25) results in:

$$\underline{\boldsymbol{R}}(z) = \underline{\widetilde{\boldsymbol{Q}}}_\beta(z)\ \underline{\boldsymbol{A}}(z) \tag{3.27}$$

3.5 Simulation Results

Figure 3.8 shows the upper triangular polynomial matrix produced from the PMQRD of the polynomial matrix previously used in the PMSVD example, $\underline{\boldsymbol{H}}(z)$ shown in Figure 3.5. As with SBR2, outer coefficient matrices can be trimmed at each iteration if they contain only a small fraction of the Frobenius norm of the input matrix, to restrict polynomial growth and reduce computational complexity.

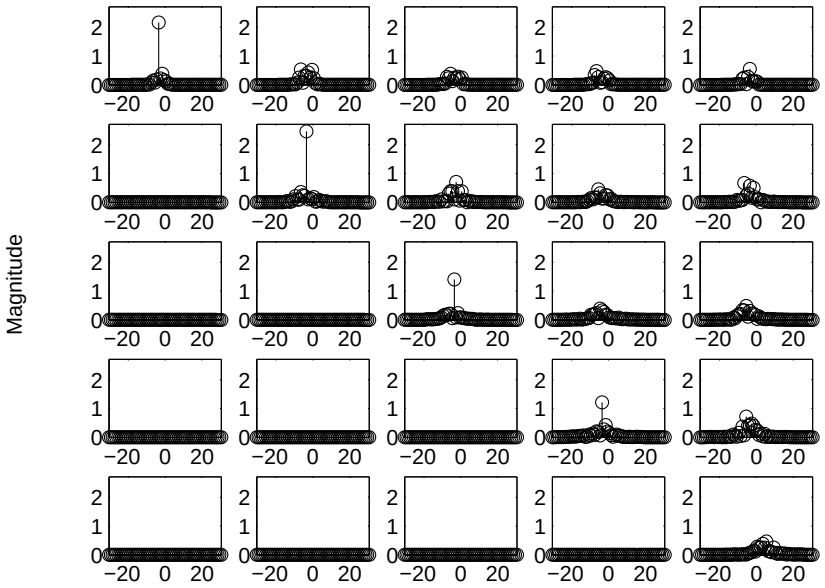

Figure 3.8: Output upper-triangular polynomial matrix produced by PMQRD, $\mu = 1 \times 10^{-6}$, $\epsilon = 1 \times 10^{-4}$.

The relative error of this decomposition was 10.6×10^{-3}, again an order of magnitude less than that typically present from MMSE channel estimation, confirming its suitability for practical implementation.

3.6 PMSVD using PMQRD Algorithm

A novel algorithm for calculating the PMSVD using the PMQRD has been proposed by Foster [53], allowing for direct calculation of the PMSVD without the need to form an input para-Hermitian matrix. Initially the PMQRD of the input matrix, $\underline{\boldsymbol{A}}(z) \in \mathbb{C}^{p \times q}$ is calculated, such that

$$\widetilde{\underline{\boldsymbol{U}}}_1(z)\, \underline{\boldsymbol{A}}(z) = \underline{\boldsymbol{R}}_1(z) \tag{3.28}$$

where $\widetilde{\underline{\boldsymbol{U}}}_1(z)$ is a $p \times p$ paraunitary matrix and $\underline{\boldsymbol{R}}_1(z)$ is a $q \times q$ upper-triangular polynomial matrix. The PMQRD of $\underline{\boldsymbol{A}}^{'}(z) = \widetilde{\underline{\boldsymbol{R}}}_1(z)$ is now calculated, essential calculating the PMQRD of a lower-triangular polynomial matrix.

$$\widetilde{\underline{\boldsymbol{V}}}_1(z)\ \underline{\boldsymbol{A}}^{'}(z) = \underline{\boldsymbol{R}}_2(z) \tag{3.29}$$

where $\widetilde{\underline{\boldsymbol{V}}}_1(z)$ is a $M_t \times M_t$ paraunitary matrix. This completes one iteration of the PMSVD by PMQRD algorithm, resulting in

$$\widetilde{\underline{\boldsymbol{V}}}_1(z)\ \widetilde{\underline{\boldsymbol{A}}}(z)\ \underline{\boldsymbol{U}}_1(z) = \underline{\boldsymbol{R}}_2(z) \tag{3.30}$$

This process is repeated until all off-diagonal coefficients are deemed sufficiently small. After β iterations resulting in

$$\underline{\boldsymbol{U}}(z)\ \underline{\boldsymbol{A}}(z)\ \widetilde{\underline{\boldsymbol{V}}}(z) = \underline{\boldsymbol{\Lambda}}(z) \tag{3.31}$$

where $\underline{\boldsymbol{U}}(z) = \underline{\boldsymbol{U}}_1(z) \ldots \underline{\boldsymbol{U}}_\beta(z)$ and $\widetilde{\underline{\boldsymbol{V}}}(z) = \widetilde{\underline{\boldsymbol{V}}}_1(z) \ldots \widetilde{\underline{\boldsymbol{V}}}_\beta(z)$. Both of these matrices are paraunitary by construction. $\underline{\boldsymbol{\Lambda}}(z)$ is a diagonal matrix containing $r = min(p, q)$ orthogonal channels. As with SBR2 the PMSVD by PMQRD algorithm will order the channels in order of power spectral density [28, 10], hence $\underline{\boldsymbol{\lambda}}_{11}(z)$ will be the strongest channel and $\underline{\boldsymbol{\lambda}}_{rr}(z)$ the weakest. Hence a PMSVD has been calculated with repeated applications of the PMQRD algorithm.

Applications of the PMQRD in this manner will result in a PMSVD, as throughout all operations of the PMSVD by PMQRD algorithm, the quantity $|a_{11}(0)|^2$ is monotonically increasing. This is a direct consequence of driving the off-diagonal polynomial elements in the first row or column of the matrix to zero, and cannot be affected by subsequent rotations applied to off-diagonal coefficients in any other column or row of the matrix. As the quantity is bounded by the total energy in the matrix, i.e. $\|\underline{\boldsymbol{A}}(z)\|_F^2$ it cannot increase indefinitely. Hence a point exists where the off-diagonal elements of the matrix are less than ϵ or some other stopping criteria in magnitude. A concise proof of convergence is available in [43].

Performing the PMSVD in this manner has several significant benefits over the SBR2 based approach. Aside from operating directly on the frequency selective MIMO channel matrix, it is computationally quicker. Moreover the paraunitary filter banks obtained from the PMSVD by PMQRD approach are significantly smaller than those obtained via SBR2. This significantly reduces the computational cost of channel equalization, which will become apparent in Chapter 4.

3.7 Conclusions

This chapter has introduced two polynomial matrix decomposition algorithms, one for calculating PMSVD and one for PMQRD. Subsequent chapters and the basis of this thesis will focus on the application and analysis of these algorithms to frequency selective MIMO channels. The operation of the SBR2 algorithm for PMEVD has been discussed and how computational complexity and performance can be significantly increased with only a minor cost to quality of matrix decomposition. This has been assessed against errors introduced by MMSE estimation of the CSI and found to be insignificant. It has then been demonstrated how a true PMSVD can be performed on any polynomial matrix by applying the SBR2 algorithm twice.

The natural extension of this Jacobi rotation matrix to polynomial matrix decomposition, PMQRD has then been demonstrated, using the computational efficient approach developed for SBR2. Finally this work has been taken one step further, and PMSVD by PMQRD has been introduced, which although only developed recently has the potential to significantly improve the performance of the MIMO systems pioneered in this thesis.

In the next chapter the PMSVD will be applied to various frequency selective MIMO channels and evaluated against existing time domain and frequency domain based solutions.

Chapter 4

Dominant Mode PMSVD Performance

4.1 Introduction

In Chapter 3 it was shown that the PMSVD of a polynomial MIMO channel matrix, $\underline{\boldsymbol{H}}(z)$ can be performed with two applications of the SBR2 algorithm. In this chapter, the application of the dominant mode of PMSVD to MIMO communications is discussed. Without loss of generality, only frequency selective MIMO systems consisting of equal number of transmit and receive antennas, i.e. $M_t = M_r$ have been considered. Generality is not lost as for a MIMO system where $M_t \neq M_r$, the PMSVD and the channel equalization techniques presented in this chapter are still readily applicable. The only caveat is the number of orthogonal channels provided by PMSVD will be reduced. However as this chapter focuses solely on exploiting the spatial properties of the dominant PMSVD mode, this is not an issue. The dominant mode, $\underline{\boldsymbol{\lambda}}(z)_{11}$ will provide the spatial sub-channel with the highest gain. Using only this mode results in a PMSVD system that does not exploit the full spatial capacity of the MIMO channel. Instead the focus in this chapter is to exploit the superior BER rate performance of the dominant mode, for low SNR environments.

Two different MIMO scenarios are considered in this chapter. A frequency selective MIMO channel with exponential power delay profile, and a frequency selective MIMO channel with constant power delay profile. Exponential power delay profile channels are commonly found in outdoor macro-cellular environments, due to the significant attenuation in non Line-of-Sight (LOS) paths. For an indoor micro-cellular environment, typically a LOS path between transmitter and receiver does not exist and the channel between each transmit-receive antenna pair is a scattering channel. Due to the rich multi-path propagating environment this results in a MIMO channel with constant power delay profile.

When using the SBR2 algorithm to calculate the PMSVD of the channel, this energy distribution has a direct effect on computational time and energy distribution within the matrices produced by the decomposition. Forming the para-Hermitian input to SBR2 as either $\widetilde{\underline{\boldsymbol{H}}}(z)\underline{\boldsymbol{H}}(z)$ or $\underline{\boldsymbol{H}}(z)\widetilde{\underline{\boldsymbol{H}}}(z)$ from a frequency selective MIMO channel with exponential power delay profile typically results in a

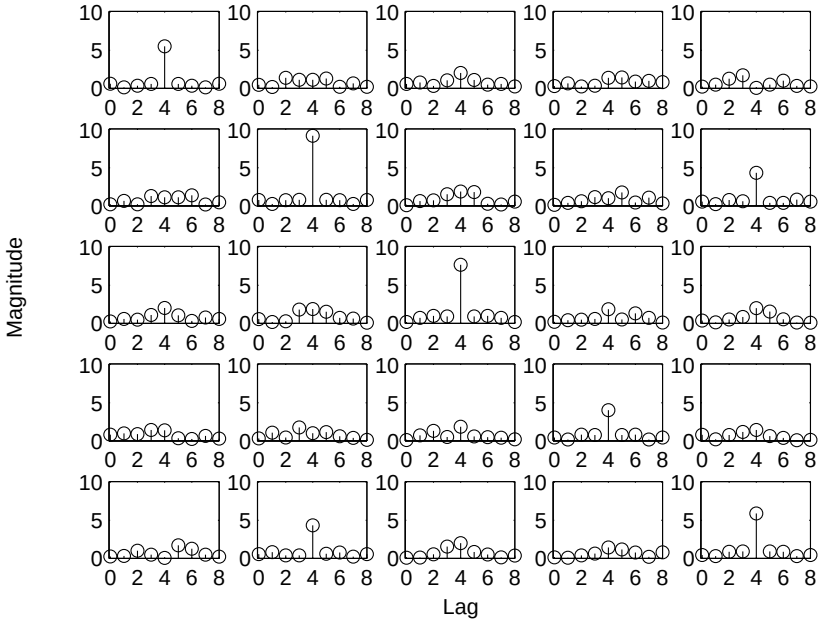

Figure 4.1: Input para-Hermitian matrix to SBR2 algorithm formed from an exponential power delay profile 5×5 MIMO channel with polynomial length $L = 5$.

input matrix that is not too dissimilar from the identity matrix, $\boldsymbol{I}$ as shown in Figure 4.1.

Hence only a small number of iterations of the SBR2 algorithm are required to fully diagonalize the input matrix, resulting in a diagonal matrix, $\underline{\boldsymbol{\Lambda}}(z)$ produced by PMSVD with a relatively low polynomial order. This allows a low complexity equalization strategy to be used to equalize the frequency selective channels produced by PMSVD. When forming the para-Hermitian input using a channel with constant power profile as shown in Figure 4.2 the percentage of the total energy distribution within the off-diagonal elements is significantly increased. Hence a larger number of iterations of the SBR2 algorithm are required, resulting in a diagonal matrix, $\underline{\boldsymbol{\Lambda}}(z)$ with a larger polynomial order and requiring a different equalization strategy.

4.2 PMSVD Architecture

Initially the PMSVD of the broadband MIMO channel, $\underline{\boldsymbol{H}}(z)$ is calculated using multiple applications of the SBR2 algorithm, as described in Chapter 3. By analogy with a conventional narrowband SVD beamformer, the process of using the i^{th} column vector of $\underline{\boldsymbol{V}}(z)$ as a transmit filter bank, $\underline{\boldsymbol{v}}_i(z) = \left[\underline{v}_{1i}(z), \underline{v}_{2i}(z), \ldots, \underline{v}_{M_t i}(z)\right]^T$ and the i^{th} row vector of $\widetilde{\underline{\boldsymbol{U}}}(z)$, i.e. $\widetilde{\underline{\boldsymbol{u}}}_i(z) = \left[\widetilde{\underline{u}}_{i1}(z), \widetilde{\underline{u}}_{i2}(z), \ldots, \widetilde{\underline{u}}_{iM_r}(z)\right]$

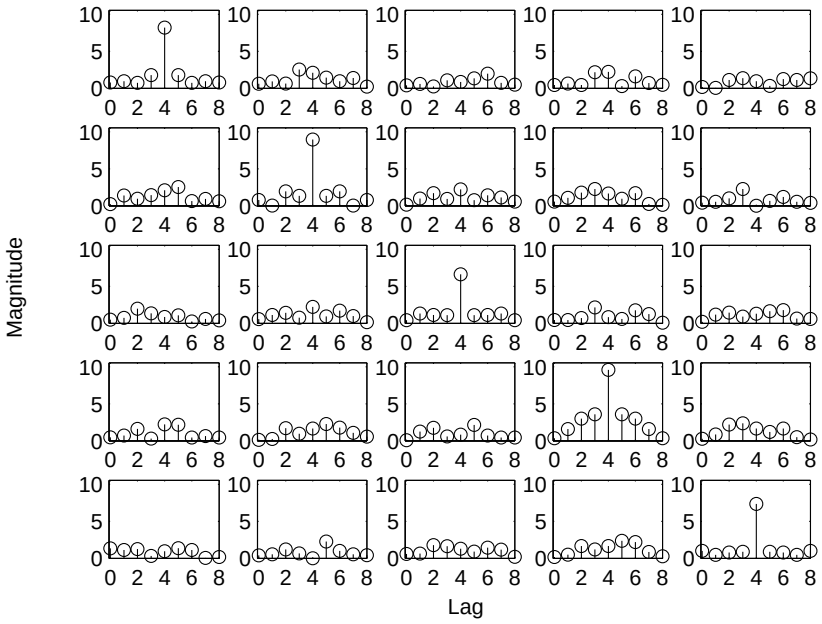

Figure 4.2: Input para-Hermitian matrix to SBR2 algorithm formed from an constant power profile 5×5 MIMO channel with polynomial length $L = 5$.

as a receive filter bank, is identical to passing the signal through the i^{th} diagonal element of $\underline{\mathbf{\Lambda}}(z)$, i.e.

$$\underline{\boldsymbol{\lambda}}_{ii}(z) = \underline{\widetilde{\boldsymbol{u}}}_i(z)\ \underline{\boldsymbol{H}}(z)\ \underline{\boldsymbol{v}}_i(z) \tag{4.1}$$

For an M_r, M_t MIMO system, $\underline{\mathbf{\Lambda}}(z)$ will be a diagonal matrix containing $r = min(M_r, M_t)$ orthogonal channels. The SBR2 algorithm will order the channels in order of power spectral density, hence $\underline{\boldsymbol{\lambda}}_{11}(z)$ will be the strongest channel and $\underline{\boldsymbol{\lambda}}_{rr}(z)$ the weakest. The decomposition of the polynomial channel matrix $\underline{\boldsymbol{H}}(z)$ into r parallel frequency selective channels (spatial-temporal modes), is depicted in Figure 4.3.

As the subchannels produced by PMSVD are FIR in nature and therefore frequency selective, further processing is required at the receiver to equalize each subchannel. As previously mentioned the distribution of energy within $\underline{\boldsymbol{H}}(z)$ directly affects the distribution of energy within $\mathbf{\Lambda}(z)$ resulting in two different equalization approaches which are now discussed. Ta *et al* [54, 55] have proposed a joint optimal precoding and block decision feedback equalization (BDFE) based solution to PMSVD channel subchannel equalization. However, their approach focuses on joint optimal transmitter-receiver filterbank design to minimize the mean square error (MSE) between input and output symbols, analogous to the transceiver optimization proposed by Vucic and Boche [37]. Their approach is distinctly

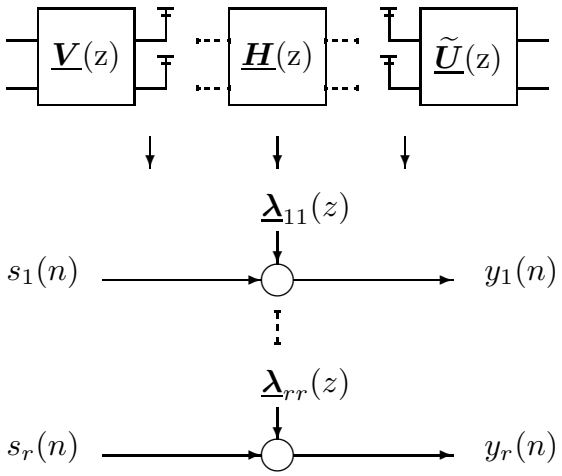

Figure 4.3: PMSVD system diagram representing decomposition of a frequency selective MIMO channel into r spatial-temporal modes.

different to the approach proposed in this chapter, as the focus is on reducing the redundancy introduced in block based MIMO-OFDM transmission schemes to cancel interbin interference. Hence it has not been considered.

4.3 Exponential Channels

A MIMO channel with an exponential power delay profile and an exponential decaying factor of $\psi = 0.8$ is considered, i.e.

$$h_{ij}(k) = \alpha \exp^{-\psi(k-1)} w(k) \qquad , i, j \in \{1, 2, \ldots, 5\}$$
$$, k = 1, \ldots, L \tag{4.2}$$

where $h_{ij}(k)$ is the k^{th} multipath coefficient, between the i^{th} transmit antenna and j^{th} receive antenna, $w(k)$ is a zero-mean complex Gaussian random variable, and the parameter α is chosen to normalize the average channel gain to unity.

Figure 4.4 shows a typical subchannel impulse response sequence for the dominant subchannel, $\underline{\boldsymbol{\lambda}}_{11}(z)$ derived from a polynomial channel matrix, $\underline{\boldsymbol{H}}(z)$ with an exponential power delay profile. Notice that for the dominant subchannel, most of the energy is concentrated in five significant taps (19-23). A Viterbi equalizer at the receiver is used to equalize the spatial-temporal subchannel [56]. Therefore, as in commonplace in wireless communications the significant five taps are extracted and

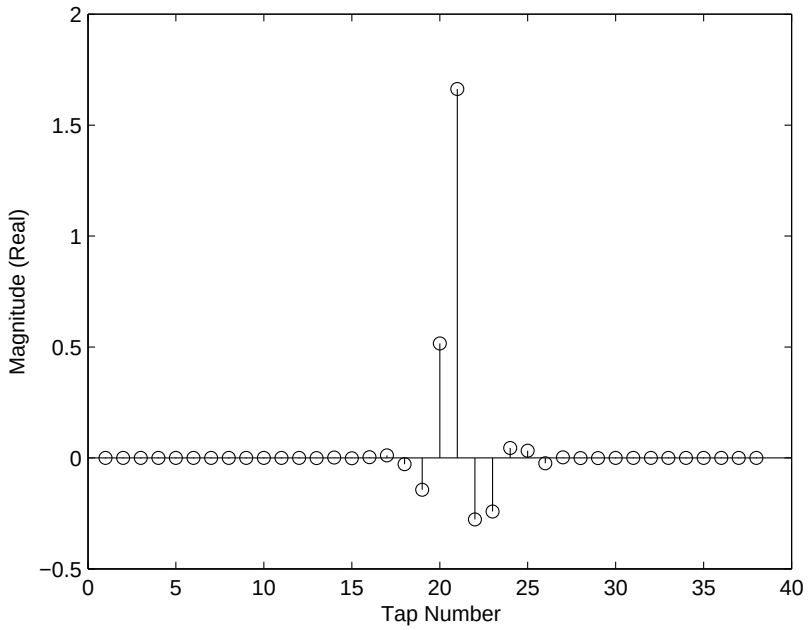

Figure 4.4: Typical $\underline{\boldsymbol{\lambda}}_{11}(z)$ plot showing a polynomial channel produced by SBR2 for a 5×5 MIMO channel, $L = 5$. with exponentially decaying elements.

passed to the Viterbi equalizer.

4.3.1 Viterbi Equalization

Recent mobile radio systems such as GSM already employ Viterbi equalization at the receiver to combat intersymbol interference (ISI) due to fast fading and the multipath propagation environment. The number of states in the Viterbi algorithm [56], and hence its complexity, increases exponentially with the length of the channel impulse response. To limit the hardware complexity, the channel impulse response (CIR) is often truncated to a manageable length [57]. In the case of GSM the CIR is generally truncated to five taps. This ensures the delay introduced in the equalization stage is acceptable for real-time voice communications, and this five tap approach has been carried over to the PMSVD implementation.

An overview of the Viterbi algorithm operation follows. Viterbi algorithm performs estimation of the input sequence of a discrete time finite-state Markov process. As the multipath wireless channel acts as Markov process it can be readily applied to FIR channel equalization. The algorithm runs from time instant $t = 0$ to $t = \tau$, and the state sequence is represented as $\boldsymbol{S} = (S_0, S_1, \ldots, S_{\tau-1}, S_\tau)$ [31]. The multistep evolution of the path through the underlying Markov graph is viewed as a multistage replication, i.e. a trellis diagram [58].

At each branch at time t on the path x in the trellis, the Euclidean distance or branch metric, denoted by v_t^x is calculated. The path metric, corresponding to path x denoted by $\mu_t^{(x)}$ is given by $\mu_t^{(x)} = \mu_{t-1}^{(x)} + v_t^x$. It is assumed that noise terms corrupting the received sequence are independent [59]. Algorithm 4.1 provides a summary of the operation of the Viterbi Algorithm.

Algorithm 4.1 Summary of the Viterbi algorithm

Set initial values
$t = 0,\ S_0 = 0,\ \mu_0^{(x)}(S_0 = 0) = 0,\ \mu_0^{(x)}(S_0 \neq 0) = \infty$
for $t = 1$ to $t = \tau$ **do**
  Compute branch metrics for all branches entering a node at time t.
  Compute path metrics for all paths entering a node at time t.
  Compute path metrics for all paths entering a node and find the survivor path for each node.
  Store the survivor path and path metric for each node.
  $t = t++$
end for
The survivor at node S_τ is the maximum likelihood path.

Computational Cost

The Viterbi algorithm was considered hopelessly complex in 1967 when it was initially published [58], due to its significant memory storage requirements. During the late 1970's when computing power caught back up it was used for error correction on the Voyager space probes and has since found its way into virtually every communication system. The computational cost of the Viterbi equalizer for BPSK modulated symbols is of the order 2^k operations, where k denotes the polynomial order of the SISO channel to be equalized. As all second generation cellular phones and above use the Viterbi algorithm (over a billion users) a significant amount of research has been carried out into reducing computational cost. The A* algorithm [60] combines the reliability and performance of the Viterbi algorithm while running efficiently as a sequential decoder when the SNR is high. The lazy Viterbi algorithm [61] builds upon this further, reducing complexity and also enabling application to continuous streams of data.

Despite this it is still impractical for mobile devices, limited by computational power and memory storage to operate on channel with $k > 8$, therefore an alternative approach is required for channels with large delay spread.

4.4 Constant Profile Channels

A MIMO channel with constant power delay profile with equal average gain for each tap, i.e. $\psi = 0$ in (4.2) is now considered. This channel model is applicable to indoor wireless local area networks [62, 63]. Figure 4.5 shows a typical subchannel impulse response for the dominant subchannel,

$\underline{\boldsymbol{\lambda}}_{11}(z)$ derived from such a polynomial channel matrix, $\underline{\boldsymbol{H}}(z)$ with constant power profiles. Subchannel length is typically between 70-90 taps but significant coefficients are clustered in the middle. However the Viterbi equalizer can no longer be used due to its high computational cost. Hence a coded approach is used to allow the inclusion of a low complexity iterative (turbo) equalizer at the receiver.

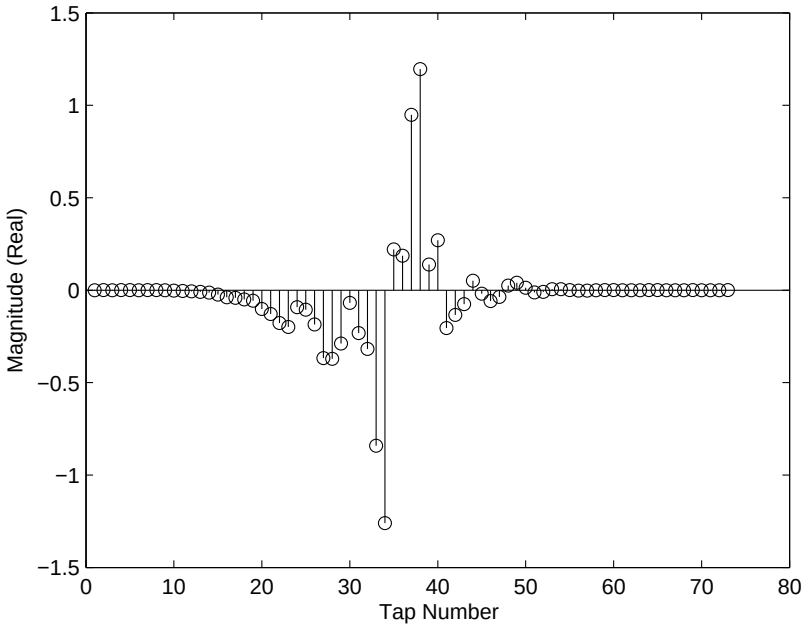

Figure 4.5: Typical $\underline{\boldsymbol{\lambda}}_{11}(z)$ plot showing a polynomial channel produced by SBR2 for a 5×5 MIMO channel, $L = 5$, with constant power profile.

4.4.1 Turbo Equalization

Turbo Equalization [64] is an iterative equalization and decoding technique that can achieve impressive performance gains for coded data transmission over intersymbol interference (ISI) channels. Repeating the equalization and decoding tasks on the same set of data and incorporating soft feedback from the decoder into the equalization process generally yields significant improvements in the BER [65]. This joint equalization and decoding technique requires the data stream to be encoded.

Transmitter Architecture

A binary data sequence, s_n of length N to be transmitted is convolutionally encoded, to produce a coded output, c_n. Typically throughout this thesis the code formatting polynomials in (4.3) are used

as per the global system for mobile (GSM) CS1-CS3 [52].

$$\begin{aligned} G0 &= 1 + D^3 + D^4 \\ G1 &= 1 + D^1 + D^3 + D^4 \end{aligned} \tag{4.3}$$

To ensure that errors appear random and to avoid long error bursts, an interleaver is used to randomize the encoded bits, x_n prior to transmission. The combination of the convolutional encoder, interleaver and channel represents a serial concatenated encoder as shown in Figure 4.6.

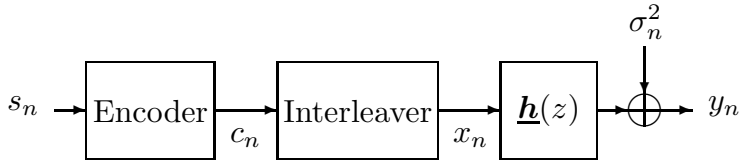

Figure 4.6: Transmitter section of the SBR2 system forming a serial concatenated encoder.

Receiver Architecture

The receiver structure is shown in Figure 4.7. It is assumed the channel coefficients $\boldsymbol{\lambda}_{ii}(z)$ are known to the receiver and do not vary in time within each block.

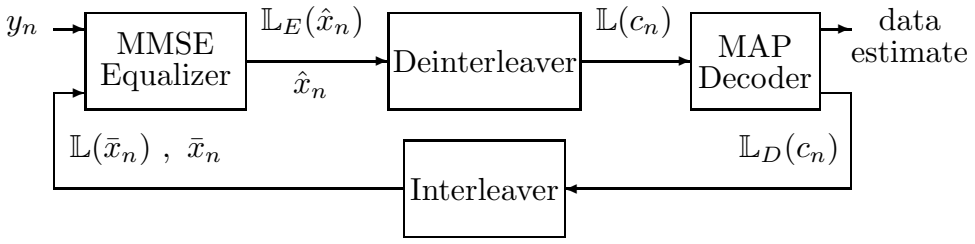

Figure 4.7: Receiver section of the SBR2 system.

The $\mathbb{L}$ operator $\mathbb{L}(x)$ is applied to quantities $x \in \{+1, -1\}$ and is given by

$$\mathbb{L}(x) \equiv \ln\left(P\left(x = +1\right)/P\left(x = -1\right)\right) \tag{4.4}$$

i.e. the log likelihood ratio (LLR).

MMSE Equalizer using A Priori Information

The MMSE equalizer computes estimates $\hat{x}_n$ of the transmitted symbols x_n from the received symbols y_n by minimizing the cost function $E\left\{|x_n - \hat{x}_n|^2\right\}$ [64] where $\hat{x}_n$ represents the soft output from the MMSE equalizer, and $E\{\cdot\}$ denotes the statistical expectation operator.

For a particular subchannel $\underline{\lambda}_{ii}(z)$ the channel is denoted as $h_0 + h_1 z^{-1}, \ldots, h_{L-1} z^{-(L-1)}$ where L represents the channel length. We only consider taps of $\underline{\lambda}_{ii}(z)$ that are greater than $\sigma^2/(M_r M_t)$ where σ^2 represents the noise variance. We set the length of the equalizer, M, to capture these taps of interest. The channel convolution matrix, $\boldsymbol{H}_c$ of dimensions $M \times (M + L - 1)$ takes the form:

$$\boldsymbol{H}_c = \begin{bmatrix} h_0 & h_1 & \ldots & h_{L-1} & 0 & \ldots & 0 \\ 0 & h_0 & h_1 & \ldots & h_{L-1} & \ldots & 0 \\ & & & \ddots & \ddots & \ddots & \ddots \\ 0 & \ldots & 0 & h_0 & h_1 & \ldots & h_{L-1} \end{bmatrix} \tag{4.5}$$

Let $\boldsymbol{h}_{c_M}$ denote the M^{th} column of $\boldsymbol{H}_c$ containing the most energy. For a single input MMSE equalizer this will always be the middle column. Assuming symbols are temporally uncorrelated, we write $E\left\{(\boldsymbol{x}_n - \bar{\boldsymbol{x}}_n)(\boldsymbol{x}_n - \bar{\boldsymbol{x}}_n)^H\right\}$ as a diagonal matrix $diag(\boldsymbol{v})$ where the n^{th} element of $\boldsymbol{v}$ is $v_n = 1 - \bar{x}_n^2$ and $\bar{x}_n$ denotes the interleaved soft estimates of the transmitted symbol from the MAP decoder output. The MMSE weight vector, $\boldsymbol{w}_n$ is given by [65] [64]:

$$\boldsymbol{w}_n = (\boldsymbol{H_c} \times diag(\boldsymbol{v}_n) \times \boldsymbol{H}_c^H + \sigma^2 \boldsymbol{I})^{-1} \boldsymbol{h}_{c_M} \tag{4.6}$$

The MMSE equalizer output $\hat{x}_n$ is used to obtain the difference between the posteriori and a prior LLR as follows:

$$\begin{aligned} \mathbb{L}_E(\hat{x}_n) &= \ln \frac{p\{x_n = +1|_{\hat{x}_n}\}}{p\{x_n = -1|_{\hat{x}_n}\}} - \ln \frac{p\{x_n = +1\}}{p\{x_n = -1\}} \\ &= \ln \frac{p\{\hat{x}_n|_{s_n=+1}\}}{p\{\hat{x}_n|_{s_n=-1}\}} \\ &= \frac{4\Re\{\hat{x}_n\}}{1 - \boldsymbol{h}_{c_M}^T \boldsymbol{w}_n} \end{aligned} \tag{4.7}$$

where $\Re\{\hat{x}_n\}$ denotes the real component of the quantity $\{\hat{x}_n\}$.

Unlike the Viterbi equalizer, the computational cost of the MMSE equalizer grows linearly with tap length, rather than exponentially. As a consequence, equalization of channels with 100 taps or greater of interest is entirely feasible, hence it perfectly suited for solving the delay spread introduced

in constant profile channels.

MAP Decoder

The maximum *a posteriori* (MAP) algorithm [66] computes the posteriori probability of symbols from Markov sources transmitted through discrete memoryless channels[1]. Since the output of a convolutional coder passed through the equalized frequency selective channel forms a Markov source the MAP algorithm can be used for maximum *a posteriori* probability decoding of convolutionally encoded code [67]. Unlike the Viterbi algorithm which minimizes the probability of selecting an incorrect path through the trellis, the MAP algorithm is optimal in terms minimizing the decoded BER [68]. For each transmitted symbol the MAP decoder generates a hard estimate (using thresholding) and a soft output, $\mathbb{L}(c_n)$ in the form of the *a posteriori* probability of the received sequence [31]. A short overview of the MAP algorithm now follows:

As with the Viterbi algorithm, the MAP algorithm covers the time period from time instant $t = 0$ to $t = \tau$, and the state sequence during is represented as $\boldsymbol{S} = (S_0, S_1, \ldots, S_{\tau-1}, S_\tau)$. The number of possible states is M_s. Given a received symbol sequence, $\boldsymbol{y}$ the MAP algorithm calculates for each decoded bit, u_t the probability that this bit was 1 or -1, equivalent to finding the *a posteriori* LLR $\mathbb{L}(u_t|\boldsymbol{y})$, given by

$$\mathbb{L}(u_t|\boldsymbol{y}) = \ln\left(\frac{P\left(u_t = +1|\boldsymbol{y}\right)}{P\left(u_t = -1|\boldsymbol{y}\right)}\right) \tag{4.8}$$

Assuming the previous state, denoted $S_{t-1} = s'$ and the present state, denoted $S_t = s$ are known in the trellis then u_t, i.e. the input bit that triggered the state transition can be determined. The received sequence $\boldsymbol{y}$ can be broken down into three constituent parts:

- α - probability of starting in the current state, S_{t-1}.
- γ - probability of a transition from state S_{t-1} to S_t.
- β - probability of ending in the state S_t.

Initially $\gamma_t^i(s', s)$ is calculated for $t = 1, 2, \ldots, \tau$, $i = 0, 1$ and for $s = 0, 1, \ldots, M_s$. i corresponds to the binary input triggering the transition. $\gamma_t^i(s', s)$ is given by

$$\gamma_t^i(s', s) = \exp\left(\frac{\left|\boldsymbol{x}_t - \boldsymbol{y}_t\right|^2}{2\sigma^2}\right) \tag{4.9}$$

where $\boldsymbol{x}_t$ denotes the modulated symbol in the trellis and σ^2 is the noise variance. It assumed that the start and end state of the sequence are known. This is achieved by flushing the state of the

[1] Also commonly referred to as the BCJR algorithm after its authors, Bahl, Cocke, Jelinek, and Raviv

convolutional encoder in the transmitter with either zeros or ones prior and post transmission. In this thesis, zeros have been used for flushing, hence $\alpha_0(0) = 1$ and $\alpha_0(s) = 0$ for $s \neq 0$ and $\beta_\tau(0) = 1$ and $\beta_\tau(s) = 0$ for $s \neq 0$. Although sub-optimum, prior knowledge of the start and end state of the sequence is not required for the MAP decoder to function. For this scenario the probability of all possible start and end states is equal, i.e. $\alpha_0(s) = \beta_\tau(s) = \frac{1}{M_s}$ for $s = 0, 1, \ldots, M_s - 1$.

It is now possible to iteratively calculate the values of α for $t = 1, 2, \ldots, \tau$, known as the forward recursion:

$$\alpha_t(s) = \sum_{s'=0}^{M_s} \sum_{i=0}^{i=1} \alpha_{t-1}(s') \gamma_t^i(s', s) \tag{4.10}$$

Similarly the backward recursion iteratively calculate the values of β for $t = \tau - 1, \ldots, 1, 0$.

$$\beta_t(s) = \sum_{s'=0}^{M_s} \sum_{i=0}^{i=1} \beta_{t+1}(s') \gamma_{t+1}^i(s, s') \tag{4.11}$$

Equations (4.10) and (4.11) can be calculated independently in parallel to reduce overall computational time. The LLR $\mathbb{L}(u_t|\boldsymbol{y})$ is given as [68, 31]:

$$\mathbb{L}(u_t|\boldsymbol{y}) = \ln \left(\frac{\sum_{(s',s) \Rightarrow u_t+1} \alpha_{t-1}(s') \ \gamma_t^1(s', s) \ \beta_t(s)}{\sum_{(s',s) \Rightarrow u_t-1} \alpha_{t-1}(s') \ \gamma_t^0(s', s) \ \beta_t(s)} \right) \tag{4.12}$$

A full description of the operation of the MAP algorithm is available in [66].

Algorithm 4.2 Summary of the MAP algorithm

Set initial values for α_0 and β_τ.
$t = 0, \ S_0 = 0, \ \mu_0^{(x)}(S_0 = 0) = 0, \ \mu_0^{(x)}(S_0 \neq 0) = \infty$
for $t = 1$ to $t = \tau$, $s = 0$ to $M_s - 1$ and $i = 0, 1$ **do**
  $\gamma_t^i(s', s) = \exp\left(\frac{|\boldsymbol{x}_t - \boldsymbol{y}_t|^2}{2\sigma^2}\right)$
end for
Calculate Forward Recursion
for $t = 1$ to $t = \tau$ and $s = 0$ to $M_s - 1$ **do**
  $\alpha_t(s) = \sum_{s'=0}^{M_s} \sum_{i=0}^{i=1} \alpha_{t-1}(s') \gamma_t^i(s', s)$
end for
Calculate Backward Recursion
for $t = \tau - 1$ to 0 and $s = 0$ to $M_s - 1$ **do**
  $\beta_t(s) = \sum_{s'=0}^{M_s} \sum_{i=0}^{i=1} \beta_{t+1}(s') \gamma_{t+1}^i(s, s')$
end for
Calculate Log-Likelihood Ratios
for $t < \tau$ **do**
  $\mathbb{L}(u_t|\boldsymbol{y}) = \ln \left(\frac{\sum_{(s',s) \Rightarrow u_t+1} \alpha_{t-1}(s') \ \gamma_t^1(s', s) \ \beta_t(s)}{\sum_{(s',s) \Rightarrow u_t-1} \alpha_{t-1}(s') \ \gamma_t^0(s', s) \ \beta_t(s)} \right)$
end for

Interleaver Design

When processing soft information as an input to the MMSE equalizer or the MAP decoder, it is assumed that the soft information about a given bit is an independent piece of information [65]. This allows sub-optimal algorithms to be used reducing computational complexity in both the equalizer and decoder. If the decoder formulates its soft information about a given bit, based on soft information provided to it from the equalizer about exactly the same bit, then the equalizer cannot consider this information to be independent of its channel observations [65]. This in effect creates a feedback loop between the two constituent parts of the turbo equalizer, with the MMSE equalizer informing the MAP decoder about a given bit, and then the MAP decoder simply re-informing the MMSE equalizer with information it already knows.

In a practical sense this can lead to the turbo equalizer becoming stuck in local minima. Interleaving prevents this from occurring, such that a large number of iterations can be carried out before cyclic behavior becomes apparent. By increasing the number of iterations in the joint equalization and decoding process, BER performance can be significantly improved with the obtainable capacity of the channel becoming close to that of the channels Shannon limit [31].

To this end a Pseudo-Random or S-Random interleaver [69] has been used. The S-Random interleaver interleaves a block of bits while ensuring that the minimum depth, i.e. the distance between two bits after interleaving that were adjacent prior to interleaving is of a specified value. The greater the depth, the greater the performance of the turbo equalizer. However depth is limited by both the number of bits in each block to be interleaved and computational time for interleaver design. To this end in the subsequent simulations an S-Random interleaver with a depth of 28 bits has been used to gain maximum performance. The interleaver has been designed using an algorithm available in the Coded Modulated Library [70].

4.5 Dominant Mode Performance

We are now in a position to assess the performance of the dominant mode, $\underline{\boldsymbol{\lambda}}_{11}(z)$ in a PMSVD MIMO system. A wide sense stationary (WSS) situation where the channel coefficients have been assumed to be unchanged within each data block, but allowed to change between data blocks according to a zero mean complex circular Gaussian distribution has been considered. WSS implies that the second-order time statistics of the channel are stationary and is justified in wireless channels over short periods [3]. The number of time slots of the channel, $N = 1024$. The bit error rate has been computed for 1000 Monte Carlo simulations.

4.5.1 Exponentially Decaying Channels

A transmitter antenna selection (TAS) scheme has been used as a TDMA benchmark. TAS operates by transmitting exclusively through the best antenna that results in the highest possible SNR at the receiver, creating a single-input multi-output (SIMO) subset of the MIMO system. The received signal at each antenna is then fed into a multiple-input Viterbi equalizer. Identical channels have been used for SBR2 and TAS. The modulation scheme used is BPSK for evaluation purposes but extension to larger constellations is straightforward. The total transmission power budgets for SBR2 and TAS are identical. Figures 4.8 and 4.9 show the BER performance of the TAS and SBR2 schemes for a range of MIMO orders. Diversity gain manifests itself in increasing the magnitude of the slope of the BER curve [3], clearly visible in the dramatic improvement in BER performance in a 2×2 MIMO system over a SISO system for both schemes. For example a 10dB gain in SNR is observed at BER 10^{-3} for the SBR2 scheme.

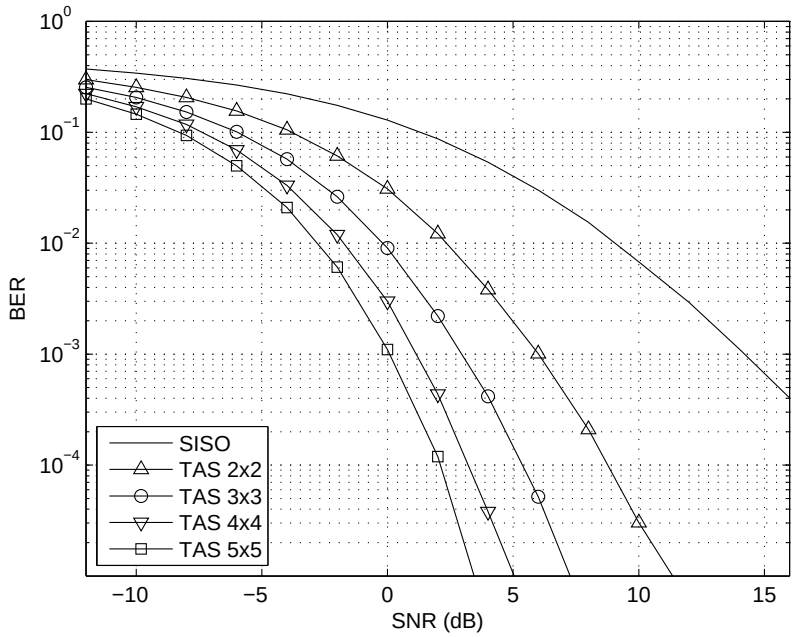

Figure 4.8: Average BER results for TAS scheme for a range of MIMO orders, $L = 5$, with exponentially decaying elements.

Figure 4.10 directly compares TAS and dominant mode SBR2 BER performance for a range of MIMO channels and clearly shows the benefit of the SBR2 algorithm. BER performance is far superior to the TAS scheme, for example a 4dB gain in SNR is observed at BER 10^{-3} for a 5×5 MIMO channel, making SBR2 potentially highly suitable for TDMA based MIMO wireless systems where decoding continuous streams of data is required. Note the very low SNR range is due to the diversity gain of

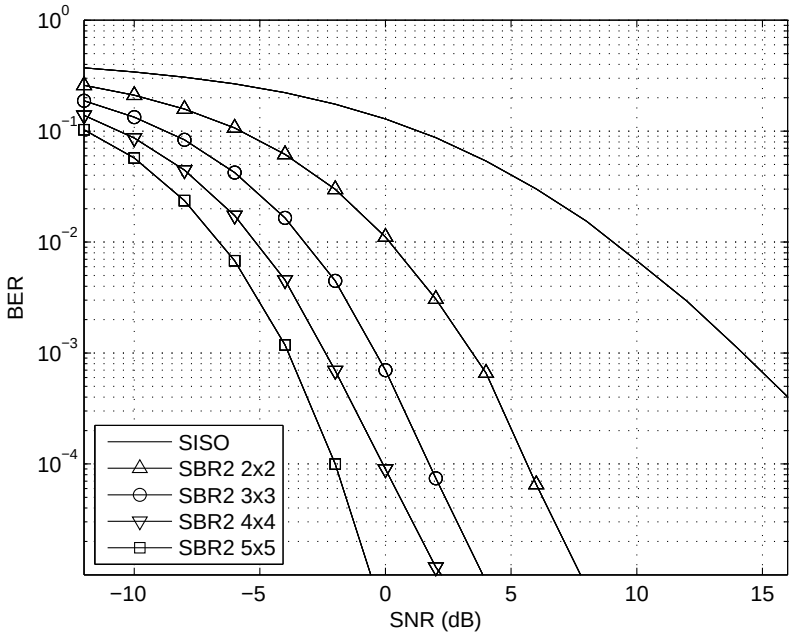

Figure 4.9: Average BER results for dominant mode SBR2 scheme for a range of MIMO orders, $L = 5$, with exponentially decaying elements.

the 5×5 MIMO system.

The proposed SBR2 scheme has also been compared with an MIMO-OFDM SVD scheme. The number of bits sent in each block, $N = 1024$. The total transmission power budgets for SBR2 and MIMO-OFDM SVD are identical. The MIMO-OFDM scheme operates almost identically to the MIMO-OFDM scheme described in Chapter 2, with the addition of the SVD operation being carried out within each individual narrowband tone. Hence for $\boldsymbol{H}_n[k]$, the frequency response of the narrowband MIMO channel corresponding to the k^{th} tone of the MIMO channel matrix $\underline{\boldsymbol{H}}(z)$, the SVD of $\boldsymbol{H}_n[k]$ is calculated. As with the SBR2 scheme only the dominant mode within each narrowband will be chosen for transmission.

Figure 4.11 shows that both the SBR2 and MIMO-OFDM SVD methods perform identically. OFDM transmission incurs on average a loss in spectral efficiency of $(L-1)/(N+L-1)$ on account of the cyclic prefix. If $N \gg L$, this loss is negligible [3] so this has not been considered. Figure 4.12 shows the frequency response of the dominant SBR2 and MIMO-OFDM SVD mode for one of the channels used. As can be seen both systems have a virtually identical frequency response. The only slight difference in performance is due to the trimming of the polynomial matrices within the SBR2 algorithm [50]. This does not occur within the MIMO-OFDM SVD system as the DFT and SVD operations and inherently lossless. Therefore the proposed time domain SBR2 approach provides a

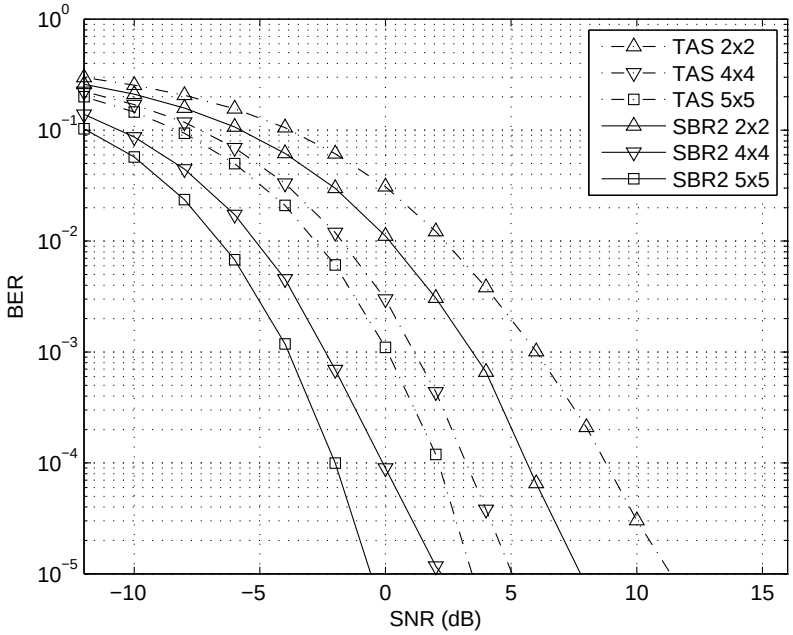

Figure 4.10: Average BER results for dominant mode SBR2 and TAS schemes for a range of MIMO orders, $L = 5$, with exponentially decaying elements.

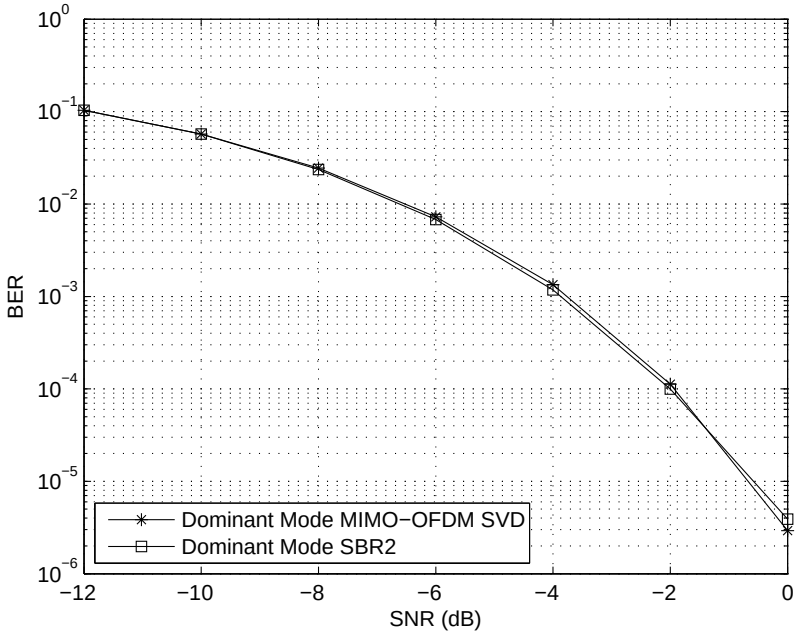

Figure 4.11: Average BER results for dominant mode SBR2 and MIMO-OFDM SVD schemes for a 5×5 MIMO channel, $L = 5$, with exponentially decaying elements.

similar performance as the discrete frequency domain based MIMO-OFDM system. The proposed approach however is more generic so that MIMO wireless systems based on TDMA could also benefit.

Additionally, unlike DFT based decompositions (which require storage of data and also incur the associated block delay at the receiver), the proposed scheme operates using spatial-temporal filters in the time domain, hence it is more suitable for decoding continuous streams of data without requiring storage of signals for DFTs and unnecessary block delays.

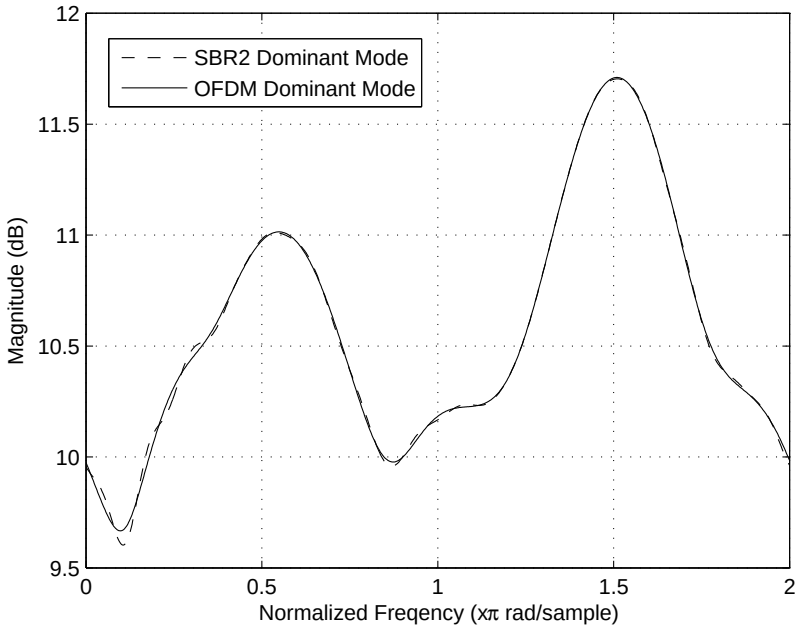

Figure 4.12: Frequency response of the dominant mode for SBR2 and MIMO-OFDM SVD for a 5×5 MIMO channel, $L = 5$,with exponentially decaying elements.

4.5.2 Constant Profile Channels

The BER performance of SBR2 for constant power delay profile channels is now shown. Again the dominant mode of SBR2 has been compared with a TAS scheme as a TDMA benchmark. For TAS the received signal at each antenna is fed into a multiple-input iterative MMSE equalizer and the equalization and decoding scheme is identical to the SBR2 system. The modulation scheme is BPSK. The number of time slots of the channel, $N = 2048$. The bit error rate has been computed for 1000 Monte Carlo simulations. Figures 4.13 and 4.14 show the BER performance of the TAS and SBR2 schemes for a range of MIMO orders.

Again the dramatic improvement in BER performance in a 2×2 MIMO system over a SISO system is clearly visible for both schemes, with a 10dB gain in SNR observed at BER 10^{-3} for the SBR2 scheme. Figure 4.15 directly compares TAS and dominant mode SBR2 BER performance for a 5×5 MIMO channel and clearly shows the benefit of the SBR2 scheme. BER performance is far superior

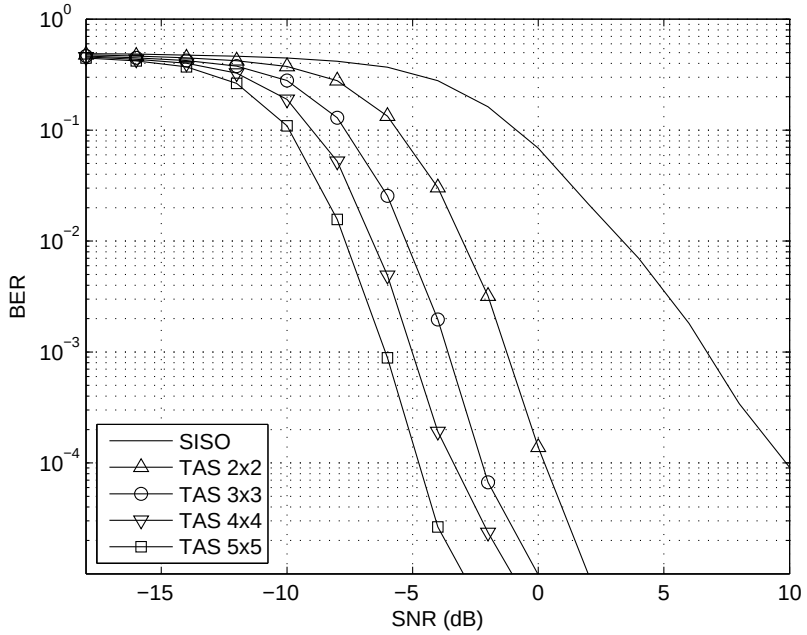

Figure 4.13: Average BER results for TAS scheme for a range of MIMO orders, $L = 5$, with constant power profile.

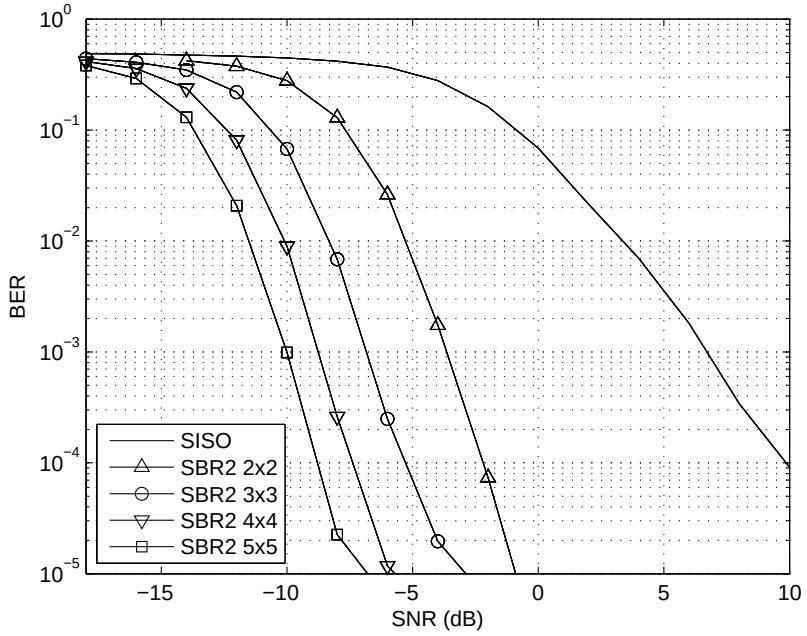

Figure 4.14: Average BER results for dominant mode SBR2 scheme for a range of MIMO orders, $L = 5$, with constant power profile.

to the TAS scheme, again with a 4dB gain in SNR at BER 10^{-3}.

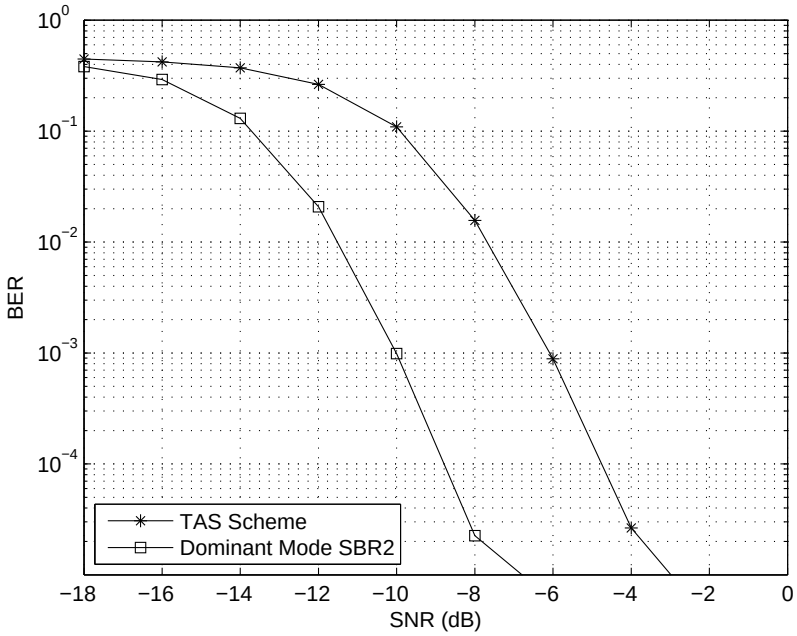

Figure 4.15: Average BER results for dominant mode SBR2 and TAS schemes for a 5×5 MIMO channel, $L = 5$, with constant power profile.

4.6 Dominant Mode Performance with Channel Estimation Error

The scenario is now considered where the receiver has imperfect channel knowledge. $\underline{\boldsymbol{H}}(z)$ has been estimated using an LSE channel estimator with a training sequence of length $N_t = 50$. Only an $M_r = M_t = 5$ frequency selective MIMO system has been considered. Again, the MIMO channel is assumed to be WSS. The bit error rate has been computed for 1000 Monte Carlo simulations. CSI error in the PMSVD implementation will result in $\underline{\boldsymbol{\Lambda}}(z)$ being only approximately diagonal. Therefore if multiple modes of $\underline{\boldsymbol{\Lambda}}(z)$ are used simultaneously for transmission, orthogonality between modes will be lost and they will interfere with each other. As we are only using the dominant for transmission in this scenario, CSI error will cause the transmit and receive beams to be misaligned. This results in an overall reduced gain of the dominant spatial subchanel used. For an OFDM system, CSI will result in co-channel interference between all subcarriers leading to decreased system

4.6.1 Exponentially Decaying Channels with Channel Estimation Error

Figure 4.16 compares the proposed SBR2 based PMSVD scheme with a TAS scheme as a TDMA benchmark. Again PMSVD provides a significant improvement in BER performance, with a 2dB gain

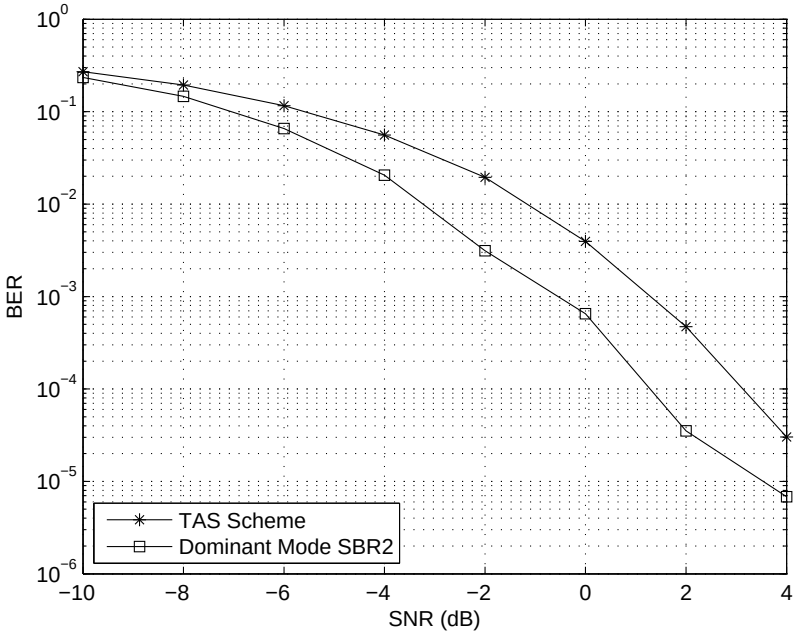

Figure 4.16: Average BER results for dominant mode SBR2 and TAS schemes for a 5×5 MIMO channel, $L = 5$, with exponentially decaying elements and training sequence of length $N_t = 50$.

in SNR observed at BER 10^{-3} for the SBR2 scheme.

Figure 4.17 compares the BER performance of the dominant mode of the SBR2 scheme with that of a MIMO-OFDM system. Forming the input para-Hermitian matrix to the SBR2 algorithm from an inaccurate estimate of the channel and its paraconjugate effectively results in squaring the errors in the channel estimate. Hence the performance of the SBR2 scheme is degraded and is now outperformed by the MIMO-OFDM scheme. For example at BER 10^{-3} the MIMO-OFDM scheme has a 1.5dB gain in SNR.

Figure 4.18 compares the BER performance of the dominant MIMO-OFDM SVD scheme against PMSVD calculated by PMQRD. As PMSVD by PMQRD operates directly on the channel matrix it is more robust to errors in the CSI than the SBR2 approach. Hence the performance of the PMQRD by PMSVD scheme is identical to that of MIMO-OFDM. Therefore the proposed time domain PMSVD approach still provides a similar performance to that of the discrete frequency domain based MIMO-OFDM system, even in the presence of incorrect CSI. This validates the robustness of the proposed PMSVD approaches.

4.6.2 Constant Profile Channels with Channel Estimation Error

Again this work is repeated for BER performance of SBR2 for constant power delay profile random

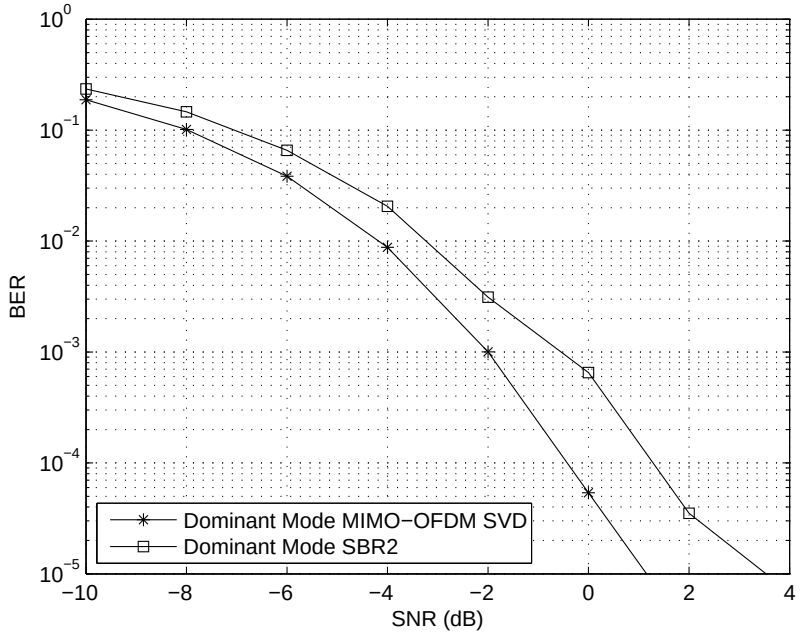

Figure 4.17: Average BER results for dominant mode SBR2 and MIMO-OFDM SVD schemes for a 5×5 MIMO channel, $L = 5$, with exponentially decaying elements and training sequence of length $N_t = 50$.

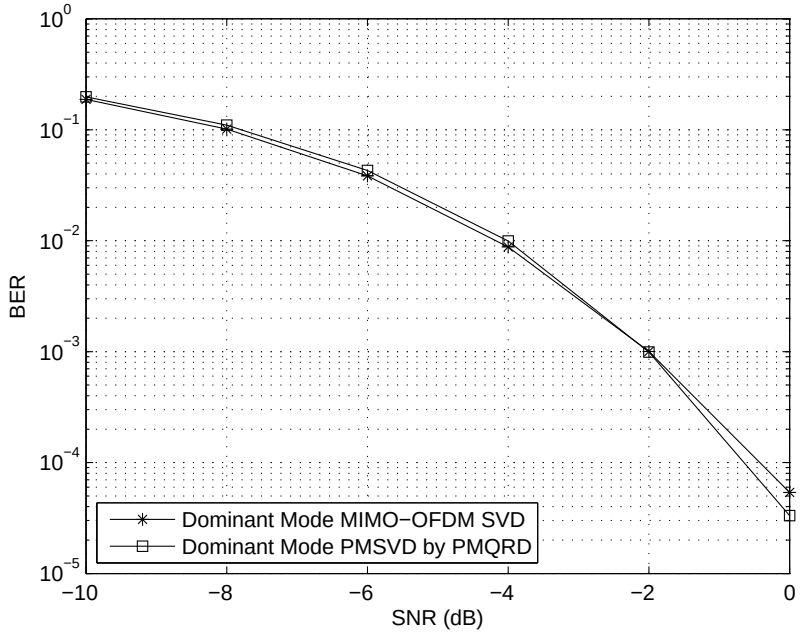

Figure 4.18: Average BER results for dominant mode MIMO-OFDM SVD and PMSVD by PMQRD schemes for a 5×5 MIMO channel, $L = 5$, with exponentially decaying elements and training sequence of length $N_t = 50$.

channels with CSI error. The dominant mode of SBR2 has been compared with a TAS scheme as a TDMA benchmark. Once again a multiple-input iterative MMSE equalizer is used and the equalization and decoding scheme is identical to that of the SBR2 system. Figure 4.19 compares the TAS, SBR2 and PMSVD by PMQRD schemes. As expected the BER performance of the PMSVD schemes is significantly greater than that of TAS, for example a gain in SNR of 3dB at BER 10^{-3}. Although the PMSVD by PMQRD is more robust to CSI error, both PMSVD schemes perform near identically. This is due to the robustness of the turbo equalization approach, and the introduction of error correction coding within the MIMO system.

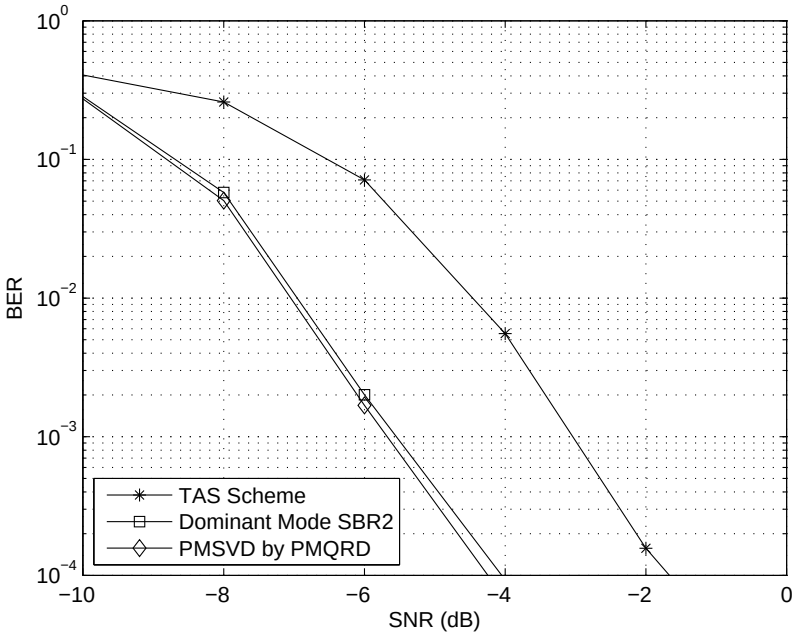

Figure 4.19: Average coded BER results for TAS, dominant mode SBR2 and PMSVD by PMQRD schemes for a 5×5 MIMO channel, $L = 5$, with constant power profile and training sequence of length $N_t = 50$.

4.6.3 Computational Complexity Analysis

Previously in Chapter 3 it was stated that the computational complexity of the SBR2 algorithm was significantly less than that of the operation of the equalization and decoding schemes used and was therefore suitable for use in a MIMO communications system. Key results from the MATLAB profiler are now presented to backup this claim. As the turbo equalization approach for constant profile channels is significantly more complex than that of the Viterbi approach for exponential power delay profile channels only constant profile channels have been considered. Table 4.1 shows the computational time of the SBR2, PMSVD by PMQRD, MAP Decoder and MMSE Equalizer components of the MIMO

communications simulation for a range of SNR's, averaged over 50 Monte Carlo simulations.

	SNR - 6dB	**SNR - 4dB**	**SNR - 2dB**
Function	*Total Time (s)*	*Total Time (s)*	*Total Time (s)*
PMSVD by SBR2	19.46	19.00	21.98
MAP Decoder	6.58	6.59	6.55
PMSVD by PMQRD	4.50	4.59	4.06
MMSE Equalizer	0.90	1.02	1.21

Table 4.1: Computational complexity analysis for 5×5 MIMO channel with constant power profile and polynomial length $L = 5$.

As expected the SBR2, PMSVD by PMQRD and MAP Decoder elements' computational time is independent of SNR. In this scenario imperfect CSI has simulated, again with a training sequence of length $N_t = 50$. Hence as the CSI is dependent on the SNR the time required for PMSVD fluctuates. The MMSE equalizer is of a minimum length of 10 taps, and only considers taps with an absolute value greater than $\frac{\sigma^2}{M_r \times M_t}$. Therefore increasing SNR also increases MMSE equalizer complexity, resulting in the steady increase in computational time.

From table 4.1 it is clear that PMSVD by SBR2 is the most computationally complex operation. As PMSVD by PMQRD outperforms the SBR2 approach to PMSVD in terms of BER and is more robust to CSI error, this result is inconsequential. The key result is that the MAP Decoding operation takes longer than that of PMSVD by PMQRD, and that MAP Decoders of comparable complexity are already implemented in existing communication systems. Again the key point to emphasize is that the computational complexity of the MAP Decoder is independent of SNR and that at -2dB the PMSVD by PMQRD system provides both an acceptable level of BER performance and reduced computational time than the MAP Decoder. Therefore it is not unreasonable to assume that the PMSVD by PMQRD approach could be implemented in real-time with the current generation of hardware in mobile devices.

Is is also important to remind ourselves that both PMSVD algorithms are still currently in the research stage. A MATLAB implementation is highly suited for creating a proof of concept reference model, as the MATLAB language enables rapid code development and testing, with the caveat of the trade-off in efficiency of the code generated. The computational speed can be significantly increased by implementing the algorithm in a lower level language, such as C++. Furthermore with a fixed application and clearly defined hardware constraints a tailor made efficient implementation of the PMSVD would be possible. For example, currently in MATLAB the results presented are simulated using default double-precision floating point numerical presentation. In the real world, with limited accuracy in the CSI, single-precision representation could be used without decreasing system

performance, but significantly reducing computational time and memory storage requirements.

4.7 Conclusions

In this chapter the PMSVD has been applied to frequency selective MIMO channels. The proposed technique decomposes a MIMO frequency selective channel into a number of SISO frequency selective channels yielding multiple spatial modes for spatial multiplexing. The performance of the dominant mode has been compared with that of a conventional transmit antenna selection scheme and found to provide superior diversity performance. Comparing the system to a conventional MIMO-OFDM SVD approach results in identical system BER performance.

The robustness of the PMSVD approach has been validated with the inclusion of results demonstrating system performance in the presence of the CSI error. For this scenario the numerical operation of the SBR2 algorithm, i.e. operating on a para-Hermitian input matrix limits the accuracy of the PMSVD approach. This problem is mitigated using the PMSVD by PMQRD algorithm. Therefore the work of Pauraj, Nabar and Gore [3] has been successfully extended to the frequency selective broadband scenario, confirming the benefits of PMSVD for MIMO communications.

The proposed PMSVD scheme is most suitable for TDMA based systems and enables a wider range of access schemes not possible with a MIMO-OFDM SVD approach, where the broadband channel can be split into a set of narrow bands. In particular for frequency selective channels with exponential power delay profile, a sliding window Viterbi algorithm can be used for channel equalization. Sliding window Viterbi computes the maximum likelihood path based on a set number of previous samples, and can operate on continuous streams of data. The PMSVD approach therefore is more suitable for decoding continuous streams of data without requiring storage of signals for DFT's and incurring block delays inherent in a MIMO-OFDM scheme.

In the next chapter the equalization approaches are applied to a PMQRD based MIMO communications system, where significant benefits of the time domain PMQRD approach are found to provide superior BER performance over a MIMO-OFDM QR based system.

Chapter 5

Diversity Techniques using PMQRD

5.1 Introduction

As demonstrated in Chapter 2, for a frequency flat MIMO channel the QR decomposition can be applied at the receiver to reduce the MIMO channel equalization problem to a set of decision feedback based single channel equalization problems. In this chapter, the PMQRD from Chapter 3 is applied to frequency selective MIMO channels to exploit the benefits of QR decomposition in a doubly selective scenario. Recalling from 3, the PMQRD of the noise free multipath MIMO channel $\underline{\boldsymbol{H}}(z)$ is given as:

$$\underline{\boldsymbol{H}}(z) = \underline{\boldsymbol{Q}}(z)\ \underline{\boldsymbol{R}}(z) \tag{5.1}$$

Propagating a set of source signals through $\underline{\boldsymbol{H}}(z)$ and filtering them with $\underline{\widetilde{\boldsymbol{Q}}}(z)$ at the receiver allows exploitation of the upper triangular structure of $\underline{\boldsymbol{R}}(z)$ to reduce the MIMO channel equalization problem to a set of single channel equalization problems. As with PMSVD, the single channels produced by PMQRD are FIR in nature and additional processing is required at the receiver to overcome the delay spread. To this end the turbo equalization approach used in the previous chapter is applied once again. To further exploit the spatial multiplexing provided by PMQRD and maximize the diversity gain afforded by the MIMO channel, three types of encoder architecture based on Bell Laboratories Layered Space Time (BLAST) encoding have been implemented. Each BLAST based scheme is evaluated against an identical MIMO-OFDM QR based scheme.

The robustness of the proposed scheme to CSI error is again considered and finally a single carrier based MIMO-OFDM scheme is implemented in an attempt to match the performance benefits of the proposed PMQRD scheme using a frequency domain equalization approach.

5.2 The Application of PMQRD to MIMO Channel Equalization

Without loss of generality a frequency selective MIMO system is considered of equal number transmit and receive antennas, i.e. $M_r = M_t$. A set of source signals of length N, $\boldsymbol{s}(t) \in \mathbb{C}^{M_t \times 1}$ for

$t \in \{0, 1, \ldots, T-1\}$ are propagated through the MIMO wireless channel, $\underline{\boldsymbol{H}}(z)$, received and filtered with $\underline{\widetilde{\boldsymbol{Q}}}(z)$, as shown in Figure 5.1.

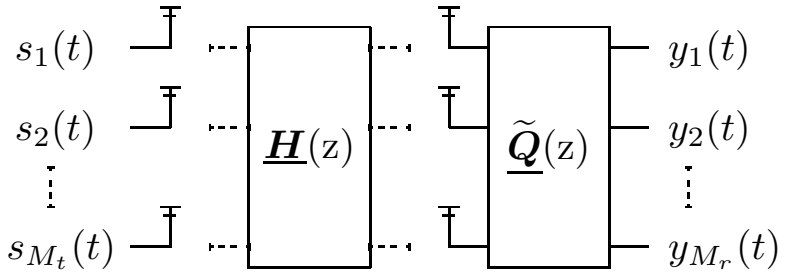

Figure 5.1: PMQRD system diagram.

The set of received signals, $\boldsymbol{y}(t)$ are expressed as (5.2) where $\boldsymbol{n}$ denotes an additive Gaussian noise process with variance $\sigma^2 \boldsymbol{I}_{M_r}$.

$$\underline{\boldsymbol{y}}(z) = \underline{\widetilde{\boldsymbol{Q}}}(z)\ \underline{\boldsymbol{H}}(z)\ \underline{\boldsymbol{s}}(z) + \underline{\widetilde{\boldsymbol{Q}}}(z)\ \boldsymbol{n}(z) \tag{5.2}$$

From (5.1), the convolutive mixing model can be rewritten as (5.3), where $\underline{\boldsymbol{n}}'(z) = \underline{\widetilde{\boldsymbol{Q}}}(z)\ \underline{\boldsymbol{n}}(z)$.

$$\underline{\boldsymbol{y}}(z) = \underline{\boldsymbol{R}}(z)\ \underline{\boldsymbol{s}}(z) + \underline{\boldsymbol{n}}'(z) \tag{5.3}$$

5.2.1 Iterative Interference Cancellation

As with QR decomposition for flat fading channels, by exploiting the upper triangular structure of the polynomial matrix $\underline{\boldsymbol{R}}(z)$, the MIMO channel problem can now be transformed into a set of M_r equalization problems using back substitution. The M_t^{th} source signal is expressed as (5.4)

$$\underline{\boldsymbol{y}}_{M_r}(z) = \underline{\boldsymbol{r}}_{M_r M_r}(z)\ \underline{\boldsymbol{s}}_{M_t}(z) + \underline{\boldsymbol{n}}'_{M_r}(z) \tag{5.4}$$

Once $\boldsymbol{s}_{M_r}$ is retrieved its contribution to $\boldsymbol{y}_{M_r-1}$ is canceled as follows

$$\underline{\boldsymbol{y}}_{M_r-1}(z) - \underline{\boldsymbol{r}}_{M_r-1 M_r}(z)\ \underline{\boldsymbol{s}}_{M_t}(z) = \underline{\boldsymbol{r}}_{M_r-1 M_r-1}(z)\ \underline{\boldsymbol{s}}_{M_t-1}(z) + \underline{\boldsymbol{n}}'_{M_r-1}(z) \tag{5.5}$$

which again is a single channel equalization problem. Therefore the i^{th} single channel equalization

problem can be formulated as

$$\underline{\boldsymbol{y}}_i(z) - \sum_{j=i+1}^{M_r} \underline{\boldsymbol{r}}_{ij}(z)\ \underline{\boldsymbol{s}}_j(z) = \underline{\boldsymbol{r}}_{ii}(z)\ \underline{\boldsymbol{s}}_i(z) + \underline{\boldsymbol{n}}'_i(z) \tag{5.6}$$

providing the streams $\underline{\boldsymbol{s}}_{i+1}(z), \ldots, \underline{\boldsymbol{s}}_{M_t}(z)$ have been previously recovered.

5.3 Channel Model

In these simulations a MIMO system with three antennas at the transmitter and receiver has been considered. The temporal length, L of the channel between each transmitter and receiver is five. The channel has a constant power delay profile with equal average gain for each tap. Channels with exponential power delay profile have also been simulated and similar performance results for these channels as presented here can be found in appendix B.

5.4 Horizontal BLAST Encoding

Horizontal Bell Laboratories Layered Space Time (H-BLAST) [15] is a sub-optimal encoding architecture used to simplify receiver design and attains a maximum diversity order of M_r as any given substream is transmitted from only one transmit antenna and received by M_r antennas [3]. The transmitter architecture is shown in Figure 5.2.

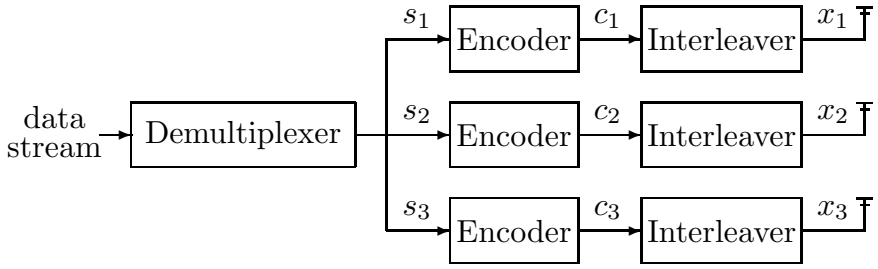

Figure 5.2: H-BLAST transmitter architecture.

The data stream is first demultiplexed into three substreams, $\boldsymbol{s}_1, \boldsymbol{s}_2, \boldsymbol{s}_3$. Each substream is then independently convolutionally encoded, interleaved and symbol mapped prior to transmission. Once again the code formatting polynomials in (4.3) as per GSM CS1-CS3 [52] have been used.

To ensure that errors appear random and to avoid long error bursts, an interleaver is used to randomize the encoded bits prior to transmission. An S-Random interleaver with a depth of 28 bits has been used to gain maximum performance [70].

5.4.1 H-BLAST Receiver Design

The received signals are filtered with $\underline{\widetilde{\boldsymbol{Q}}}(z)$ as shown in Figure 5.1, yielding the received substreams, y_1, y_2, y_3. Each substream is turbo equalized prior to the application of the iterative interference cancellation scheme previously described.

Algorithm 5.1 Summary of the H-BLAST receiver.

Receive and **filter** streams with $\underline{\boldsymbol{Q}}(z)$.
for $i = Mr : -1 : 1$ **do**
  Formulate channel equalization problem
  $\boldsymbol{y}_i - \sum_{j=i+1}^{M_r} \underline{\boldsymbol{r}}_{ij}(z)\ \boldsymbol{x}_j = \underline{\boldsymbol{r}}_{ii}(z)\ \boldsymbol{x}_i + \boldsymbol{n}'_i$
  for Turbo equalize i^{th} stream **do**
    Calculate soft estimate of transmitted signal, $\boldsymbol{x}_i$ via MMSE equalizer.
    De-interleave and calculate $\boldsymbol{c}_i$.
    Calculate hard estimate of transmitted signal, $\boldsymbol{s}_i$ and updated soft estimate of $\boldsymbol{c}_i$ via MAP decoder.
    Interleave $\boldsymbol{c}_i$ to form $\boldsymbol{x}_i$.
  end for
end for
Multiplex streams to obtain original data stream.

5.4.2 H-BLAST Results

A wide-sense quasi stationary (WSQS) situation has been considered. The bit error rate has been computed for 1000 Monte Carlo simulations. The modulation scheme used is BPSK for evaluation purposes but extension to large constellations is straightforward. The number of time slots of the channel, $N = 2048$. Initially it is assumed the receiver has perfect channel knowledge.

A MIMO-OFDM QR scheme has been used as a benchmark. As with MIMO-OFDM SVD, the frequency selective channel is decomposed into N orthogonal frequency flat MIMO channels. The data stream undergoes the same H-BLAST encoding process as the PMQRD based scheme prior to application of OFDM. The standard QR decomposition is then applied with each narrowband tone. The iterative cancellation within the receiver is performed on each tone individually and finally a Viterbi decoder is used to remove the error correction coding. Again as $N \gg L$ the negligible loss in spectral efficiency has not been considered.

Figure 5.3 directly compares the proposed PMQRD and MIMO-OFDM QR schemes. BER performance of PMQRD is far superior to the MIMO-OFDM QR scheme, for example a 5dB gain in SNR is observed at BER 10^{-3}. For a MIMO-OFDM QR scheme, the information in each individual transmitted symbol is constrained to a single narrowband tone. Figure 5.4 shows the typical frequency response for the SISO channel $\underline{\boldsymbol{R}}_{33}(z)$. Individual tones may have poor gains due to the frequency selective nature of the MIMO channel, resulting in degraded system performance. However in the

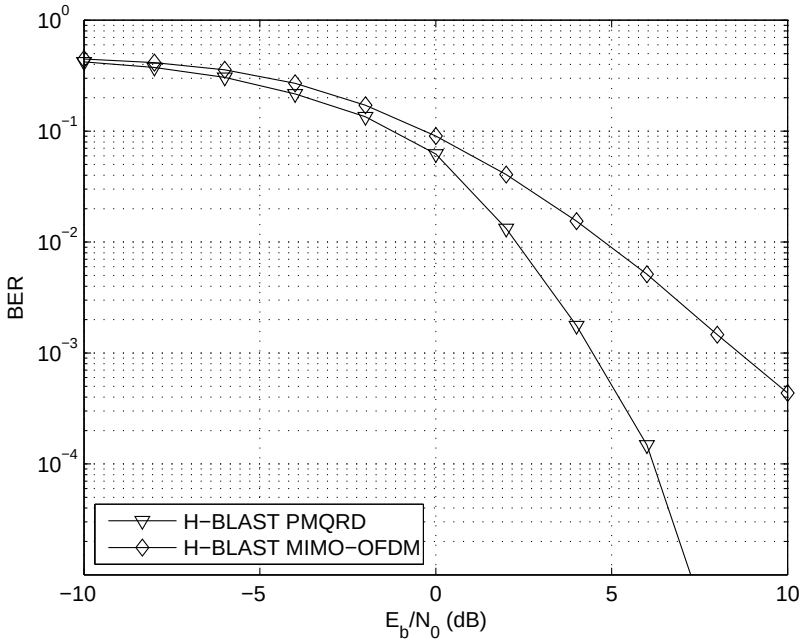

Figure 5.3: Average coded BER results for H-BLAST PMQRD and MIMO-OFDM QR schemes for a 3×3 MIMO channel, $L = 5$, with constant power profile.

PMQRD based system the information in each symbol is spread across the entire frequency bandwidth, making the system more robust to frequency selectivity, resulting in superior performance. This makes PMQRD highly suitable for MIMO-QR based applications where the transmitter has no prior channel knowledge, for example digital video broadcasting.

5.4.3 H-BLAST Optimal Detection Ordering

The performance of the iterative interference cancellation scheme is affected significantly by the order in which the components of $\boldsymbol{x}$ are detected. An optimal detection ordering (ODO) scheme can significantly improve system performance. This is achieved by swapping the columns of $\underline{\underline{\boldsymbol{H}}}(z)$ and performing the PMQRD. A permutation of the columns of $\underline{\underline{\boldsymbol{H}}}(z)$ exists such that $\|\boldsymbol{r}_{3,3}\|_F$ is maximal. Wolniansky *et al* have shown [71] that for a frequency flat channel $\boldsymbol{H}$, the column permutation of $\boldsymbol{H}$ where maximizing $\|r_{i+1,i+1}\|$ given that $\|r_{i,i}\|$ is already maximal yields the order of optimum detection.

For a frequency selective MIMO scenario this amounts to finding the column permutation of $\underline{\underline{\boldsymbol{H}}}(z)$ where maximizing $\|\boldsymbol{r}_{i+1,i+1}\|_F$ given that $\|\boldsymbol{r}_{i,i}\|_F$ is already maximal. This ensures that for the M_r^{th} equalized stream, the best possible estimate of the M_t^{th} transmitted signal is obtained (assuming $M_r = M_t$). Any errors present in the estimate of $\boldsymbol{s}_{M_t}$ will lead to sub-optimum iterative cancellation of the

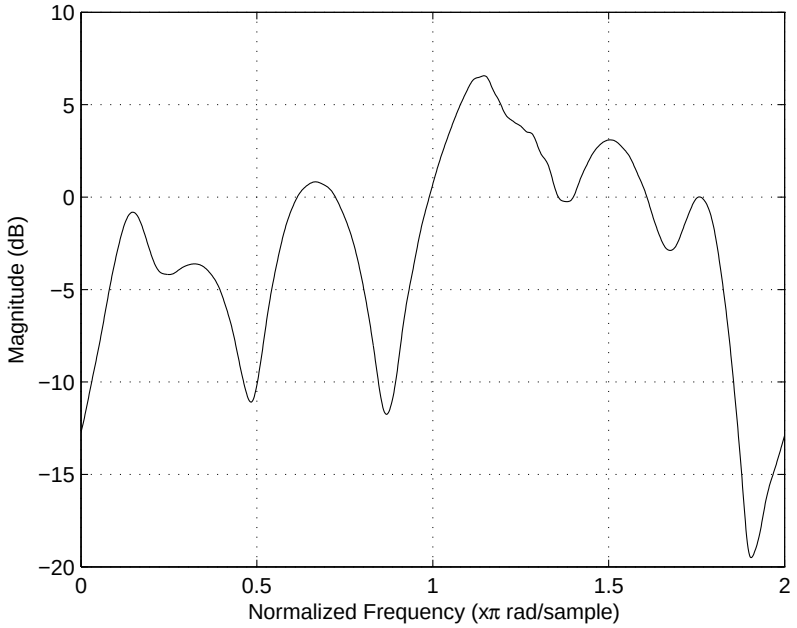

Figure 5.4: Typical frequency response of the SISO channel $\underline{\boldsymbol{R}}_{33}(z)$ obtained by MIMO-OFDM QR for a 3×3 MIMO channel, $L = 5$ with constant power profile.

subsequent substreams. Even for a modest order MIMO system this propagation of errors will lead to significant performance degradation. Hence maximizing the Frobenius norms in this manner minimizes the likelihood of error propagation within the iterative cancellation scheme. Wolninansky *et al* simply use a brute force approach to compute the optimum column permutation of $\underline{\boldsymbol{H}}(z)$ [71]. Calculating every possible column permutation is only possible for a low order MIMO system where the additional computational cost is relatively inexpensive, even if it must be carried out individually within each narrowband tone, as per a MIMO-OFDM QR ODO scheme. However this quickly becomes infeasible for modest order MIMO systems. Wubben *et al* [72] have developed a sorted QR decomposition that not only calculates the QR decomposition of a scalar matrix but attempts to optimally order the upper triangular matrix, $\boldsymbol{R}$. This results in a system with a small degradation in BER performance over the optimum brute force approach, but with a significant reduced computational cost. However as this approach is based on the Gram-Schmidt algorithm for computing QR decomposition and not readily applicable to PMQRD, a brute force approach has been applied here.

Implementation of the ODO scheme requires no modification of the transmitter architecture, and the entire process is carried out at the receiver. The modified receiver design is summarized in algorithm 5.2.

Algorithm 5.2 Summary of the H-BLAST ODO receiver.

Calculate $\underline{\boldsymbol{Q}}(z)$ and $\underline{\boldsymbol{R}}(z)$ for optimum permutation of columns of $\underline{\boldsymbol{H}}(z)$.
Receive and **filter** streams with $\underline{\boldsymbol{Q}}(z)$.
for $i = Mr : -1 : 1$ **do**
  Formulate channel equalization problem
  $\boldsymbol{y}_i - \sum_{j=i+1}^{M_r} \underline{\boldsymbol{r}}_{ij}(z)\ \boldsymbol{x}_j = \underline{\boldsymbol{r}}_{ii}(z)\ \boldsymbol{x}_i + \boldsymbol{n}'_i$
  for Turbo equalize i^{th} stream **do**
    Calculate soft estimate of transmitted signal, $\boldsymbol{x}_i$ via MMSE equalizer.
    De-interleave and calculate $\boldsymbol{c}_i$.
    Calculate hard estimate of transmitted signal, $\boldsymbol{s}_i$ and updated soft estimate of $\boldsymbol{c}_i$ via MAP decoder.
    Interleave $\boldsymbol{c}_i$ to form $\boldsymbol{x}_i$.
  end for
end for
Permute equalized signals to obtain original streams $\boldsymbol{s}_1, \boldsymbol{s}_2, \boldsymbol{s}_3$.
Multiplex streams to obtain original data stream.

5.4.4 H-BLAST Optimal Detection Ordering Results

Again a MIMO-OFDM QR scheme has been used as a benchmark. For the OFDM scheme, optimal detection ordering has been applied separately to each narrowband MIMO channel. Figure 5.5 directly compares the proposed PMQRD ODO and MIMO-OFDM QR ODO schemes.

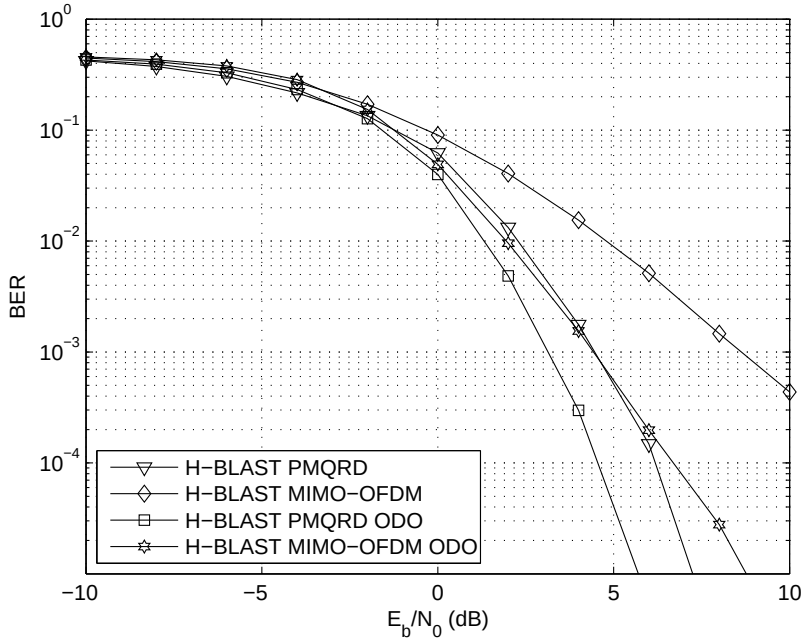

Figure 5.5: Average coded BER results for H-BLAST PMQRD and MIMO-OFDM QR schemes incorporating ODO for a 3×3 MIMO channel, $L = 5$, with constant power profile.

Again PMQRD significantly outperforms MIMO-OFDM QR for an ODO implementation, for example a 2.5dB gain in SNR is observed at BER 10^{-4}. Also note the significant performance in

both schemes incorporating ODO, for example a 2dB gain in SNR at BER 10^{-4} in the PMQRD scheme incorporating ODO and a substantial 8dB gain in SNR at BER 10^{-3} for the MIMO-OFDM QR scheme incorporating ODO. This significant increase in MIMO-OFDM QR performance is due to the fact that ODO affectively mitigates the problems of individual tones having low gain. However the optimum permutation of the columns in each narrowband tone is unique to each tone and must be calculated individually, significantly increasing the computational cost.

5.5 Vertical BLAST Encoding

Vertical-BLAST [71] or V-BLAST encoding architecture is shown in Figure 5.6. The data stream undergoes convolutional encoding, interleaving and symbol mapping prior to demultiplexing into M_t sub-streams. This form of encoding is potentially optimal since each information bit is spread across multiple antennas. The full spatial diversity of M_r, M_t however can only be obtained if the codeword used is of length $M_r M_t$ [10] which is highly unlikely for most reasonable order MIMO systems.

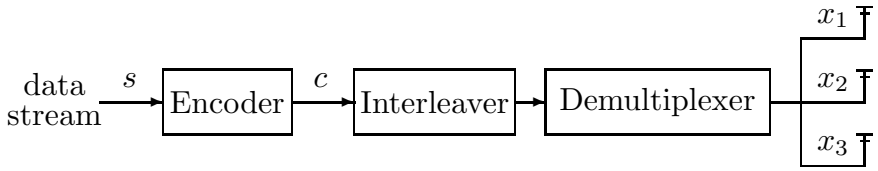

Figure 5.6: V-BLAST transmitter architecture.

5.5.1 V-BLAST Receiver Design

V-BLAST significantly increases the computational complexity of the receiver. As the streams can no longer be MAP decoded independently, the memory storage requirements for calculating all the states in the trellis are increased by a factor of M_t. Increasing the codeword length for optimum diversity exploitation increases MAP decoding complexity exponentially [10]. Hence realizing the full benefits of the V-BLAST architecture is impractical in most situations.

5.5.2 V-BLAST Results

Figure 5.7 shows results for both PMQRD and MIMO-OFDM QR for a V-BLAST architecture. Additional results have been included for ODO implementations. Again PMQRD provides superior performance, with a gain in SNR of 4 and 5dB for MIMO-OFDM QR and MIMO-OFDM QR implementations at a BER of 10^{-3} respectively.

Note that there is no significant difference in performance between the PMQRD and PMQRD ODO implementations. In an H-BLAST implementation, if $\underline{\boldsymbol{r}}_{M_r M_r}$ has poor gain, than independent

Algorithm 5.3 Summary of the V-BLAST receiver.

Receive and **filter** streams with $\underline{\boldsymbol{Q}}(z)$.
for Turbo-equalization loop **do**
  for $i = Mr : -1 : 1$ **do**
    Formulate channel equalization problem
    $\boldsymbol{y}_i - \sum_{j=i+1}^{M_r} \underline{\boldsymbol{r}}_{ij}(z)\ \boldsymbol{x}_j = \underline{\boldsymbol{r}}_{ii}(z)\ \boldsymbol{x}_i + \boldsymbol{n}'_i$
    Calculate soft estimate of transmitted signal, $\boldsymbol{x}_i$ via MMSE equalizer.
  end for
  Multiplex streams
  De-interleave and calculate $\boldsymbol{c}$.
  Calculate hard estimate of transmitted signal, $\boldsymbol{s}$ and updated soft estimate of $\boldsymbol{c}$ via MAP decoder.
  Interleave $\boldsymbol{c}$ to form $\boldsymbol{x}$.
  De-multiplex into transmitted streams.
end for
Obtain final estimate of transmitted data stream.

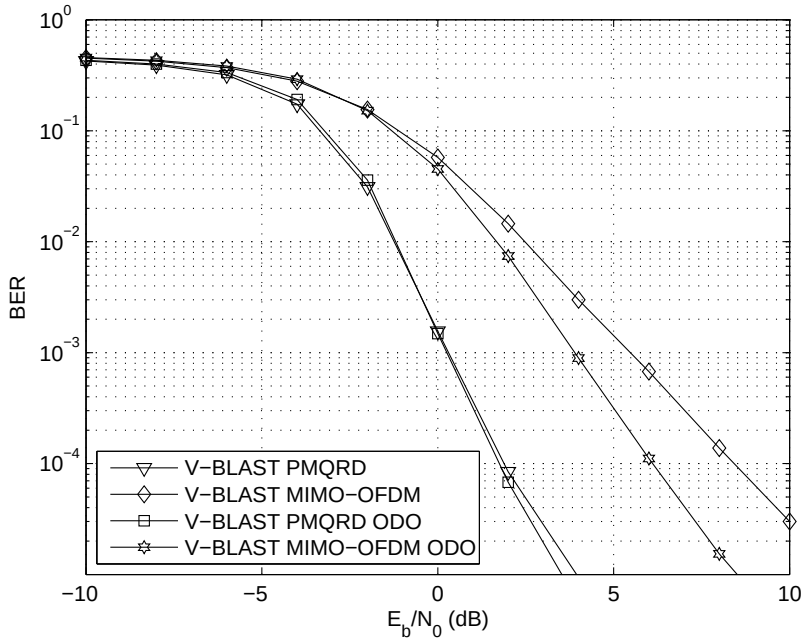

Figure 5.7: Average coded BER results for V-BLAST PMQRD and MIMO-OFDM QR schemes incorporating ODO for a 3×3 MIMO channel, $L = 5$, with constant power profile.

MMSE equalization and MAP decoding of the M_r^{th} stream will result in the likelihood of the entire recovered signal $\underline{\boldsymbol{s}}_{M_t}$ being corrupt. This incorrect estimate of $\underline{\boldsymbol{s}}_{M_t}$ will then back propagate through the iterative cancellation scheme causing further corruption in all recovered streams. ODO for H-BLAST negates this providing a significant performance boost. In a V-BLAST implementation the entire iterative cancellation process is carried out prior to MAP decoding. As there is a de-interleaving operation prior to the MAP operation, these errors will become significantly spread out and the ECC present is able to correct for these errors. Additionally the soft feedback to the MMSE equalizer will

make the equalization step robust to back propagation of errors in the iterative cancellation scheme. Therefore the V-BLAST architecture inherently provides the benefits of ODO, and the performance of the two schemes is identical.

Note the PMQRD approach still provides the additional robustness of spreading the information in each transmitted symbol across the entire frequency bandwidth, making it robust to deep fading. For MIMO-OFDM QR subsequent tones may all be in deep fade and hence ODO in this scenario provides a significant performance boost.

5.6 Diagonal BLAST Encoding

Diagonal-BLAST or D-BLAST encoding is an encoding architecture that combines the simplicity of H-BLAST encoding with the performance benefits of V-BLAST encoding [71]. The data stream is first demultiplexed into three substreams, s_1, s_2, s_3. Each substream is then independently convolutionally encoded and interleaved, again using the code formatting polynomials in (4.3). An S-random interleaver with a depth of 28 bits is again used to randomize the encoded bits prior to transmission. The data streams are then rotated, so that the bit stream-antenna association is periodically cycled [3]. This allows a diversity gain of $M_r M_t$ while maintaining a low computational complexity at the receiver. The D-BLAST architecture is shown in Figure 5.8.

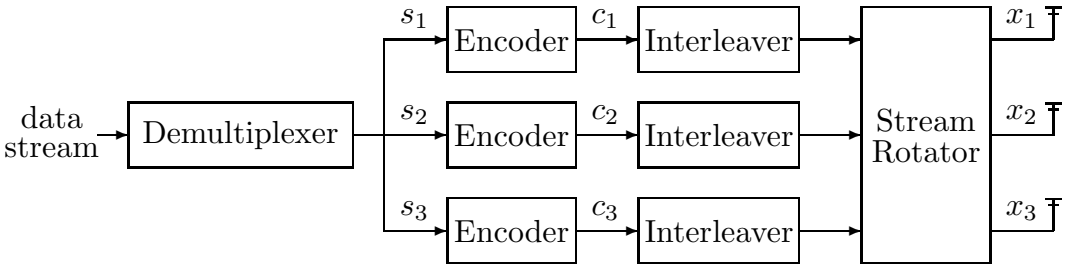

Figure 5.8: D-BLAST transmitter architecture.

5.6.1 D-BLAST Receiver Design

D-BLAST receiver design is more akin to an H-BLAST receiver. The computational cost of the MAP algorithm remains the same as that of the H-BLAST implementation, yet provides equal performance to that in the V-BLAST implementation. Note that the individual MAP decoding operations for each stream can be performed simultaneously. When implemented on hardware supporting parallel processing the D-BLAST algorithm therefore is the fastest of the all the BLAST algorithms. Assuming that the number of simultaneous MAP decoding operations supported in parallel is the same as

the number of receive antennas then D-BLAST will take approximately $1/M_r$ of the time required for an H-BLAST implementation.

Algorithm 5.4 Summary of the D-BLAST receiver.

Receive and **filter** streams with $\underline{\boldsymbol{Q}}(z)$.
for Turbo-equalization loop **do**
  for $i = Mr : -1 : 1$ **do**
    Formulate channel equalization problem
    $\boldsymbol{y}_i - \sum_{j=i+1}^{M_r} \underline{\boldsymbol{r}}_{ij}(z)\ \boldsymbol{x}_j = \underline{\boldsymbol{r}}_{ii}(z)\ \boldsymbol{x}_i + \boldsymbol{n}_i'$
    Calculate soft estimate of transmitted signal, $\boldsymbol{x}_i$ via MMSE equalizer.
  end for
  De-rotate the streams.
  De-interleave each stream.
  Calculate hard estimate of transmitted signals, $\boldsymbol{S}$ and updated soft estimates of $\boldsymbol{C}$ via MAP decoder.
  Interleave coded streams.
  Rotate streams to form $\boldsymbol{X}$
end for
Multiplex streams to obtain original data stream.

5.6.2 D-BLAST Results

Figure 5.9 compares both PMQRD and MIMO-OFDM QR D-BLAST implementations and includes ODO results. As with V-BLAST, both PMQRD implementations perform identically due to the performance increase from exploiting the full diversity gain of the channel. Note the significant performance benefits of a gain in 5dB in SNR at BER 10^{-4} over the MIMO-OFDM QR ODO implementation. This is again due to the information in each individual transmitted symbol being spread across the entire frequency bandwidth in the PMQRD based system, providing robustness to deep channel fading not possible by constraining the information in each individual transmitted symbol to a single narrowband tone as found in the MIMO-OFDM QR D-BLAST implementations.

Figure 5.10 compares the performance of all PMQRD ODO BLAST schemes. As expected as the H-BLAST scheme only attains a diversity gain of M_r it has the weakest performance. As V-BLAST and D-BLAST effectively attain the full diversity gain of $M_r M_t$ they have identical performance with a increase in SNR of 3dB at BER 10^{-3}.

5.7 Channel Estimation Error

The scenario where the receiver has imperfect channel knowledge is now considered. Again a least squares channel estimator as described in Chapter 2 has been implemented. Figure 5.11 shows the average relative error in channel estimation for 1000 Monte Carlo simulations. Even with a relatively low SNR it is possible to obtain a reasonably accurate estimation of the channel, for example a relative

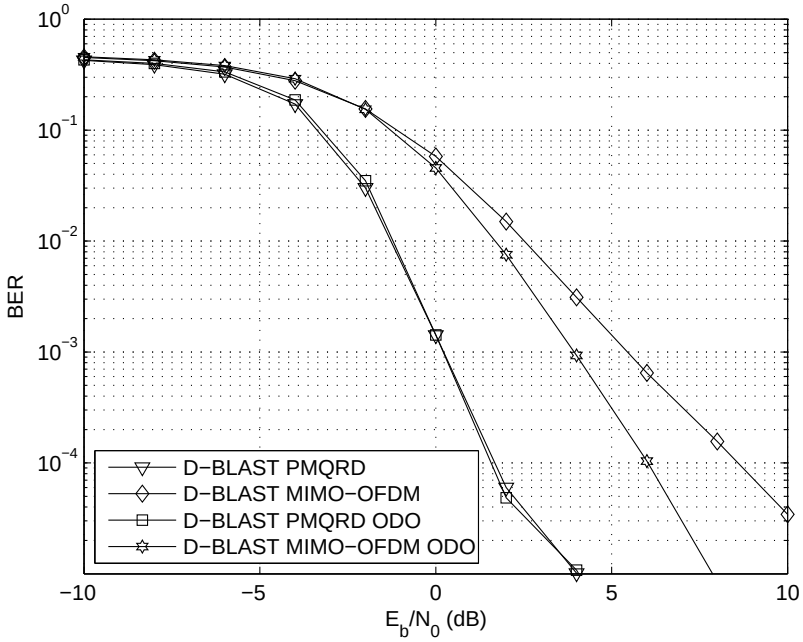

Figure 5.9: Average coded BER results for D-BLAST PMQRD and MIMO-OFDM QR schemes incorporating ODO for a 3×3 MIMO channel, $L = 5$, with constant power profile.

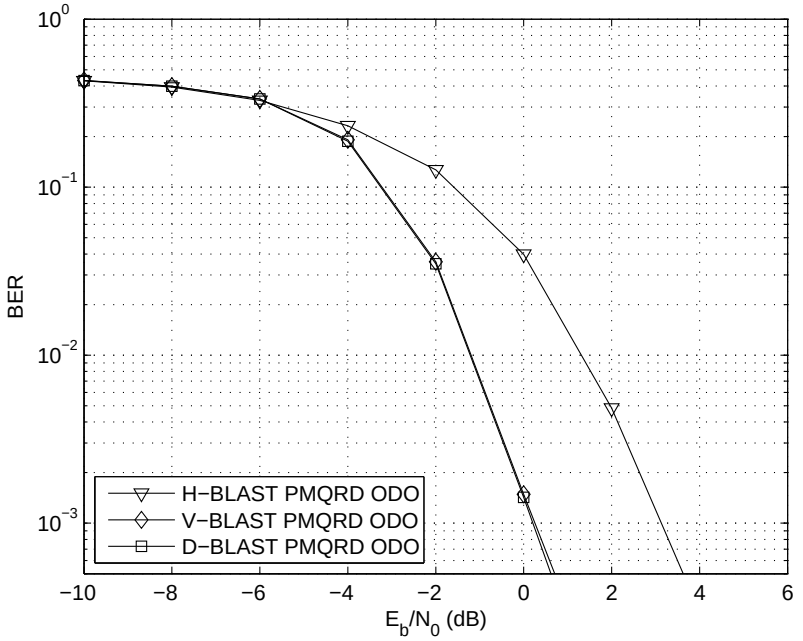

Figure 5.10: Average coded BER results for BLAST PMQRD ODO for a 3×3 MIMO channel, $L = 5$, with constant power profile.

error of 0.27 at an SNR of 2dB.

Figure 5.12 shows the impact of channel estimation error on BER performance. The BER rate

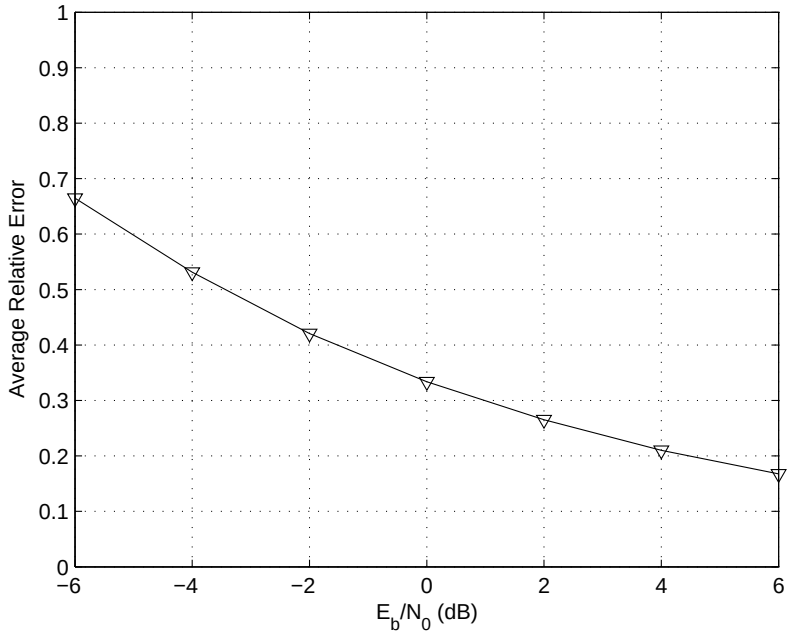

Figure 5.11: Average relative error in channel estimation for a 3×3 MIMO channel, $L = 5$ with constant power profile and training sequence of length $N_t = 50$.

has been computed for 1000 Monte Carlo simulations. The modulation scheme used is BPSK. The number of time slots of the channel, $N = 2048$. The length of the training sequence, $N_t = 50$. Simulations have been performed for both D-BLAST PMQRD ODO and D-BLAST MIMO-OFDM QR ODO schemes. Again the clear benefit of PMQRD is visible, with a gain in SNR of 4dB at BER 10^{-3}.

So far in this chapter three types of BLAST architecture have been evaluated. It has been found in every simulation that the PMQRD approach significantly outperforms MIMO-OFDM QR. The algorithm has also been shown to be robust to CSI error, confirming its suitability for real world applications. The PMQRD approach has significant performance benefits. Spreading the information in each transmitted symbol across the entire frequency bandwidth automatically makes the system robust to deep channel fading.

A key design constraint in realizing wireless communications systems is the peak-to-average power ratio (PAPR). For an OFDM based scheme, the IFFT operation at each transmit antenna results in a relatively high PAPR. Therefore, nonlinearities may get overloaded by high signal peaks, causing intermodulation distortion in the transmitted signal [73], and undesired out-of-band radiation. If radio frequency (RF) power amplifiers are operated without large power back-offs, it is impossible to keep the out-of-band power below specified limits, leading to very inefficient amplification and expensive

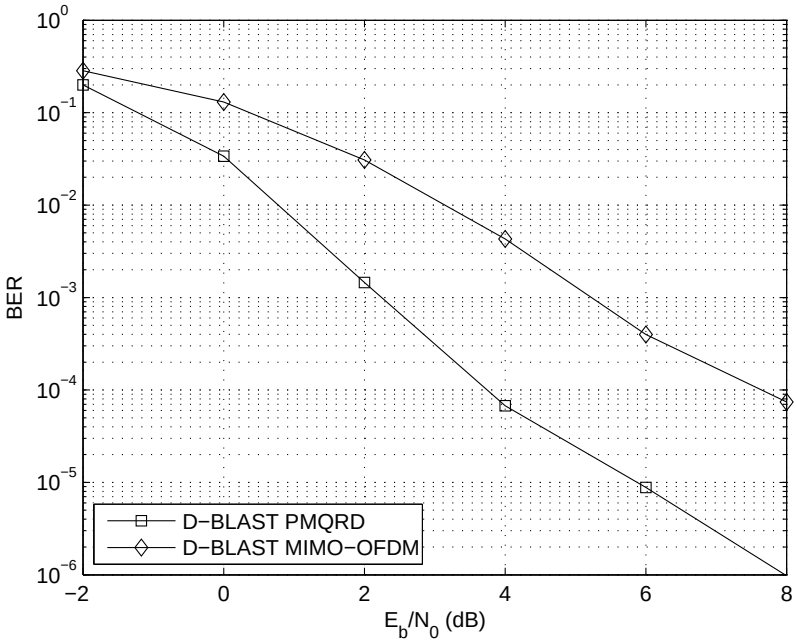

Figure 5.12: Average coded BER results for D-BLAST PMQRD and MIMO-OFDM QR schemes for a 3×3 MIMO channel, $L = 5$, with constant power profile with channel estimation error.

transmitters [74]. In addition, signal components originating from bins other than the considered one give rise to interbin interference (IBI) [75]. In the presence of channel estimation error IBI is significantly increased, leading to degraded performance of a MIMO-OFDM based scheme.

In a PMQRD implementation the PAPR is dictated by the modulation scheme used, not the DFT. Hence for modulation schemes with constant transmit energy per symbol the PAPR will be unity. This significantly reduces the cost and design of the amplifier stage and allows for more power efficient amplifier design. For modulation schemes with variable transmit energy per symbol, the PAPR of PMQRD system will still be significantly less than that of OFDM, reducing transmitter complexity and cost. Although the PMQRD scheme is also susceptible to channel estimation error, its BER performance is still significantly greater, demonstrating the robustness of the proposed PMQRD scheme.

5.8 Single Carrier OFDM

Although the proposed PMQRD has been show to significantly outperform MIMO-OFDM QR in every scenario, the greatest advantage of the PMQRD approach is the reduction in PAPR at the transmitter. Increased BER performance is always welcomed, but the ability to operate power efficient amplifiers at mobile base stations is paramount. With the current global focus on reducing carbon

emissions in all industries and formation of new international groups to provide green solutions, such as the International Partnership for Energy Efficiency Cooperation (IPEEC), the mobile cellular industry must significantly change its environmental model to meet global standards. Energy costs account for as much as half of a mobile operators operating expenses, so improving energy-efficiency is not only beneficial for the environment but also makes commercial sense for operators [76]. This is highlighted by the fact that in the UK most mobile operators will switch of the third generation (3G) Enhanced Data rates for GSM Evolution (EDGE) component of their mobile networks to save electricity and running costs in the early hours of the morning and rely entirely on the previous second generation (2G) General Packet Radio Service (GPRS). GPRS is a 2G technology compatible with both 2G and 3G cellular systems and although the data rates are significantly slower than EDGE this is offset by the lack of demand for the EDGE service during in the early hours [77].

A single carrier OFDM system, like the PMQRD approach allows the modulation scheme to dictate the PAPR and has an identical PAPR to the proposed PMQRD scheme. A basic SISO implementation of a single carrier OFDM system is shown in Figure 5.13. Essentially the IFFT operation at the transmitter has been shifted to the receiver. The only operation carried out at the transmitter is the addition of the cyclic prefix, hence the modulation scheme dictates the PAPR. Recalling from Chapter 2, the cyclic prefix renders the channel impulse response circulant. The impulse response of the resulting circulant channel, $\boldsymbol{H}_c$ may be expressed again as

$$\boldsymbol{H}_c = \boldsymbol{D}^H \, \boldsymbol{\Sigma} \, \boldsymbol{D} \tag{5.7}$$

Where $\boldsymbol{D}$ denotes the discrete Fourier transform matrix, normalized by a factor of $1/\sqrt{N}$ (2.23). For Figure 5.13, $\boldsymbol{y''}$ is simply expressed as

$$\boldsymbol{y''} = \boldsymbol{D}^H \, \boldsymbol{\Sigma} \, \boldsymbol{D} \, \boldsymbol{s} \tag{5.8}$$

The FFT operation cancels out the discrete Fourier transform matrix, $\boldsymbol{D}^H$, allowing $\hat{\boldsymbol{y}}$ to be reduced to

$$\begin{aligned} \hat{\boldsymbol{y}} &= \boldsymbol{D} \, \boldsymbol{D}^H \, \boldsymbol{\Sigma} \, \boldsymbol{D} \, \boldsymbol{s} \\ \hat{\boldsymbol{y}} &= \boldsymbol{\Sigma} \, \boldsymbol{D} \, \boldsymbol{s} \end{aligned} \tag{5.9}$$

For this SISO scenario, the channel equalizer is simply $\boldsymbol{\Sigma}^{-1}$. Combined with the final IFFT

operation which cancels out $\boldsymbol{D}$, $\boldsymbol{y}$ becomes the transmitted signal $\boldsymbol{s}$

$$\begin{aligned} \boldsymbol{y} &= \boldsymbol{D}^H \, \boldsymbol{\Sigma}^{-1} \, \boldsymbol{\Sigma} \, \boldsymbol{D} \, \boldsymbol{s} \\ \hat{\boldsymbol{y}} &= \boldsymbol{D}^H \, \boldsymbol{D} \, \boldsymbol{s} \\ \hat{\boldsymbol{y}} &= \boldsymbol{s} \end{aligned} \tag{5.10}$$

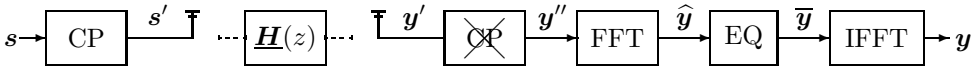

Figure 5.13: SISO single carrier OFDM architecture.

Extending this to approach to the MIMO scenario, Figure 5.14 shows the complete system up to the equalization stage.

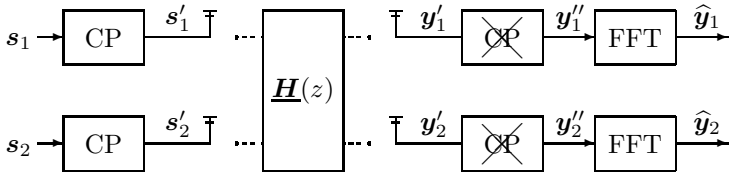

Figure 5.14: MIMO single carrier OFDM architecture.

The received signal $\hat{\boldsymbol{y}}$ is can be written in vector form as

$$\begin{bmatrix} \hat{\boldsymbol{y}}_1 \\ \hat{\boldsymbol{y}}_2 \end{bmatrix} = \begin{bmatrix} diag(\boldsymbol{\Sigma}_{11}) & diag(\boldsymbol{\Sigma}_{12}) \\ diag(\boldsymbol{\Sigma}_{21}) & diag(\boldsymbol{\Sigma}_{22}) \end{bmatrix} \begin{bmatrix} \boldsymbol{D} \, \boldsymbol{s}_1 \\ \boldsymbol{D} \, \boldsymbol{s}_2 \end{bmatrix} \tag{5.11}$$

and for the n^{th} symbol of the received signal $\hat{\boldsymbol{y}}$

$$\begin{bmatrix} \hat{\boldsymbol{y}}_1(n) \\ \hat{\boldsymbol{y}}_2(n) \end{bmatrix} = \begin{bmatrix} \boldsymbol{\Sigma}_{11}(n) & \boldsymbol{\Sigma}_{12}(n) \\ \boldsymbol{\Sigma}_{21}(n) & \boldsymbol{\Sigma}_{22}(n) \end{bmatrix} \begin{bmatrix} \boldsymbol{D}(n,:) \, \boldsymbol{s}_1 \\ \boldsymbol{D}(n,:) \, \boldsymbol{s}_2 \end{bmatrix} \tag{5.12}$$

Calculating the QR decomposition of the n^{th} tone and using $\boldsymbol{Q}^H$ as filterbank reduces the MIMO equalization problem to upper triangular form as before. Once again it is a simple decision feedback process to iteratively cancel the transmitted signals from the received signals. Eq 5.13 shows the equalization problem for the n^{th} tone. Assuming QR decomposition has been properly carried out,

$\boldsymbol{R}_{21}(n) = 0$.

$$\begin{bmatrix} \hat{\boldsymbol{y}}_1(n) \\ \hat{\boldsymbol{y}}_2(n) \end{bmatrix} = \begin{bmatrix} \boldsymbol{R}_{11}(n) & \boldsymbol{R}_{12}(n) \\ \boldsymbol{R}_{21}(n) & \boldsymbol{R}_{22}(n) \end{bmatrix} \begin{bmatrix} \boldsymbol{D}(n,:)\ \boldsymbol{s}_1 \\ \boldsymbol{D}(n,:)\ \boldsymbol{s}_2 \end{bmatrix} \tag{5.13}$$

Eq 5.13 clearly shows the critical problem with this approach. Unlike the MIMO-OFDM QR approach described previously we are no longer recovering the n^{th} transmitted symbol from each antenna, $\boldsymbol{S}(n)$, we are recovering the n^{th} symbol of the FFT of the transmitted symbol sequence from each antenna. Denoting the FFT of the i^{th} symbol stream as $\boldsymbol{\xi}_i = \boldsymbol{D}\ \boldsymbol{s}_i$, if the n^{th} element of $\boldsymbol{\xi}_i$ is significantly corrupted, due to the n^{th} tone of the MIMO frequency selective channel undergoing deep fade, performing the IFFT will no longer corrupt only the estimate of $\boldsymbol{s}_i(n)$, but the entire estimate of the symbol sequence $\boldsymbol{s}_i$. When this occurs, in particular for a V-BLAST and D-BLAST implementation exploiting the full diversity gain of the channel not only is the i^{th} symbol sequence lost, but the received streams can no longer be iteratively canceled from eachother and the entire packet is lost. Figure 5.15 shows the average coded BER for a single carrier MIMO-OFDM system, averaged over 1000 Monte Carlo simulations and compared with MIMO-OFDM QR. A D-BLAST architecture system has been implemented identical to those previously described in this chapter. As can be clearly seen the single carrier implementation cannot provide any real performance, even at the relatively high SNR of 10dB.

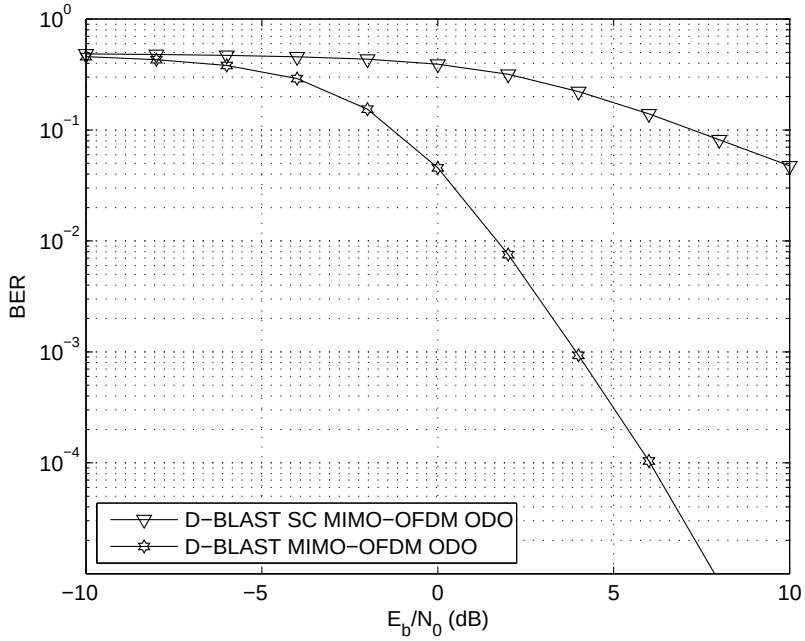

Figure 5.15: Average coded BER results for D-BLAST MIMO-OFDM QR schemes incorporating ODO for a 3×3 MIMO channel, $L = 5$, with constant power profile.

However, Figure 5.15 does not provide the full picture. Focusing on the 1000 Monte Carlo simulations carried out at an SNR of 10dB, Figure 5.16 shows a histogram of the BER obtained in each simulation run. As can be seen for a significant percentage, around 75% of the Monte Carlo simulations operate as expected and although not obtainable from the histogram, 657 of the 1000 Monte Carlo simulations had a coded BER of less than 9.7×10^{-4}, i.e. they recovered the transmitted signal in its entirety free from errors. As previously shown in Figure 5.4, the frequency selective nature of the MIMO channel can cause certain tones to be in deep fade, when this occurs the BER performance is degraded to such an extent that the entire packet is unrecoverable. This is clearly visible in the results as there are packets with a BER rate between 0.4 and 0.5, i.e. the receiver has had a 50% chance of correctly estimating each transmited bit. Note for the equivalent standard MIMO-OFDM QR approach over 1000 Monte Carlo simulations, no packets produced a BER higher than 1×10^{-3}.

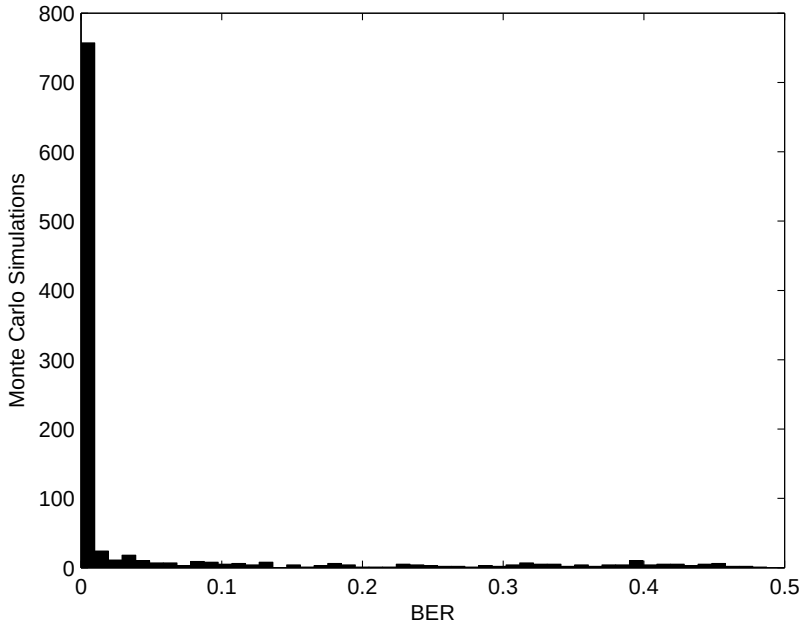

Figure 5.16: Histogram of coded BER results for 1000 Monte Carlo simulations of a D-BLAST SC MIMO-OFDM QR scheme incorporating ODO for a 3×3 MIMO channel, $L = 5$, with constant power profile at an SNR of 10dB.

The typical solution to this problem is to use an adaptive modulation scheme at the transmitter [78] to adapt the constellations for the subchannels according to their respective channel gains and avoid using tones in deep fade [79], known as bit loading [80, 81]. This technique however only applies to a bidirectional transmission system where the channel transfer function estimated at the receiver can be fed back to the transmitter. Hence it is not suitable for implementation in a QR based system

where no feedback path exists.

5.9 Conclusion

In this chapter the PMQRD has been applied and analyzed to frequency selective MIMO channels. Application of the proposed PMQRD technique reduces the MIMO channel equalization problem to a set of decision feedback based single channel equalization problems. The performance of the PMQRD system has been evaluated for BLAST architecture communications systems incorporating either horizontal, vertical or diagonal encoding. Comparing the proposed PMQRD time domain solution to an identical MIMO-OFDM QR frequency domain solution has yielded several important results. In an OFDM system, receiver decisions are made carrier by carrier, which makes some decisions highly unreliable, whereas the decision reliability in single-carrier systems is dictated by the SNR averaged over the entire channel bandwidth [82]. This has been shown clearly in the results with the superior BER performance of the PMQRD based scheme over MIMO-OFDM QR in every scenario. The robustness of the proposed approach has again been verified for system performance in the presence of CSI error.

Furthermore, the PAPR of the PMQRD scheme is dictated by the modulation scheme used at the transmitter. Hence for low complexity PSK modulation schemes such as BPSK and QPSK, the PAPR is unity. This allows for optimal power amplifier design within the transmitter, minimizing operating and design costs while maximizing energy efficiency. Although a single carrier OFDM approach is capable of providing the same benefit, it has been shown that without a feedback path between receiver and transmitter to mitigate the effect of individual tones being in deep fade, such a system is unworkable for a BLAST architecture communications system.

In the next chapter we combine PMSVD at the transmitter and PMQRD at the receiver to create a MIMO multiuser (MIMO-MU) system, capable of true time domain broadband beamforming for the MIMO-MU downlink channel.

Chapter 6

Downlink Multi-User MIMO for Frequency Selective Channels

6.1 Introduction

In the preceding chapters the individual application of PMSVD and PMQRD to frequency selective MIMO channels has been discussed. In this chapter the benefits of both techniques are combined for a downlink multi-user MIMO (MU-MIMO) scenario (often also commonly referred to as spatial division multiple access (SDMA) [83, 84]). For applications such as wireless LAN's and cellular telephony, MIMO systems will likely be deployed in environments where a single base station must communicate with multiple users simultaneously. MU-MIMO systems have the potential to combine the high capacity achievable with MIMO processing with the benefits of space-division multiple access [85]. For this scenario there are two communications problems to consider, the uplink, whereby multiple users transmit data simultaneously to the base station, and the downlink, whereby the base station transmits data simultaneously to multiple users. Typically for the uplink channel, users are unable to coordinate with each other and therefore the challenge is for the base station to separate the users. For the downlink channel the challenge is for the base station to design transmit vectors while considering the co-channel interference of other users [25]. The primary benefit of MU-MIMO to wireless systems is not the multiple access capability, but the additional channel reuse within a cell to increase spectral efficiency [3].

MU-MIMO is particularly well suited to satellite applications. As users on the ground have a direct LOS path to the satellite with no scattering component, the signals received at the satellite have no angular spread [3]. Assuming the multiple users are at well separated angles it is relatively straightforward to direct co-channel pencil beams with minimum cross interference [86]. Conversely a terrestrial MU-MIMO cellular system is significantly more complex due to the multipath scattering environment and typically the high mobility of mobile users [87].

In this chapter a downlink MU-MIMO scenario has been considered, consisting of a single transmitter base station equipped with multiple antennas communicating with multiple users. Initially the application and implementation of an instantaneous MU-MIMO mixing channel is discussed. SVD is

used at the transmitter to design orthogonal transmit vectors for each user. Each user is equipped with multiple receive antennas and the transmitter is capable of transmitting multiple independent data streams to each user, therefore QR decomposition is used at the receiver side to equalize the MU-MIMO channel and recover the transmitted data streams. This work is then generalized to convolutive MU-MIMO mixing channels, where the PMSVD using SBR2 [21] is used to design orthogonal transmit vectors at the base station and PMQRD to equalize the resulting channel at the receiver. Throughout this work an identical MU-MIMO OFDM scheme is used as a benchmark. Finally the robustness of the proposed scheme to CSI is considered and the benefits of the time-domain polynomial approach discussed.

6.2 Instantaneous Mixing MIMO-MU Transmission

Consider initially an instantaneous mixing scenario whereby a base-station communicates with K wireless users. The base-station is equipped with M_t transmit antennas, and the j^{th} user is equipped with M_{r_j} receive antennas. It is assumed that the base station has perfect CSI of the channel between itself and each user, furthermore it assumed that each user has perfect CSI of the channel between itself and the base station. The total number of antennas over all the receivers, M_r is defined as $M_r = \sum_{i=1}^{K} M_{r_i}$. The noise free channel matrix from the base station to the j^{th} user is denoted as $\boldsymbol{H}_j \in \mathbb{C}^{M_{r_j}, M_t}$, and the associated transmit filter bank by $\boldsymbol{M}_j \in \mathbb{C}^{M_t \times M_{r_j}}$. A set of source signals of length T for the j^{th} user, $\boldsymbol{s}_j(t) \in \mathbb{C}^{M_{r_j} \times 1}$, for $t \in \{0, 1, \ldots, T-1\}$ are propagated through $\boldsymbol{H}_j$. Therefore the set of received signals at the j^{th} receiver, $\boldsymbol{y}_j(t) \in \mathbb{C}^{M_{r_j} \times 1}$ is

$$y_j(t) = \sum_{i=1}^{K} \boldsymbol{H}_j \ \boldsymbol{M}_i \ s_i(t) + n_j(t) \tag{6.1}$$

where $n_j(t)$ denotes an additive Gaussian noise process with variance $\sigma^2 \boldsymbol{I}_{M_{r_j}}$ and $\boldsymbol{M}_i$ denotes the transmit filter bank for the i^{th} user. To reduce interference between users the goal therefore is to design a transmit filter such that $\boldsymbol{H}_i \ \boldsymbol{M}_j = \boldsymbol{0}$ for $i = 1, 2, \ldots, K$ and $i \neq j$.

6.2.1 Singular Value Decomposition

The design of the transmit filter for the j^{th} user, $\boldsymbol{M}_j$ is obtained via the SVD. Extending the MIMO-MU notation, $\widehat{\boldsymbol{H}}_j$ is used to denote the channel matrix for all users other than the j^{th} user

combined, i.e.

$$\widehat{\boldsymbol{H}}_j = \begin{bmatrix} \boldsymbol{H}_1 \\ \vdots \\ \boldsymbol{H}_{j-1} \\ \boldsymbol{H}_{j+1} \\ \vdots \\ \boldsymbol{H}_K \end{bmatrix} \tag{6.2}$$

The SVD of $\widehat{\boldsymbol{H}}_j$ is shown in (6.3). As $\widehat{\boldsymbol{H}}_j$ is a tall matrix of dimensions $(M_r - M_{r_j}, M_t)$, $\widehat{\boldsymbol{\Lambda}}_j$ will be a fat diagonal matrix containing $r = min(M_r - M_{r_j}, M_t)$ orthogonal channels.

$$\widehat{\boldsymbol{H}}_j = \widehat{\boldsymbol{U}}_j \ \widehat{\boldsymbol{\Lambda}}_j \ \widehat{\boldsymbol{V}}_j^H \tag{6.3}$$

where $\widehat{\boldsymbol{\Lambda}}_j$ takes the form

$$\widehat{\boldsymbol{\Lambda}}_j = \begin{bmatrix} \lambda_{11} & 0 & \dots & \dots & \dots & \dots & 0 \\ 0 & \lambda_{22} & 0 & \dots & \dots & \dots & 0 \\ \vdots & & \ddots & \ddots & & & \vdots \\ 0 & \dots & 0 & \lambda_{rr} & 0 & \dots & 0 \end{bmatrix} \tag{6.4}$$

The SVD of $\widehat{\boldsymbol{H}}_j$ can therefore be expressed as

$$\widehat{\boldsymbol{H}}_j = \widehat{\boldsymbol{U}}_j \ \widehat{\boldsymbol{\Lambda}}_j \ \left[\widehat{\boldsymbol{V}}_j^{(1)} \ \widehat{\boldsymbol{V}}_j^{(0)}\right]^H \tag{6.5}$$

where $\widehat{\boldsymbol{V}}_j^{(1)}$ holds the first r right singular vectors and $\widehat{\boldsymbol{V}}_j^{(0)}$ holds the last $M_t - r$ right singular vectors. Thus $\widehat{\boldsymbol{V}}_j^{(0)}$ forms an orthogonal basis for the null space of $\widehat{\boldsymbol{H}}_j$ [25]. Setting $\boldsymbol{M}_j = \widehat{\boldsymbol{V}}_j^{(0)}$ therefore fulfills the design criteria of

$$\boldsymbol{H}_i \ \boldsymbol{M}_j = \boldsymbol{0} \tag{6.6}$$

for $i = 1, 2, \dots, K$ and $i \neq j$.

6.2.2 Receiver Design

Assuming perfect interference cancellation between users, the signal received by the j^{th} user will

be

$$y_j(t) = \boldsymbol{H}_j \ \boldsymbol{M}_j \ s_j(t) + n_j(t) \tag{6.7}$$

QR decomposition can therefore be applied at the receiver to exploit the diversity gain afforded by the MU-MIMO channel and to simplify MU-MIMO channel equalization. Formulating the QR decomposition of the product of the modulation matrix and channel and using $\boldsymbol{Q}_j^H$ as a receive filter bank results in

$$\begin{aligned} y_j(t) &= \boldsymbol{Q}_j^H \ \boldsymbol{H}_j \ \boldsymbol{M}_j \ s_j(t) + n_j(t) \\ y_j(t) &= \boldsymbol{R}_j \ s_j(t) + n_j(t) \end{aligned} \tag{6.8}$$

where $\boldsymbol{Q}_j\boldsymbol{R}_j = \boldsymbol{H}_j \ \boldsymbol{M}_j$. As discussed in Chapter 2 the upper triangular property of the matrix $\boldsymbol{R}_j$ can now be exploited to transform the MIMO channel equalization problem into a set of M_{r_j} single channel equalization problems using back substitution and solved accordingly.

6.2.3 Results

Figure 6.1 shows the average BER for the first user in a narrowband MU-MIMO system consisting of three users, each equipped with two antennas and a transmitter base station equipped with six antennas. The three curves represent the average BER rate when the base station is transmitting to only the first user, the first and second user and finally all three users. QR decomposition is used at the receiver to equalize the MU-MIMO channel, but no BLAST scheme or error correction coding is implemented. The total transmission power budget is identical for each user and is independent of the number of users of the MU-MIMO system. The modulation scheme used is BPSK. BER results have been computed for 1000 Monte Carlo simulations. As can be seen from the results, the average BER rate for the first user at a given SNR remains constant regardless whether the base station is transmitting to the other users or not. This confirms that the transmitter is correctly designing the filter bank for each user such that the signals intended for any single user are transmitted in the null space of all other users.

6.3 Convolutive Mixing MIMO-MU Transmission

We now extend this work to the frequency selective MU-MIMO scenario. Once again the transmitter base station contains M_t transmit antennas and the j^{th} user is equipped with M_{r_j} receive antennas. The noise free multipath channel matrix from the base station to the j^{th} user is denoted as $\underline{\boldsymbol{H}}_j(z) \in \mathbb{C}^{M_{r_j}, M_t}$, and the associated filterbank by $\underline{\boldsymbol{M}}_j(z) \in \mathbb{C}^{M_t \times M_{r_j}}$.

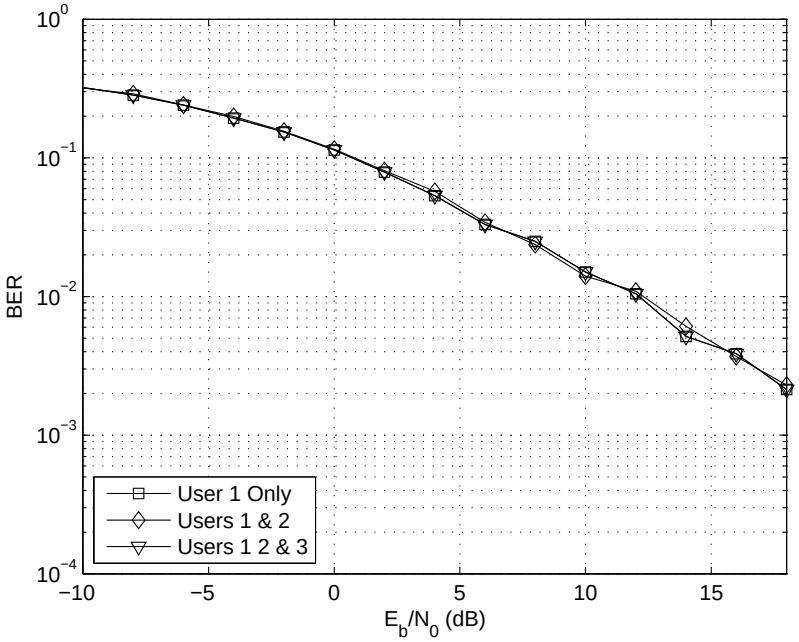

Figure 6.1: Average BER results for User 1 when the base station is transmitting to User 1, Users 1 & 2 and Users 1,2 & 3 simultaneously.

6.3.1 PMSVD at the Transmitter

Extending the MIMO-MU notation developed previously, $\underline{\widehat{\boldsymbol{H}}}_j(z)$ denotes the multipath MIMO channel matrix for all users other than the j^{th} user combined, i.e.

$$\underline{\widehat{\boldsymbol{H}}}_j(z) \quad = \quad \begin{bmatrix} \underline{\boldsymbol{H}}_1(z) \\ \vdots \\ \underline{\boldsymbol{H}}_{j-1}(z) \\ \underline{\boldsymbol{H}}_{j+1}(z) \\ \vdots \\ \underline{\boldsymbol{H}}_K(z) \end{bmatrix} \tag{6.9}$$

The PMSVD of $\underline{\widehat{\boldsymbol{H}}}_j(z)$ can now be formulated using the SBR2 algorithm. Recalling from Chapter 3 the input to the SBR2 algorithm must possess the para-Hermitian property. Forming the para-Hermitian matrix, $\underline{\boldsymbol{R}}(z)$ as $\underline{\boldsymbol{R}}(z) = \underline{\widetilde{\widehat{\boldsymbol{H}}}}_j(z)\underline{\widehat{\boldsymbol{H}}}_j(z)$ and performing a PMEVD yields the paraunitary matrix, $\underline{\boldsymbol{V}}(z)$ as per (3.16). The PMSVD of $\underline{\widehat{\boldsymbol{H}}}_j(z)$ is shown in (6.10). Again due to $\underline{\widehat{\boldsymbol{H}}}_j(z)$ being a tall matrix, performing PMSVD will result in $\underline{\widehat{\boldsymbol{\Lambda}}}_j(z)$ as a fat diagonal polynomial matrix containing

$r = min(M_r - M_{r_j}, M_t)$ orthogonal channels.

$$\begin{aligned} \widehat{\underline{\boldsymbol{H}}}_j(z) &= \underline{\widehat{\boldsymbol{U}}}_j(z)\ \underline{\widehat{\boldsymbol{\Lambda}}}_j(z)\ \underline{\widehat{\boldsymbol{V}}}_j^H(z) \\ &= \underline{\widehat{\boldsymbol{U}}}_j(z)\ \underline{\widehat{\boldsymbol{\Lambda}}}_j(z)\ \left[\underline{\widehat{\boldsymbol{V}}}_j^{(1)}(z)\ \underline{\widehat{\boldsymbol{V}}}_j^{(0)}(z)\right]^H \end{aligned} \tag{6.10}$$

$\underline{\widehat{\boldsymbol{V}}}_j^{(0)}(z)$ now forms an orthogonal basis vector for the null space of $\widehat{\underline{\boldsymbol{H}}}_j(z)$. Setting $\underline{\boldsymbol{M}}_j(z) = \underline{\widehat{\boldsymbol{V}}}_j^{(0)}(z)$ again fulfills the design criteria of

$$\underline{\boldsymbol{H}}_i(z)\ \underline{\boldsymbol{M}}_j(z) = \mathbf{0} \tag{6.11}$$

for $i = 1, 2, \ldots, K$ and $i \neq j$.

6.3.2 PMQRD at the Receiver

To equalize the resulting frequency selective MIMO channel between transmitter base station and the j^{th} user, PMQRD is used at the receiver. Again, assuming perfect interference cancellation between users, calculating the PMQRD of $\underline{\boldsymbol{H}}_j(z)\ \underline{\boldsymbol{M}}_j(z)$ and using $\underline{\boldsymbol{Q}}_j^H(z)$ as a receive filter bank reduces the MIMO channel equalization problem to a set of single channel equalization problems.

$$\begin{aligned} \underline{\boldsymbol{y}}_j(z) &= \underline{\boldsymbol{Q}}_j^H(z)\ \underline{\boldsymbol{H}}_j(z)\ \underline{\boldsymbol{M}}_j(z)\ \underline{\boldsymbol{s}}_j(z) + \underline{\boldsymbol{n}}_j(z) \\ \underline{\boldsymbol{y}}_j(z) &= \underline{\boldsymbol{R}}_j(z)\ \underline{\boldsymbol{s}}_j(z) + \underline{\boldsymbol{n}}_j(z) \end{aligned} \tag{6.12}$$

To fully exploit the diversity gain afforded by the multipath channel, a D-BLAST encoding scheme has been implemented as shown in Figure 6.2. Prior to transmission the data stream for the j^{th} user is demultiplexed into M_{r_j} substreams which are independently convolutionally encoded and interleaved and finally stream rotated to obtain the maximum spatial diversity afforded by the MU-MIMO channel.

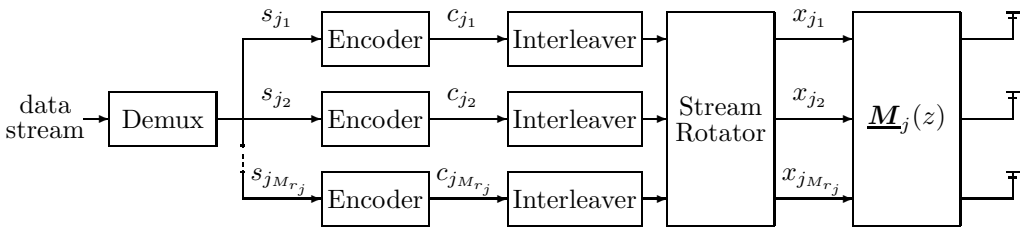

Figure 6.2: D-BLAST MU-MIMO transmitter architecture.

Note the flexibility provided by the encoder in the D-BLAST architecture. A potential problem in

MU-MIMO systems is the near-far problem [88], where one user is significantly closer to the transmitter base station than an other, resulting in the far user operating in a more strongly attenuated channel. Although the transmitter can allocate transmit power independently to different users, maximizing achievable throughput of the entire MU-MIMO using a waterpouring technique typically results in a solution at the expense of the user with the most attenuated channel [85]. Using the D-BLAST encoding architecture the transmitter can use a generator polynomial with a code rate appropriate to the channel capacity [67] and provides a simple method for solving this problem while maintaining quality of service for other users.

6.4 Channel Model

Without loss of generality a downlink MU-MIMO scenario has been modeled, consisting of a base station transmitting to multiple users. The number of antennas at the basestation, M_t is six. The number of users, K is three and the number of antennas at each user, M_{r_j} is two. The temporal length, L of the channel between each transmitter and receiver is five. Frequency selective MIMO channels with both an exponential power delay profile and a constant power delay profile have been considered to model both outdoor macro-cellular environments and indoor micro-cellular environments. As per Chapter 4, the MIMO channel with an exponential power delay profile has an exponential decaying factor of $\psi = 0.8$ as in (4.2).

6.5 Results

A WSQS situation has been considered. The bit error rate has been computed for 1000 Monte Carlo simulations. The modulation scheme used is BPSK for evaluation purposes but extension to large constellations is straightforward. The number of time slots of the channel, $N = 2048$. Initially it is assumed the receiver has perfect channel knowledge. The code formatting polynomials in (4.3) as per GSM CS1-CS3 [52] have been used for each user.

A MU-MIMO OFDM scheme has been used as a benchmark. As with previous MIMO-OFDM incarnations, the frequency selective channel is decomposed into N orthogonal frequency flat MU-MIMO channels. For the j^{th} user, the SVD operation at the transmitter is carried out within each narrowband tone of $\underline{\hat{\boldsymbol{H}}}_j(z)$. Hence for $\hat{\boldsymbol{H}}_j[k]$, the frequency response of the narrowband MU-MIMO channel corresponding to the k^{th} tone of the MU-MIMO channel matrix $\underline{\hat{\boldsymbol{H}}}_j(z)$, the SVD of $\hat{\boldsymbol{H}}_j[k]$ is calculated, as with the MIMO-OFDM SVD technique demonstrated in Chapter 4. The data stream undergoes the same D-BLAST encoding process as the PMQRD based scheme prior to application of OFDM. At the receiver the standard QR decomposition is applied within each narrowband tone and

the iterative cancellation within the receiver is performed on each tone individually.

6.5.1 Constant Power Profile

Figure 6.3 shows the average coded BER performance for the first user in a MU-MIMO system with a constant power profile. The three curves represent the average BER rate when the base station is transmitting to only the first user, the first and second user and finally all three users. The proposed polynomial matrix based scheme has been denoted PM and the benchmark MU-MIMO OFDM scheme as OFDM. As can be clearly seen the narrowband SVD approach to MU-MIMO has been successfully generalized to frequency selective channels. The average coded BER performance of the first user does not change when additional users are operating within the MU-MIMO channel. Also note this result is successfully repeated in the MU-MIMO OFDM scheme, the BER performance of the first user is independent of the number of other users using the channel.

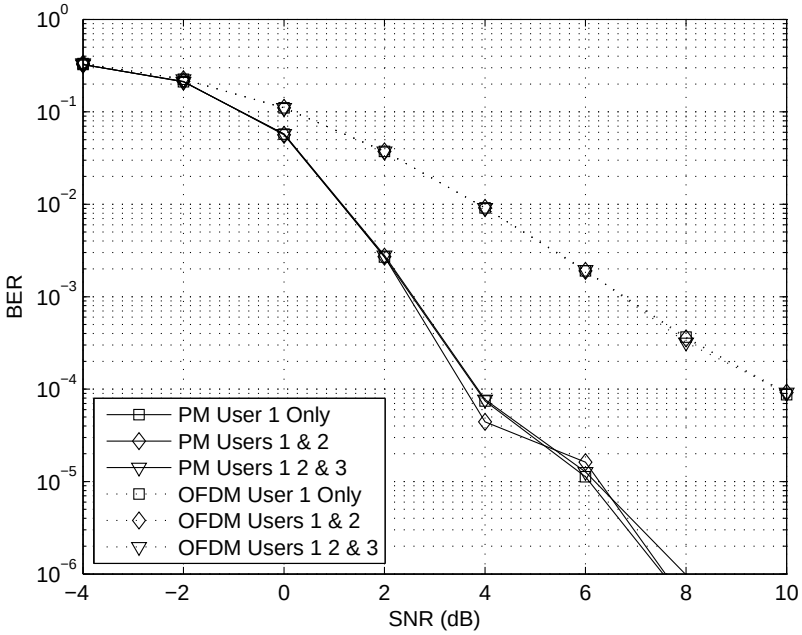

Figure 6.3: Average coded BER results for User 1 when the base station is transmitting to User 1, Users 1 & 2 and Users 1,2 & 3 simultaneously, for a MU-MIMO channel with constant power profile.

However the PM system significantly outperforms the OFDM scheme, with a gain in SNR of 3dB at a BER of 1×10^{-4}. This is entirely due to the benefits in the PMQRD approach over the MIMO-OFDM QR approach discussed in Chapter 5. Spreading the information in each transmitted symbol across the entire frequency bandwidth automatically makes the PM system robust to deep channel fading effects which significantly effect system performance in the OFDM based implementation.

6.5.2 Exponential Power Delay Profile

Figure 6.4 repeats the experiment for a MU-MIMO system with exponential power delay profile. Again the three curves represent the average BER rate when the base station is transmitting to only the first user, the first and second user and finally all three users. PM and OFDM based implementations have been considered. Again we see both MU-MIMO are successful and BER performance is independent of users of the channel. The proposed PM system outperforms the OFDM scheme, with a gain in SNR of 4dB at a BER of 1×10^{-3}.

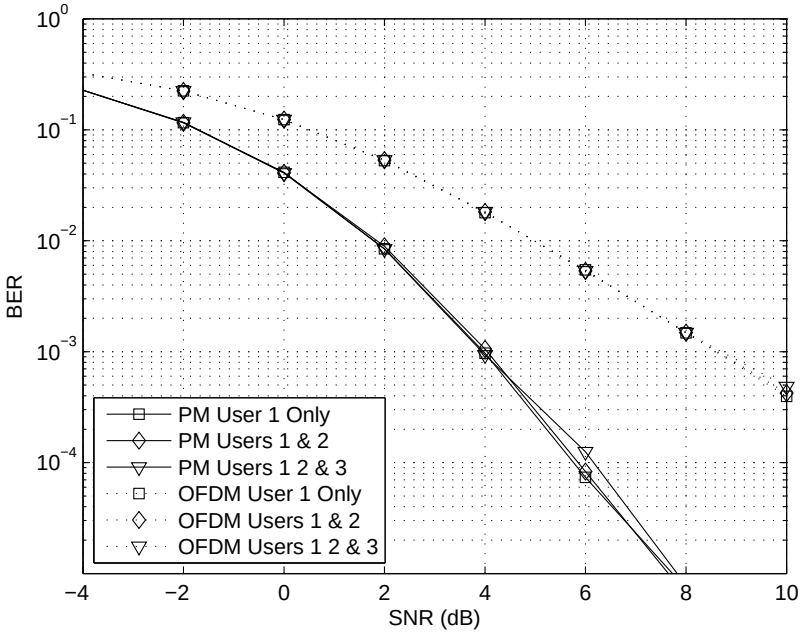

Figure 6.4: Average coded BER results for User 1 when the base station is transmitting to User 1, Users 1 & 2 and Users 1,2 & 3 simultaneously, for a MU-MIMO channel with exponential power delay profile.

6.6 Channel Estimation Error

The scenario where both the transmitter and receiver have imperfect channel knowledge is now considered. For a MU-MIMO scenario imperfect CSI will have a significant impact on the performance of all users. Imperfect CSI at the transmitter will destroy the orthogonality of the transmitted streams for each user and result in interference between transmitted streams. Hence the signals received by each user will contain not only background noise but additional noise proportional to the number of additional users operating in the MU-MIMO channel. Furthermore CSI error will result in degradation in the performance of the iterative cancellation scheme within the receiver, as previously demonstrated

in Chapter 5. The length of the training signal used, $N_t = 50$.

6.6.1 Constant Power Profile

Figure 6.5 shows the average coded BER performance for the first user when the base station is transmitting to only the first user, the first and second user and finally all three users. As can be seen, the BER performance degrades with the addition of other users with a loss in SNR of 3dB for a BER of 1×10^{-4} when all three users are operating simultaneously. This is mirrored in the results for the OFDM implementation, shown in Figure 6.6 with a loss in SNR of 2dB for a BER of 1×10^{-3} when all three users are operating simultaneously.

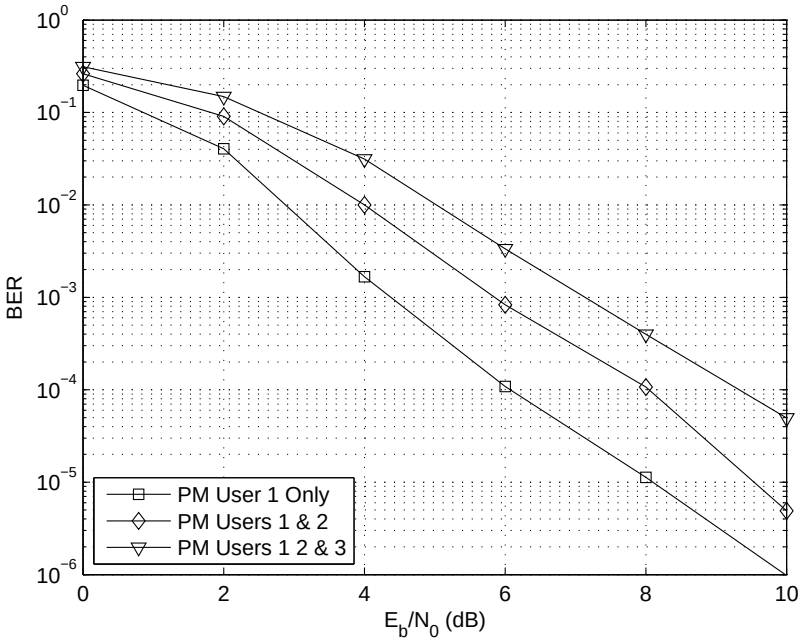

Figure 6.5: Average coded BER results for User 1 when the base station is transmitting to User 1, Users 1 & 2 and Users 1,2 & 3 simultaneously, for a MU-MIMO channel with constant power profile.

Figure 6.7 shows the average coded BER for each individual user when each all three users are transmitting simultaneously. Note the BER for any user when using a given scheme is identical at any SNR. Again the proposed PM approach significantly outperforms OFDM with a gain in SNR of 4dB at BER 1×10^{-3}.

6.6.2 Exponential Power Delay Profile

Figures 6.8 and 6.9 repeat the previous results for exponential power delay profile channels. The figures show the average coded BER performance for the first user when the base station transmits to only the first user, the first and second user and all three users. As expected the BER performance

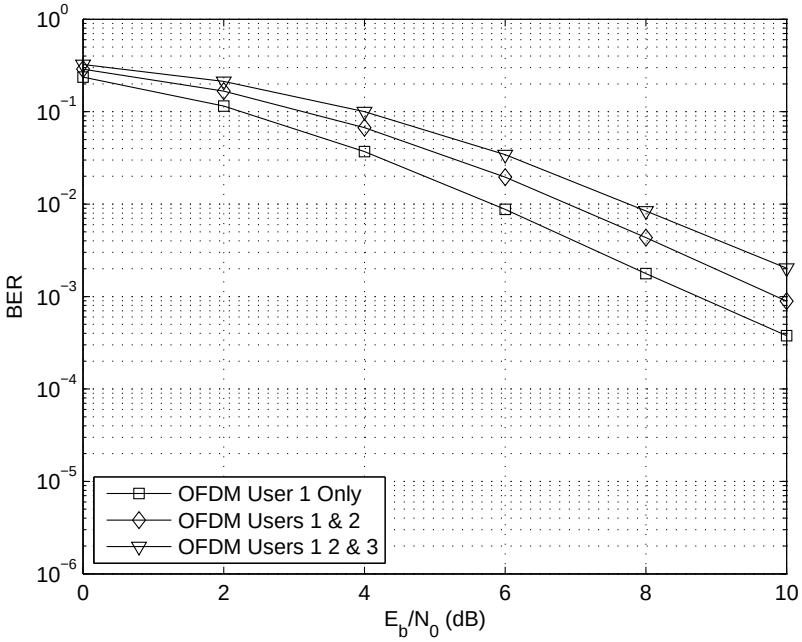

Figure 6.6: Average coded BER results for User 1 when the base station is transmitting to User 1, Users 1 & 2 and Users 1,2 & 3 simultaneously, for a MU-MIMO channel with constant power profile.

degrades with the addition of other users, with a loss in SNR of 2dB at BER 1×10^{-3} for the first user when all three users are transmitting simultaneously. OFDM suffers a similar loss in SNR of 2dB at a BER of 1×10^{-3} for the first user when all three users are operating simultaneously.

Finally Figure 6.10 shows the average coded BER for each individual user when all three users are transmitting simultaneously for the proposed PM and OFDM approaches. Once again the proposed PM approach outperforms OFDM with a gain in SNR of 6dB at BER 1×10^{-3}.

6.7 Conclusion

The SVD approach to downlink MU-MIMO has been successfully generalized to frequency selective MU-MIMO channels using the PMSVD. The proposed PM technique is robust to CSI error and outperforms a conventional OFDM based implementation for every scenario. The SBR2 algorithm has been used to design the transmit filter banks at the transmitter for each user. As shown in Chapter 4, operating on $\widetilde{\widehat{\underline{\boldsymbol{H}}}}_j(z)\widehat{\underline{\boldsymbol{H}}}_j(z)$ rather than directly on $\widehat{\underline{\boldsymbol{H}}}_j(z)$ will square the effect of CSI error, resulting in degraded system performance. A solution to this is already available in the form of the PMSVD by PMQRD algorithm, detailed in the same chapter. However this algorithm was not available at the time of implementation and hence the now redundant SBR2 approach was used. The performance of the proposed PM scheme therefore can be further improved by replacing the SBR2

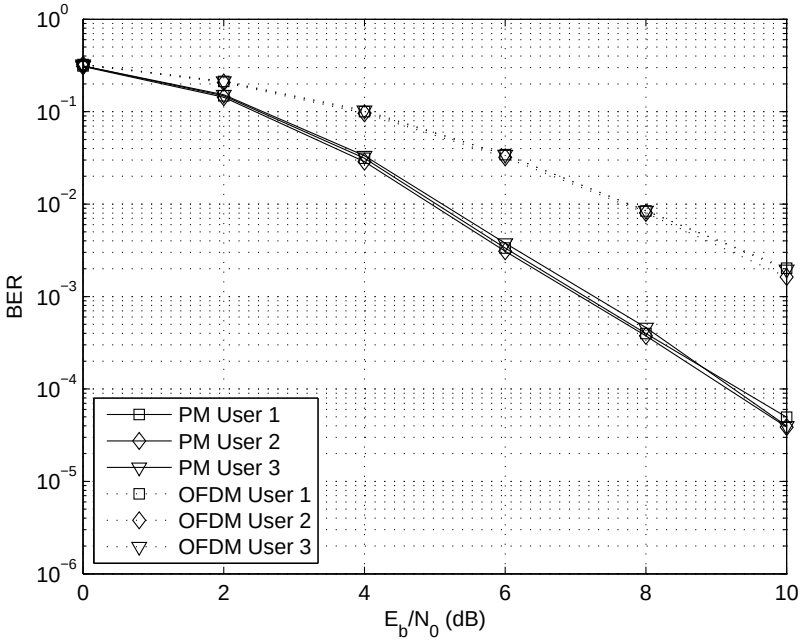

Figure 6.7: Average coded BER results for all users transmitting simultaneously, for a MU-MIMO channel with constant power profile.

algorithm with the PMSVD by PMQRD algorithm.

A significant advantage of the proposed PM technique is carried over from the dominant mode PMSVD work of Chapter 4. As the proposed scheme is entirely time domain based it does not require the storage of signals for DFTs and incur the block delays inherent in a MU-MIMO OFDM scheme. The benefits of using PQMRD at the receiver are also apparent, as with the PMQRD work of Chapter 5, spreading the information in each transmitted symbol across the entire frequency bandwidth makes the system robust to deep channel fading. This results in the dramatic performance increase over a MU-MIMO OFDM scheme. For a MU-MIMO OFDM scheme to provide a similar level of BER performance, an adaptive bit loading scheme must be implemented at the transmitter [79], resulting in a significant computational overhead.

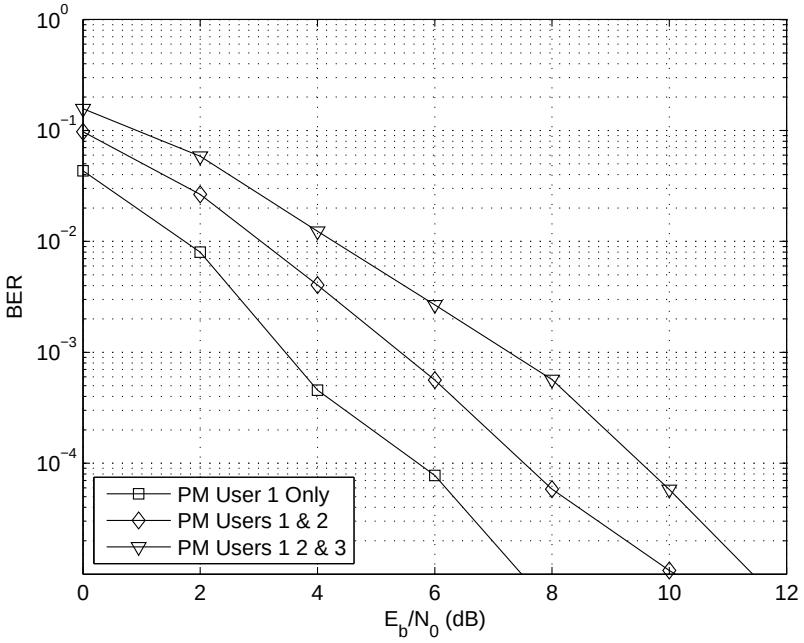

Figure 6.8: Average coded BER results for User 1 when the base station is transmitting to User 1, Users 1 & 2 and Users 1,2 & 3 simultaneously, for a MU-MIMO channel with exponential power delay profile.

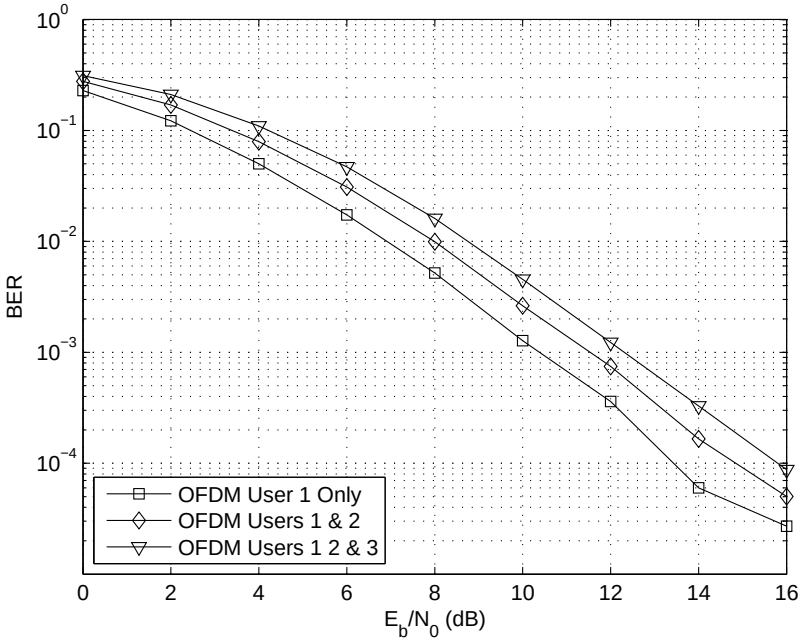

Figure 6.9: Average coded BER results for User 1 when the base station is transmitting to User 1, Users 1 & 2 and Users 1,2 & 3 simultaneously, for a MU-MIMO channel with exponential power delay profile.

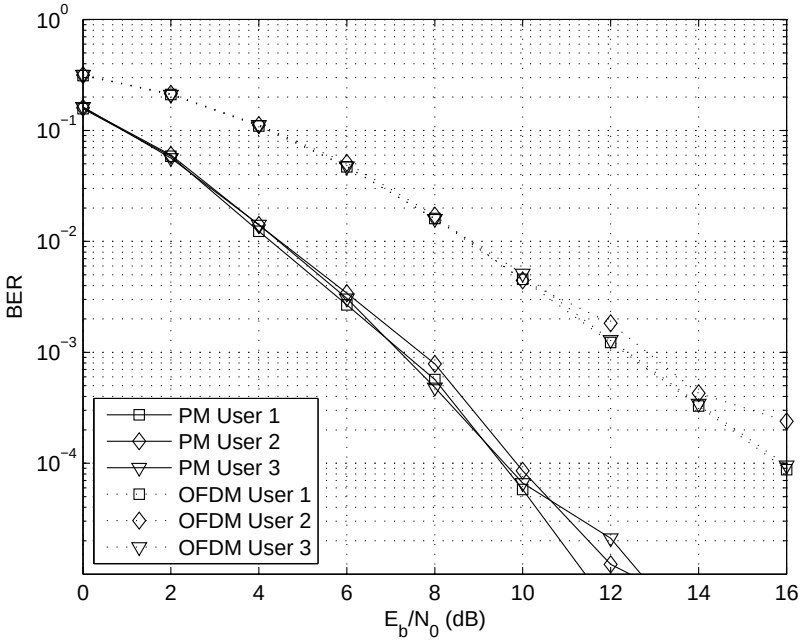

Figure 6.10: Average coded BER results for all users transmitting simultaneously, for a MU-MIMO channel with exponential power delay profile.

Chapter 7

Conclusions

The original problem with applying the SBR2 algorithm to frequency selective MIMO channels was the inability to satisfactorily process the large polynomial channel length produced by PMSVD. Initially the only polynomial matrix channels considered were those with a constant power profile. This automatically eliminated using Viterbi algorithm to equalize the channel response, due to the computational cost. A number of different approaches were tried, namely attempting to reduce the channel impulse response using channel shortening techniques. Capitalizing on the considerable experience available within the engineering department [89, 90], two distinct approaches were attempted. Firstly the shortening of the paraunitary filter banks, $\underline{\boldsymbol{U}}(z)$ and $\underline{\boldsymbol{V}}(z)$ produced by PMSVD was considered. It was hoped that this would produce a diagonal polynomial matrix, $\underline{\boldsymbol{\Lambda}}(z)$ with not only a reduced polynomial length, but that also the energy distribution within would be concentrated in a small number of significant taps, enabling the application of Viterbi equalization.

This approach was unsuccessful as the frequency response of $\underline{\boldsymbol{U}}(z)$ and $\underline{\boldsymbol{V}}(z)$ were found to be too complex to replicate accurately with shorter filter banks. As a consequence the product of $\underline{\widetilde{\boldsymbol{U}}}(z)\ \underline{\boldsymbol{H}}(z)\ \underline{\boldsymbol{V}}(z)$ was no longer sufficiently diagonal. A more direct solution was to use the filter banks generated by PMSVD intact, and focus on shortening $\underline{\boldsymbol{\Lambda}}(z)$ directly. The paraunitary filter banks created by PMSVD would be used directly and channel shortening used to represent $\underline{\boldsymbol{\Lambda}}(z)$ accurately by a smaller number of taps, again allowing Viterbi equalization to be applied. This approach was also found to be unsuccessful. The errors introduced by inaccurately representing the channel degraded overall system performance such that a MIMO-OFDM SVD approach was outperforming the PMSVD system typically by 15-20 dB.

It was only until the PMSVD was applied to MIMO channels with exponential power delay profile, where the energy is concentrated in a few significant taps as a natural effect of the properties of the channel and enabling the use of the Viterbi algorithm were the benefits first realized. Encouraged by this result, a turbo equalization based solution was subsequently implemented to mitigate the effects of constant power profile channels. This work is illustrated in the fourth chapter, where the dominant mode of the PMSVD is exploited to obtain a SISO frequency selective channel with far superior BER performance to existing time domain based access schemes. The performance of the proposed

scheme was also evaluated against a frequency domain based OFDM solution. Although the BER performance of both schemes was found to be identical, the PMSVD approach enables a wider range of access schemes and is operable on continuous streams of data, providing a more flexible solution.

The turbo equalization strategy was subsequently applied to BLAST architecture schemes utilizing PMQRD at the receiver to reduce the MIMO channel equalization problem to a set of decision feedback based single channel problems. The fifth chapter provides a comprehensive review of every conceivable BLAST architecture system and showcases the significant benefits of PMQRD. PMQRD is shown to not only provide superior BER performance over a conventional OFDM based solution, but to additionally reduce power consumption and design costs at the transmitter.

Finally in chapter six both PMSVD and PMQRD were combined in a MU-MIMO downlink scenario. Application of the PMSVD at the transmitter base station enables the transmission of signals between the transmitter and a desired user within other systems users null space. Hence multiple users may share spectrum simultaneously, creating a true spatial access scheme. A D-BLAST architecture encoding scheme was used in conjunction with PMQRD at each receiver to create a MU-MIMO system resistant to deep channel fading. Again, this was compared to an existing frequency domain based OFDM solution and found to provide superior BER performance.

The main contributions of this thesis are the successful application of polynomial matrix decomposition techniques based on polynomial QR and polynomial eigenvalue decomposition to frequency selective MIMO communications. All polynomial based implementations have been shown to be robust to CSI error and demonstrate the maturity of this approach. The significant benefits over existing schemes have been discussed and documented.

7.1 Suggestions for Future Work

This section presents suggested developments to the work in this thesis and future applications of polynomial matrix decomposition techniques within the field of MIMO communications.

7.1.1 Developments in Thesis Material

Due to recent development of the PMSVD by PMQRD algorithm, and the predictable BER performance increase it brings due to operating directly on $\underline{\boldsymbol{H}}(z)$, shown in Chapter 4, there is no further need to apply the SBR2 algorithm to frequency selective MIMO communications as it has been superseded. Due to the computational complexity and number of Monte Carlo simulations required, time did not permit the replacement of the SBR2 algorithm with the PMSVD by PMQRD in the MU-MIMO scenario. Doing so however would further mitigate the effects of CSI and provide a small,

yet significant performance boost and should be investigated.

Chapter 4 only exploits the performance of the dominant mode provided by PMSVD. This research could be extended further with the use of a frequency selective waterpouring scheme to utilize multiple modes of the PMSVD simultaneously and increase system capacity. A MIMO-OFDM scheme utilizing a bit loading scheme would provide a suitable benchmark [91, 92]. A comparison of the robustness of the schemes to CSI error would yield interesting results. When exploiting only the dominant mode in a PMSVD or MIMO-OFDM SVD scheme, CSI error does not significantly effect system performance. Although the beam pattern at the transmitter and receiver will be sub-optimum, resulting in a reduction in the gain of the signal received and increased noise, system performance is still acceptable, as shown in Chapter 4. However CSI error will destroy the orthogonality between the modes in a PMSVD or MIMO-OFDM SVD scheme, leading to a significant performance decrease when multiple spatial modes are used simultaneously due to cross mode interference.

As the significant benefits of PMQRD using optimum detection ordering have been shown in Chapter 5, there is now sufficient motivation to develop a PMQRD algorithm that can operate on any channel matrix and calculate both the optimum decomposition and relevant permutation of the channel matrix simultaneously. This would be of significant value for high order MIMO systems where the calculation of the QR decomposition for every possible permutation of the channel matrix is infeasible. An algorithm that operates directly on a given scalar channel matrix, without the need for the brute force approach used in Chapter 5 already exists [72], often referred to as the *Sorted QR Algorithm*. Sorted QR Algorithm however does not use a Givens rotation based approach to QR decomposition, and instead operates using a modified Gram-Schmidt algorithm. Therefore this approach cannot be easily generalized for the PMQRD givens rotation based approach. Further research is clearly needed in this matter.

Finally, the PMQRD algorithm is at a mature enough state to be taken out of the MATLAB simulation environment and implemented on a real-world development testbed. Given the robustness of the PMQRD approach to CSI error, it is now time to examine the robustness of the algorithm when implemented on the limited hardware found in mobile cellular systems, in particular the limited floating point accuracy available. Given the hardware constraints of a real world system a comprehensive analysis can be carried out to see if it is possible to implement a PMQRD based scheme while maintaining the performance edge over a MIMO-OFDM QR scheme.

7.1.2 Application to Cognitive Radios

The electromagnetic radio spectrum is a tightly regulated natural resource and every wireless sys-

tem requires an exclusive license from the government [93]. As spectrum availability has decreased, the cost of spectrum licenses has sky-rocketed. For example at the turn of the century, Orange, Vodafone and many other mobile operators each paid upwards of 4 billion for a twenty year 3G license [94]. However, when portions of the spectrum are scanned it is found that there exist a large number of spectrum holes [17]. In a cognitive radio application the first step at either the transmitter or receiver antenna array is to detect spectrum holes, i.e. absence of licensed users. In a narrowband, instantaneous mixing scenario there are several well established techniques for decorrelating the received signals and estimating their angle-of-arrival (AOA), based on eigenvalue decomposition, such as multiple signal classification (MUSIC) [95] and estimation of signal parameters by rotational invariance techniques (ESPRIT) [96]. Standard MUSIC and ESPRIT operate by collecting a number of samples of the signals received at each individual antenna within the array and forming their covariance matrix. Eigendecomposition is carried out on this covariance matrix to determine which eigenvectors span the signal subspace and their AOA and which eigenvectors span the noise subspace. Again however for the broadband, convolutive mixing scenario the problem requires the eigenvalue decomposition of a polynomial matrix. As with the work presented in this thesis, a typical solution to this broadband problem is to use the DFT and apply spatial spectrum estimation techniques within each narrowband. However, this ignores the relatively small but important correlations that may exist between different bands. This independent frequency bin (IFB) [97] approach limits the degree to which strong decorrelation can be achieved. It can also lead to a lack of temporal (phase) coherence across the bands, [21].

Application of the SBR2 algorithm would allow blind source separation (BSS) techniques to be directly applied to the broadband channel, and hence the accuracy of BSS can be significantly improved by operating entirely within the time domain. The additional computational complexity needed to correlate data obtained in each frequency band in a DFT based system, and the questionable accuracy of the correlation is entirely removed in an SBR2 based system. Additionally, alongside providing accurate spectrum hole location SBR2 is able to provide an entirely time domain based broadband beamformer, resulting in a complete time domain based solution to the broadband cognitive radio problem. Given the considerable benefits of operating within the time domain shown in this thesis coupled with the industrial interest in spectrum hole exploitation this would be an ideal environment for the application of polynomial matrix decomposition techniques.

Bibliography

[1] G. Corazza, "Marconis history," *Proceedings of the IEEE*, vol. 86, no. 7, pp. 1308–1311, July 1998.

[2] J. Tebo, "The history of radio detectors," *Communications Society: A Digest of News and Events of Interest to Communications Engineers*, vol. 12, no. 6, pp. 26–30, November 1974.

[3] A. Paulraj, R. Nabar, and D. Gore, *Introduction to Space-Time Wireless Communications*, 1st ed. University Press, Cambridge: Cambridge University Press, 2003.

[4] R. Marriott, "Specifications for steamship radio equipment," *Institute of Radio Engineers*, 1914.

[5] R. Schroer, "Aviation radio (a century of powered flight 1903-2003)," *IEEE Aerospace and Electronic Systems Magazine*, vol. 18, no. 7, pp. 19–26, July 2003.

[6] E. Miller, "The computer revolution," *IEEE Potentials*, vol. 8, pp. 27–31, May 1989.

[7] N. Tredennick, "Microprocessor-based computers," *Computer*, vol. 29, pp. 27–37, October 1996.

[8] A. Peled and B. Liu, *Digital Signal Processing*, 1st ed. Hoboken, New Jersey: John Wiley & Sons, 1976.

[9] R. Lyons, *Understanding Digital Signal Processing*, 2nd ed. Upper Saddle River, New Jersey: Prentice Hall, 2004.

[10] A. Goldsmith, *Wireless Communications*, 1st ed. Cambridge, England: Cambridge University Press, 2005.

[11] *Wireless Local Area Networks*, IEEE Standards Association Std. IEEE 802.11, 1997.

[12] T. Virki. (2007) Global cellphone penetration reaches 50 pct. [Online]. Available: http://www.reuters.com

[13] A. Paulraj and C. Papadias, "Space-time processing for wireless communications," *IEEE Signal Processing Magazine*, vol. 14, no. 6, pp. 49–83, Nov 1997.

[14] A. Abbas and S. Sheikh, "On understanding the nature of slow fading in los microcellular channels," in 47^{th} *Vehicular Technology Conference - Spring*, Phoenix, Arizona, USA, May 1997.

[15] G. Foschini, "Layered space-time architecture for wireless communication in a fading environment when using multi-element antennas," *Bell Labs Technical Journal (Autumn)*, pp. 41–59, 1996.

[16] B. VanVeen and K. Buckley, "Beamforming: A versatile approach to spatial filtering," *IEEE ASSP Magazine*, pp. 4–24, April 1988.

[17] S. Haykin, "Cognitive radio: Brain-empowered wireless communications," *IEEE Journal Selected Areas in Communications*, vol. 23, no. 2, pp. 201–220, February 2005.

[18] K. Watanabe, K. Ishibashi, and R. Kohno, "Performance of cognitive radio technologies in the presence of primary radio systems," in *Proceedings of the 18th Annual IEEE Symposium on Personal, Indoor and Mobile Radio Communications*, 2007.

[19] A. Scaglione, S. Barbarossa, and G. Giannakis, "Robust OFDM transmissions over frequency-selective channels with multiplicative time-selective effects," in *IEEE International Conference on Acoustic, Speech and Signal Processing (ICASSP)*, Turkey, June 2000, pp. 2677–2680.

[20] G. Giannakis, Z. Liu, X. Ma, and S. Zhou, *Space-Time Coding for Broadband Wireless Communications*, 1st ed. Hoboken, New Jersey: John Wiley & Sons, 2007.

[21] J. McWhirter, P. Baxter, T. Cooper, S. Redif, and J. Foster, "An EVD algorithm for para-Hermitian polynomial matrices," *IEEE Transactions on Signal Processing*, vol. 55, no. 5, pp. 2158–2169, May 2007.

[22] J. Foster, J. McWhirter, and J. Chambers, "An algorithm for computing the QR decomposition of a polynomial matrix," in *15^{th} International Conference on Digital Signal Processing*, Cardiff, July 2007.

[23] M. Davies, S. Lambotharan, J. Foster, J. Chambers, and J. McWhirter, "A polynomial QR decomposition based turbo equalization technique for frequency selective MIMO channels," in *69^{th} Vehicular Technology Conference - Spring*, Barcelona, Spain, April 2009.

[24] ——, "Polynomial matrix QR decomposition and iterative decoding of frequency selective MIMO channels," in *IEEE Wireless Communications and Networking Conference*, Budapest, Hungary, April 2009.

[25] Q. Spencer, A. Swindlehurst, and M. Haardt, "Zero-forcing methods for downlink spatial multiplexing in multiuser MIMO channels," *IEEE Transactions on Signal Processing*, vol. 52, pp. 461–471, February 2004.

[26] J. Foster, J. McWhirter, and J. Chambers, "A polynomial matrix QR decomposition with application to MIMO channel equalization," in *Conference Digest : 41st Asilomar Conference on Signals, Systems, and Computers*, November 2007.

[27] C. Chuah, J. Kahn, and D. Tse, "Capacity of multi-antenna array systems in indoor wireless environment," in *Proceedings of IEEE GLOBECOM*, Sydney, Australia, November 1998, pp. 1894–1899.

[28] P. Vaidyanathan, *Multirate Systems and Filter Banks*, 1st ed. Upper Saddle River, New Jersey: Prentice-Hall, 1993.

[29] G. Golub and C. Loan, *Matrix Computations*, 3rd ed. Baltimore, Maryland: The John Hopkins University Press, 1996.

[30] C. Shannon, "A mathematical theory of communication," *Bell System Technical Journal*, vol. 27, pp. 379–423, 623–656, October 1948.

[31] B. Vucetic and J. Yuah, *Turbo Codes: Principles and Applications*, 1st ed. Dordrecht, The Netherlands: Kluwer Academic Publishers, 2000.

[32] T. Cover and J. Thomas, *Elements of Information Theory*, 2nd ed. Hoboken, New Jersey: John Wiley & Sons, 2006.

[33] G. Raleigh and J. Cioffi, "Spatio-temporal coding for wireless communication," *IEEE Transactions on Communications*, vol. 46, no. 3, pp. 357–366, March 1998.

[34] S. Weinstein and P. Ebert, "Data transmission by frequency-division multiplexing using the discrete fourier transform," *IEEE Transactions on Communication Technology*, vol. COM-19, no. 5, pp. 628–634, October 1971.

[35] R. Gray. (2009) Toeplitz and circulant matrices: A review. [Online]. Available: http://ee.stanford.edu/ gray/toeplitz.pdf

[36] J. Cooley and J. Tukey, "An algorithm for the machine calculation of the complex fourier series," *Mathematics of Computation*, vol. 19, pp. 297–301, 1965.

[37] N. Vucic and H. Boche, "Robust transceiver optimization for frequency selective mimo channels," in *2nd IEEE International Workshop on Computational Advances in Multi-Sensor Adaptive Processing (CAMPSAP)*, Virgin Islands, USA, December 2007, pp. 73–76.

[38] A. Mertins, "MMSE design of redundant fir precoders for arbitrary channel lengths," *IEEE Transactions on Signal Processing*, vol. 51, no. 9, pp. 2402–2409, September 2003.

[39] P. Regalia and D. Huang, "Attainable error bounds in multirate adaptive lossless fir filters," in *IEEE International Conference on Acoustic, Speech and Signal Processing (ICASSP)*, Detroit, USA, May 1995, pp. 1460–1463.

[40] R. Lambert, M. Joho, and H. Mathis, "Polynomial singular values for number of wideband sources estimation and principal components analysis," in *Proceedings on International Conference on Independent Component Analysis*, 2001, pp. 379–383.

[41] R. Lambert, "Multichannel blind deconvolution: FIR matrix algebra and separation of multipath mixtures," Ph.D. dissertation, University of Southern California, Los Angeles, 1996.

[42] H. Smith, "On systems of linear indeterminate equations and congruences," *Philosophical Transactions, Royal Society, London*, vol. 151, pp. 293–326, 1861.

[43] J. Foster, "Algorithms and techniques for polynomial matrix decomposition," Ph.D. dissertation, Cardiff University, Cardiff, May 2008.

[44] J. Tugnait, L. Tong, and Z. Ding, "Single-user channel estimation and equalization," *IEEE Signal Processing Magazine*, vol. 17, no. 3, pp. 16–28, May 2000.

[45] H. Sampath, S. Talwar, J. Tellado, V. Erceg, and A. Paulraj, "A fourth-generation MIMO-OFDM broadband wireless system: Design, performance, and field trial results," *IEEE Communications Magazine*, vol. 40, no. 9, pp. 143–149, Sep 2002.

[46] Z. Luo and D. Huang, "General MMSE channel estimation for MIMO-OFDM systems," in *68^{th} Vehicular Technology Conference - Fall*, Calgary, Alberta, Sept 2008.

[47] ——, "Optimal and robust MMSE channel estimation for MIMO-OFDM systems," in *Proceedings of the 19th Annual IEEE Symposium on Personal, Indoor and Mobile Radio Communications*, 2008.

[48] C. Shin, R. Heath, and E. Powers, "Blind channel estimation for MIMO-OFDM systems," *IEEE Transactions on Vehicular Technology*, vol. 56, pp. 670–685, March 2007.

[49] P. Baxter and J. McWhirter, "Blind signal separation of convolutive mixtures," in *Conference Digest : 37^{th} Asilomar Conference on Signals, Systems, and Computers*, November 2003.

[50] J. Foster, J. McWhirter, and J.Chambers, "Limiting the order of polynomial matrices within the SBR2 algorithm," in *Conference Digest: IMA Mathematics in Signal Processing*, Cirencester, England, Dec 2006, pp. 93–97.

[51] C. Ta and S. Weiss, "Shortening the order of paraunitary matrices in SBR2 algorithm," in *15^{th} International Conference on Digital Signal Processing*, Cardiff, July 2007.

[52] *Technical Specification Group GERAN, Channel Coding*, 3rd Generation Partnership Project Std. 3GPP TS 05.03 V8.6.1 (2001-01), 1999.

[53] J. Foster, J. McWhirter, M. Davies, and J. Chambers, "An algorithm for calculating the QR and singular value decompositions of polynomial matrices," *IEEE Transactions on Signal Processing*, vol. 58, no. 3, March 2010.

[54] C. Ta and S. Weiss, "A design of precoding and equalisation for broadband MIMO systems," in *Conference Digest : 41^{st} Asilomar Conference on Signals, Systems, and Computers*, November 2007.

[55] ——, "Broadband SVD and non-linear precoding applied to broadband MIMO channels," in *Conference Digest : 42^{nd} Asilomar Conference on Signals, Systems, and Computers*, October 2008.

[56] A. Viterbi, "Error bounds for convolutional codes and an asymptotically optimum decoding algorithm," *IEEE Transactions on Information Theory*, vol. IT-13, pp. 260–269, 1967.

[57] J. Cheung and R. Steele, "Viterbi equalisation of mobile radio channels having large delay spreads," in *IEE Colloquium on Methods of Combating Multipaths*, January 1990, pp. 2/1–2/5.

[58] A. Viterbi, "A personal history of the Viterbi algorithm," *IEEE Signal Processing Magazine*, pp. 120–142, July 2006.

[59] G. Forney, "Maximum-likelihood sequence estimation of digital sequences in the presence of intersymbol interference," *IEEE Transactions on Information Theory*, vol. 18, no. 3, pp. 363–378, May 1972.

[60] L. Ekroot and S. Dolinar, "A* decoding of block codes," *IEEE Transactions on Communications*, vol. 44, no. 9, pp. 1052–1056, Sept 1996.

[61] J. Feldman, I. Abou-Faycal, and M. Frigo, "A fast maximum-likelihood decoder for convolutional codes," in *56^{th} Vehicular Technology Conference - Fall*, Vancouver, Canada, November 2002.

[62] G. Chapelle, "Cpm for indoor wireless channel," *IET Electronics Letters*, vol. 38, no. 21, pp. 1278–1280, October 2002.

[63] ——, "Continuous phase modulation for the indoor wireless channel," Ph.D. dissertation, University of California, San Diego, 1998.

[64] M. Tuchler, R. Koetter, and A. Singer, "Turbo equalization: Principles and new results," *IEEE Transactions on Communications*, vol. 50, no. 5, pp. 754–767, May 2002.

[65] R. Koetter, A. Singer, and M. Tuchler, "Turbo equalization: an iterative equalization and decoding technique for coded data transmission," *IEEE Signal Processing Magazine*, pp. 67–80, January 2004.

[66] L. Bahl, J. Cocke, F. Jelinek, and J. Raviv, "Optimal decoding of linear codes for minimizing symbol error rate," *IEEE Transactions on Information Theory*, vol. 20, pp. 284–287, March 1974.

[67] T. Moon, *Error Correction Coding: Mathematical Methods and Algorithms*, 1st ed. Hoboken, New Jersey: John Wiley & Sons, 2005.

[68] L. Hanzo, J. Woodward, and P. Robertson, "Turbo decoding and detection for wireless applications," *Proceedings of the IEEE*, vol. 95, no. 6, pp. 1178–1200, June 2007.

[69] S. Dolinar and D. Divsalar, "Weight distribution for turbo codes using random and nonrandom permutations," in *TDA Progress Report*, August 1995, pp. 42–122.

[70] M. Valenti. (2006) Coded modulation library. [Online]. Available: http://www.iterative-solutions.com/Matlab.htm

[71] P. Wolninansky, G. Foschini, G. Golden, and R. Valenzuela, "V-BLAST: An architecture for realizing very high data rates over the rich-scattering wireless channel," in *1998 International Symposium on Signals, Systems and Electronics*, Pisa, Sept-Oct 1998, pp. 295–300.

[72] D. Wubben, R. Bohnke, J. Rinas, V. Kuhn, and K. Kammeyer, "Efficient algorithm for decoding layered space-time codes," *IET Electronics Letters*, vol. 37, no. 22, pp. 1348–1350, October 2001.

[73] J. Proakis, *Digital Communications*, 4th ed. Avenue of the Americas, New York: McGraw-Hill, 2001.

[74] S. Muller and J. Huber, "A comparison of peak power reduction schemes for OFDM," in *Proceedings of IEEE GLOBECOM*, Phoenix, Arizona, November 1997, pp. 1–5.

[75] T. Pollet, M. V. Bladel, and M. Moeneclaey, "BER sensitivity of OFDM systems to carrier frequency offset and wiener phase noise," *IEEE Transactions on Communications*, vol. 43, no. 2/3/4, pp. 191–193, February 1995.

[76] Ericsson. (2008) Energy-saving solutions helping mobile operators meet commercial and sustainability goals worldwide. [Online]. Available: http://www.ericsson.com/ericsson/press/-facts_figures/doc/energy_efficiency.pdf

[77] G. Fettweis. (2009) 2009 IEEE wireless communications and networking conference spring keynote. [Online]. Available: http://ieee-wcnc.org/2009

[78] A. Czylwik, "Comparison between adaptive OFDM and single carier modulation with frequency domain equalization," in *47th Vehicular Technology Conference*, Phoenix, Arizona, May 1997.

[79] C. Wong, R. Cheng, K. Lataief, and R. Murch, "Multiuser OFDM with adaptive subcarrier, bit, and power allocation," *IEEE Journal on Selected Areas in Communications*, vol. 17, no. 10, pp. 1747–1758, October 1999.

[80] A. Goldsmith and S. Chua, "Variable-rate variable-power MQAM for fading channels," *IEEE Transactions on Communications*, vol. 45, no. 10, p. 12181230, October 1997.

[81] G. Forney and M. Eyuboglu, "Combined equalization and coding using precoding," *IEEE Communications Magazine*, vol. 29, no. 12, pp. 25–34, December 1991.

[82] H. Sari, G. Karam, and I. Jeanclaude, "An analysis of orthogonal frequency-division multiplexing for mobile radio applications," in *44th Vehicular Technology Conference - Spring*, Stockholm, Sweden, 1994, pp. 1635–1639.

[83] B. Ottersten, "Array processing for wireless communications," in *Proceedings of the Eighth IEEE Signal Processing Workshop on Statistical Signal and Array Processing*, Corfu, Greece, June 1996, pp. 466–473.

[84] P. Vandenameele, *Space Division Multiple Access for Wireless Local Area Networks*, 1st ed. Norwell, Massachusetts: Kluwer, 2001.

[85] Q. Spencer, C. Peel, A. Swindlehurst, and M. Haardt, "An introduction to the multi-user MIMO downlink," *IEEE Communications Magazine*, pp. 60–67, October 2004.

[86] K. King-Tim and B. Davies, "A space-division multiple-access protocol for spot-beam antenna and satellite-switched communication network," *IEEE Selected Areas in Communications*, vol. 1, no. 1, pp. 126–132, January 1983.

[87] S. Bana and P. Varaiya, "Space division multiple access (SDMA) for robust ad hoc vehicle communication networks," in *Proceedings of the 2001 IEEE Conference on Intelligent Transportation Systems*, 2001, pp. 962–967.

[88] R. Pickholtz, D. Schilling, and L. Milstein, "Theory of spread-spectrum communications," *IEEE Transactions on Communications*, vol. 30, pp. 855–884, May 1982.

[89] C. Toker, S. Lambotharan, and J. Chambers, "Joint transceiver design for MIMO channel shortening," *IEEE Transactions on Signal Processing*, vol. 55, pp. 3851–3866, July 2007.

[90] C. Toker, S. Lambotharan, J. Chambers, and B. Baykal, "Joint spatial and temporal channel-shortening techniques for frequency selective fading MIMO channels," *IEE Proceedings on Communications*, vol. 152, pp. 89–94, February 2005.

[91] P. Xia, S. Zhou, and G. Giannakis, "Adaptive MIMO-OFDM based on partial channel state information," *IEEE Transactions on Signal Processing*, vol. 52, no. 1, pp. 202–213, January 2004.

[92] P. Chow, J. Cioffi, and J. Bingham, "A practical discrete multitone transceiver loading algorithm for data transmission over spectrally shaped channels," *IEEE Transactions on Communications*, vol. 43, no. 4, pp. 773–775, Feb-Mar-Apr 1995.

[93] G. Staple and K. Werbach, "The end of spectrum scarcity," *IEEE Spectrum*, pp. 48–52, March 2004.

[94] OFCOM. (2008) Radiocommunications agency : Spectrum auctions. [Online]. Available: http://www.ofcom.org.uk/static/archive/spectrumauctions/index.htm

[95] R. Schmidt, "Multiple emitter location and signal parameter estimation," *IEEE Transactions on Antennas and Propagation*, vol. AP-34, no. 3, pp. 276–280, March 1986.

[96] A. Paulraj, R. Roy, and T. Kaliath, "A subspace rotation approach to signal parameter estimation," *Proceedings of the IEEE*, vol. 74, no. 7, pp. 1044–1045, July 1986.

[97] R. Klemm, "Space-time adaptive processing principles and applications," *IEE Radar, Sonar, Navigation and Avionics*, 1998.

[98] F. Daneshgaran, M. Laddomada, and M. Mondin, "High-rate recursive convolutional codes for concatenated channel codes," *IEEE Transactions on Communications*, vol. 52, no. 11, pp. 1846–1850, November 2004.

Appendix A

Recursive Convolutional Encoding for PMSVD Channels

A.1 Introduction

Throughout this thesis the non-recursive convolutional encoder used in GSM CS1-CS3 [52] shown in Figure A.1 has been implemented in all turbo equalization based schemes. D blocks represent 1-bit storage devices, or D flip-flops. The two output streams, $\boldsymbol{C}_1$ and $\boldsymbol{C}_2$ are interleaved together to produce the coded stream $\boldsymbol{C}$. Thus for every bit of input, there are two coded output bits, resulting in a rate $R = 1/2$ code [67]. It is convention to assume that all memory elements are initialized to zeros prior to transmission, so that the initial starting state of the encoder can be predetermined.

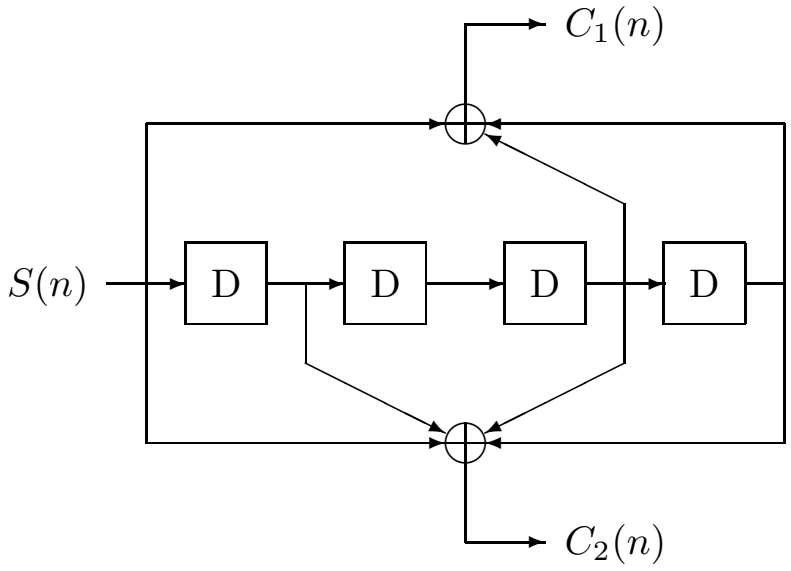

Figure A.1: GSM CS1-CS3 convolutional encoder.

For the input stream $\boldsymbol{S} = [0, 1, 1, 0, 1, 0, 1]$ the resulting outputs are $\boldsymbol{C}_1 = [0, 1, 1, 0, 0, 0, 0]$ and $\boldsymbol{C}_2 = [0, 1, 0, 1, 0, 1, 0]$. Hence the encoded interleaved stream is $\boldsymbol{C}\,[00, 11, 10, 01, 00, 01, 00]$. Commas separate the pairs of outputs at a single input time. This encoding architecture is known as a non-recursive, feedforward or FIR encoder, as the transfer function 4.3 contains only polynomial entries [67]. Each bit of the input stream $\boldsymbol{S}$ will influence the subsequent 5 bits of the output streams

$\boldsymbol{C}_1$ and $\boldsymbol{C}_2$ as it traverses the shift register. In this appendix the performance of recursive convolutional encoders are considered. A recursive encoder utilizes a feedback or IIR element to produce a convolutional encoder where each bit of the input stream will influence every subsequent coded output bit. Tuchler *et al* [65] have shown the performance of a turbo equalization scheme can be significantly improved using a recursive encoder. Assuming perfect channel equalization the performance of the turbo equalization scheme is lower bounded by the underlying 1/2 rate code used over an ISI-free channel at the same SNR. Well designed recursive encoders typically outperform their FIR counterparts, hence the aim of this appendix is to mirror the results presented by Tuchler textitet al [65] for the dominant mode PMSVD scenario presented in chapter 4.

A.2 Recursive Encoder Design

Two types of recursive encoder are implemented in this appendix. The first is based on a simple suggestion by Tuchler *et al* [65], which is to convert an existing non-recursive encoder to a recursive with the simple addition of a single one-tap IIR element. The second is a specific recursive convolutional encoder, designed for for concatenated channel encoding.

A.2.1 IIR GSM CS1-CS3

The GSM CS1-CS3 encoder can be easily modified to become recursive with the addition of the feedback path shown in Figure A.2, as suggested in [64]. Note that the addition of this feedback path will not cause a significant complexity overhead, since the required number of delay elements has remained constant.

A.2.2 High-Rate Recursive Encoder

Daneshgaran *et al* [98] have investigated a wide range of recursive convolutional encoders for concatenated channel coding. The minimum metric of a path diverging from and then remerging to the all zero path is termed the free distance, or d_{free} of a convolutional code. As encoder performance is directly proportional to d_{free}, Daneshgaran *et al* have searched for a number of recursive convolutional encoders whose distance spectra is maximal for a given number of conditions. Thus the 1/2 rate recursive generating polynomial (A.1) has been selected, due to its high value of $d_{free} = 7$. Figure A.3 shows the structure of the encoder.

$$G(D) = \left[1, \frac{23}{35}\right] \tag{A.1}$$

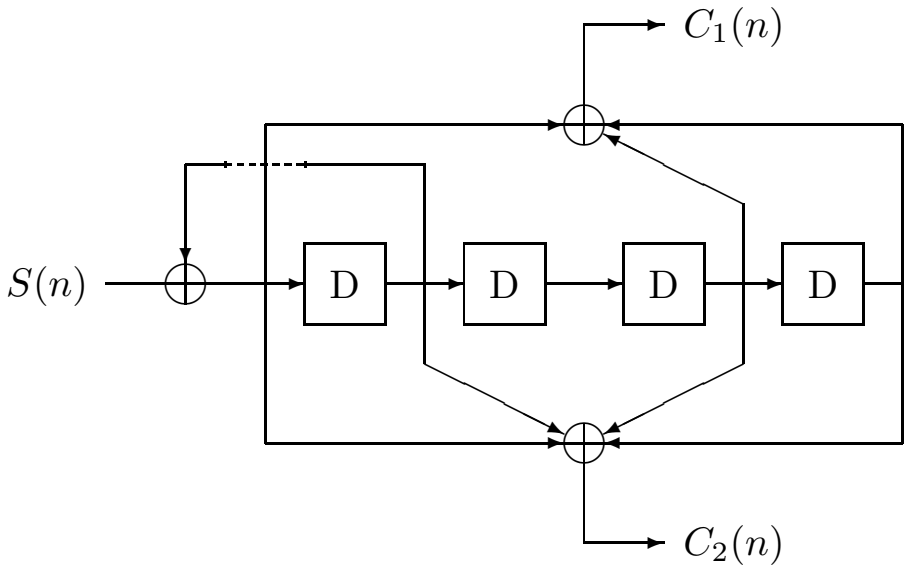

Figure A.2: GSM CS1-CS3 recursive convolutional encoder.

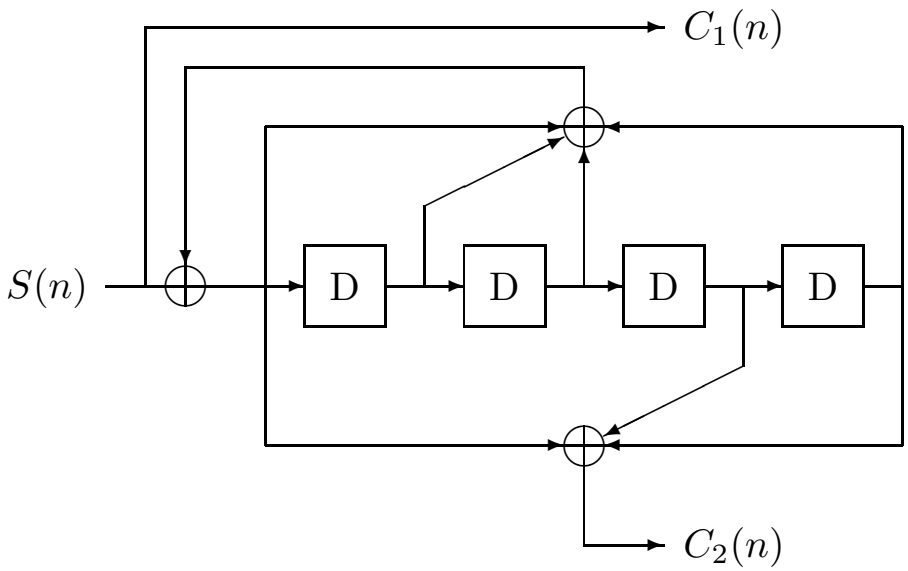

Figure A.3: High-rate Daneshgaran recursive convolutional encoder.

A.2.3 MAP Decoder Design

It is important to note that due to the IIR properties of the recursive encoders it can be difficult to flush the encoder to a known end state with only a small number of flushbits. Therefore to avoid

wasting bandwidth transmitting excessive flushbits it is necessary to set all the ending probabilities to have an equal probability, i.e. the values of $\beta_\tau(i) = 1/M_s$ for $i = 0, 1, \ldots, M_s - 1$ where M_s denotes the number of states.

A.3 Channel Model

A MIMO channel with constant power delay profile and equal average gain for each tap has been considered. The number of antennas at the transmitter and receiver is five, i.e. $M_t = M_r = 5$. The polynomial length of the channel, L is five. It is assumed both the transmitter and receiver have perfect channel knowledge.

A.4 Results

A PMSVD scheme identical to that used in chapter 4 has been implemented and the PMSVD has been calculated using the SBR2 algorithm. Again, only the BER performance of the dominant mode has been considered. The standard non-recursive GSM CS1-CS3 generating polynomial has been used as a benchmark. The bit error rate has been computed for 1000 Monte Carlo simulations. The modulation scheme used is BPSK for evaluation purposes but extension to large constellations is straightforward. The number of time slots of the channel, $N = 2048$.

Figure A.4 compares the coded BER performance of all three schemes. As can be seen, all three convolutional encoders provide a similar level of average coded BER performance. Surprisingly, both recursive encoders are outperformed by the standard non-recursive GSM CS1-CS3 encoder. For example at a BER of 1×10^{-4}, GSM CS1-CS3 outperforms both recursive encoders with a gain in SNR of 0.2 dB.

A.5 Conclusion

Recursive encoders degrade coded BER performance when applied to the dominant mode PMSVD scenario described in Chapter 4. This is due to the excessive length of the polynomial channel generated by PMSVD and the MMSE equalization strategy employed to overcome it. Recalling from Chapter 4, to reduce the computational complexity of the MMSE equalizer, the MMSE equalizer is of a minimum length of 10 taps, and only considers taps of the resulting channel $\lambda_{11}(z)$ with an absolute value greater than $\frac{\sigma^2}{M_r \times M_t}$. This provides an acceptable trade-off between computational complexity and performance. Typically the MMSE equalizer length is around 30-50 taps and hence behaves similarly to a constraint-length 30-50 convolutional codec. Since the minimum distance of the legitimate codewords is huge, once an error is made the resulting decision is a high distance codeword

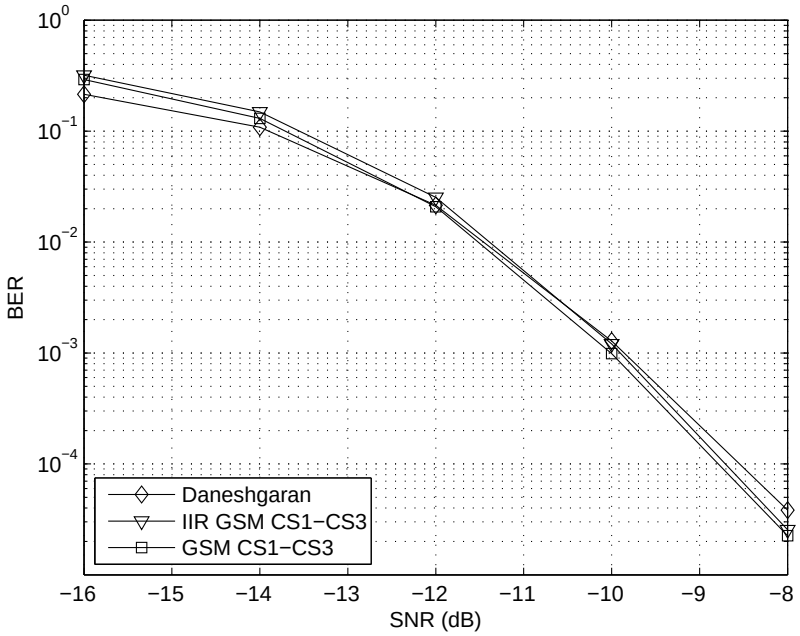

Figure A.4: Average coded BER results for dominant mode PMSVD scheme with a range of encoding schemes for a 5×5 MIMO channel, $L = 5$, with constant power profile.

that can inflict a far greater number of errors the originally existed. This effect, coupled with the sub-optimum performance of the MMSE equalizer results in error propagation between the MMSE equalizer and MAP decoder. Given the extended bit influence of the recursive architecture, this results in degraded system performance when using a recursive encoding strategy.

Although the proposed recursive encoders degrade system performance, the GSM CS1-CS3 encoder is by no means the definitive encoder to use when exploiting the dominant mode performance of the PMSVD. As the aim of Chapter 4 was to successfully implement a dominant mode PMSVD based communications system, GSM CS1-CS3 was deemed appropriate due to its use in cellular systems. However the GSM implementation does not utilize a turbo equalization strategy and hence more appropriate generating polynomials may be found for PMSVD applications. This work however is outside the scope of this thesis.

Appendix B

Diversity Techniques using PMQRD for Channels with Exponentially Decaying Power Profile

B.1 Introduction

In Chapter 5 the application of PMQRD to frequency selective MIMO channels with constant power profile was discussed. In this appendix identical techniques are applied to frequency selective MIMO channels with exponential power delay profile to demonstrate the flexibility of the proposed approach. The exponential channel model is identical to that presented in Chapter 4. Again the exponential decaying factor, $\psi = 0.8$ (in keeping with the PMSVD experiments). A MIMO system consisting of $M_r = M_t = 3$ antennas has been considered, but extension to MIMO systems with $M_r \neq M_t$ is trivial.

Application of PMSVD to MIMO channels with exponential power delay results in a frequency selective channel where the energy distribution is concentrated in a few consecutive taps, allowing a low complexity Viterbi equalizer to be applied. However this does not occur when applying PMQRD to exponential power delay MIMO channels. As a consequence the turbo equalization approach discussed in Chapter 5 for constant power profile channels is simply re-applied here.

B.2 Results

Again, a wide-sense quasi stationary (WSQS) situation has been considered. The bit error rate has been computed for 1000 Monte Carlo simulations. The modulation scheme used is BPSK for evaluation purposes but extension to large constellations is straightforward. The number of time slots of the channel, N = 2048. Initially it is assumed the receiver has perfect channel knowledge. Results have been simulated with and without ODO and again an equivalent MIMO-OFDM QR scheme has been used as a benchmark.

B.2.1 H-BLAST

Figure B.1 directly compares the proposed PMQRD and MIMO-OFDM QR schemes for a H-Blast architecture wireless system. Additional results have been included for ODO implementations. PMQRD provides superior BER performance, with a gain of 3dB in SNR at BER 10^{-3} over a MIMO-OFDM approach. ODO further increases the performance of the PMQRD scheme, with a 3dB gain in SNR over standard PMQRD and 1dB gain over MIMO-OFDM ODO at BER 10^{-3} respectively. As with constant power profile channels, ODO mitigates the effects of individual tones having poor gain in the MIMO-OFDM approach, providing the significant performance boost.

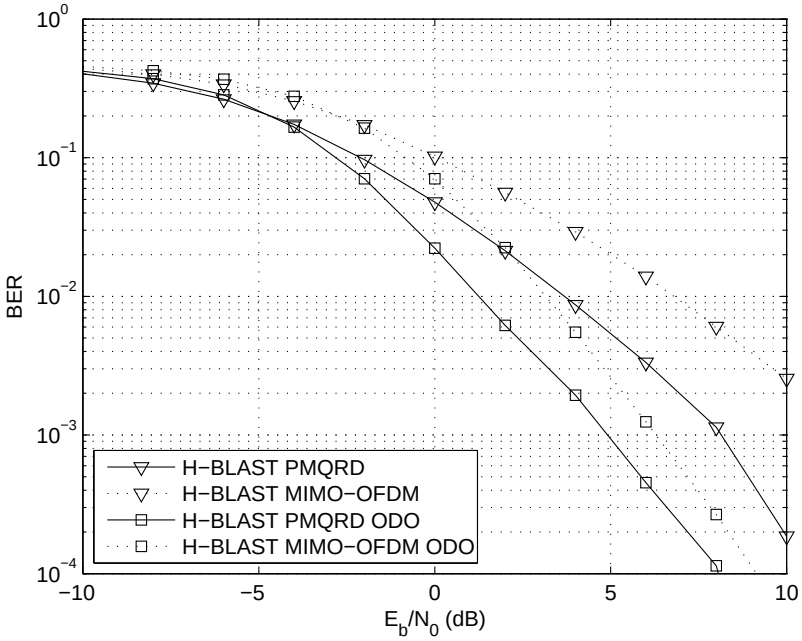

Figure B.1: Average uncoded BER results for H-BLAST PMQRD and MIMO-OFDM QR schemes incorporating ODO for a 3×3 MIMO channel, $L = 5$, with exponentially decaying elements.

B.2.2 V-BLAST

Figure B.2 repeats the previous results for a V-BLAST architecture implementation. When using channels with constant power profile the maximum diversity obtainable is $M_r M_t L$, where L denotes the polynomial length of the channel. As the V-BLAST architecture approximately provides this the benefits of ODO are negated and no-performance gain is seen with its inclusion in PMQRD based schemes. The PMQRD approach retains its superior performance over MIMO-OFDM QR due to the spreading of information in each transmitted symbol across the entire frequency bandwidth, providing

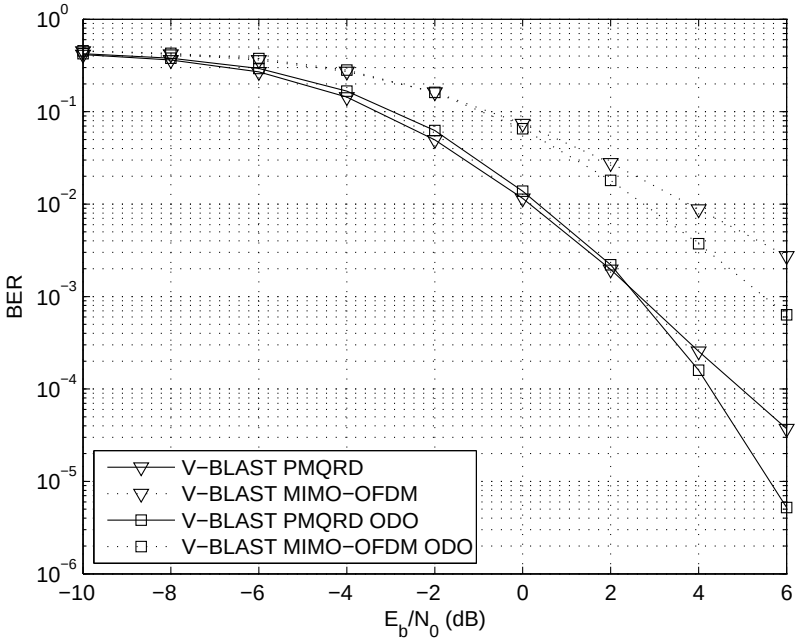

Figure B.2: Average uncoded BER results for V-BLAST PMQRD and MIMO-OFDM QR schemes incorporating ODO for a 3×3 MIMO channel, $L = 5$, with exponentially decaying elements.

additional robustness against deep fading, with a small gain of 4dB in SNR at BER 10^{-3}.

B.2.3 D-BLAST

Figure B.3 again repeats the previous simulation for a D-Blast architecture scenario. Combining the performance benefits of V-BLAST with the computational benefits of H-BLAST, once again PMQRD outperforms MIMO-OFDM QR with a gain in SNR of 3dB at BER $10^{-}3$.

B.2.4 Channel Estimation Error

Finally the scenario where the receiver has imperfect channel knowledge has once again been considered. The BER rate has been computed for 1000 Monte Carlo simulations. The modulation scheme used is BPSK. The number of time slots of the channel, $N = 2048$. The length of the training sequence, $N_t = 50$. Simulations have been performed for both D-BLAST PMQRD ODO and D-BLAST MIMO-OFDM QR ODO schemes. Figure B.4 again shows the clear performance benefits of the PMQRD approach, with a gain in SNR of 2dB at BER 10^{-3}. The algorithm has again been shown to be robust to CSI error, confirming its suitability for real world applications.

B.3 Conclusion

In this short appendix the results of Chapter 5 have been confirmed for MIMO frequency selective

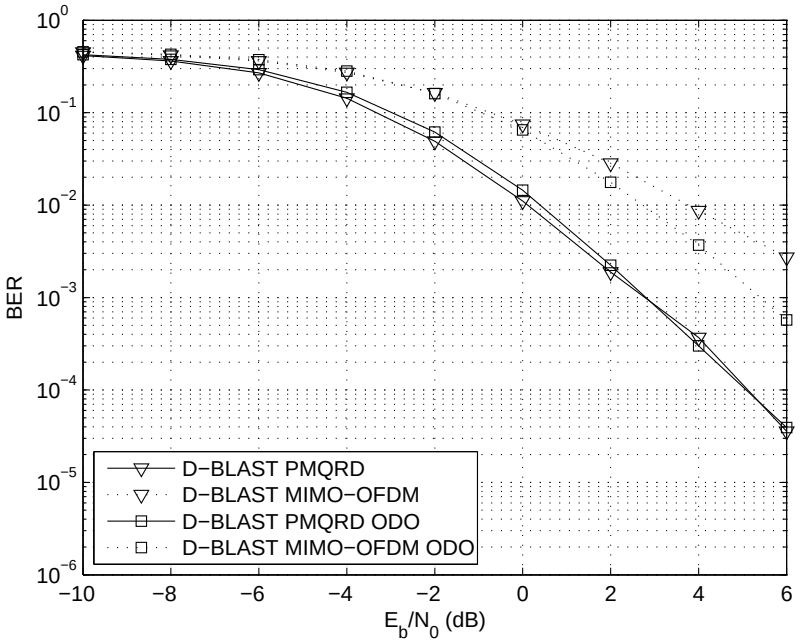

Figure B.3: Average uncoded BER results for D-BLAST PMQRD and MIMO-OFDM QR schemes incorporating ODO for a 3×3 MIMO channel, $L = 5$, with exponentially decaying elements.

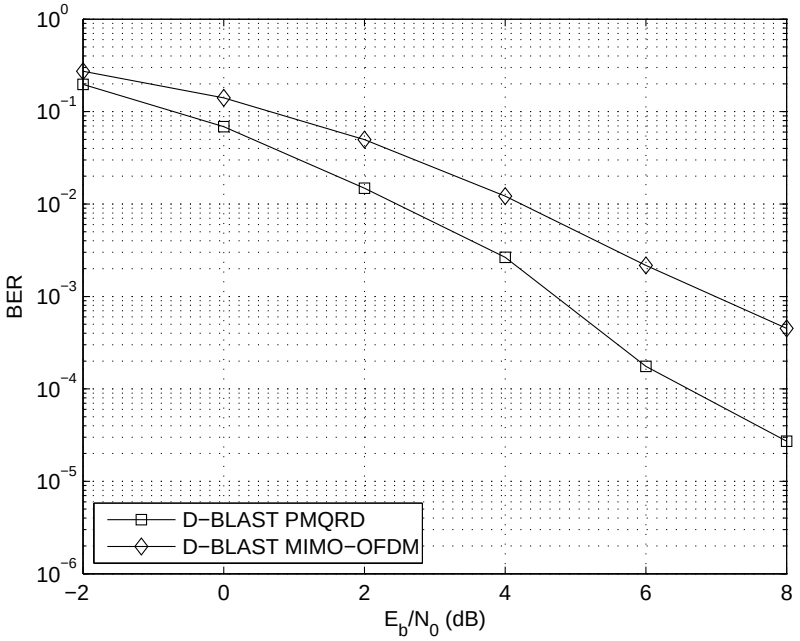

Figure B.4: Average uncoded BER results for D-BLAST PMQRD and MIMO-OFDM QR schemes incorporating ODO for a 3×3 MIMO channel, $L = 5$, with exponentially decaying elements with channel estimation error.

channels with exponential power delay profile. The key benefits of the PMQRD approach, i.e. the robustness to deep fading and reduction in peak-to-average power ratio over MIMO-OFDM QR all still apply.